

**Voltage Interactions and Commutation Failure  
Phenomena in Multi-Infeed HVDC Systems**

By:

**Ebrahim Rahimi**

A Thesis

Submitted to the Faculty of Graduate Studies in Partial  
Fulfillment of the Requirements for the Degree of

**Doctor of Philosophy**

Department of Electrical and Computer Engineering

University of Manitoba

Winnipeg, Manitoba

© Copyright by Ebrahim Rahimi 2011

## **Acknowledgments**

First and foremost, I would like to show my utmost gratitude to my thesis supervisor, Dr. Aniruddha Golé, Distinguished Professor and NSERC Industrial Research Chair in Power System Simulation, whose support, encouragement, guidance, and mentorship I will never forget. Professor Golé is one of the top experts in the HVDC transmission technology and I consider myself lucky to have had the privilege of conducting my research under his supervision.

I would like to thank Mr. Brett Davies, Dr. Ioni Fernando, and Mr. Kelvin Kent, who during the time of this thesis was prepared were part of the System Planning Department of Manitoba Hydro, for their ideas, comments, and guidance throughout my research. I appreciate their input, as it was instrumental in the success of this research.

I am also grateful to Dr. Robert Burton, a vice president at Teshmont Consultants LP and my supervisor at work, for supporting me during the creation of this thesis, for accommodating my study schedule, and for providing me with the opportunity to focus on my research even when the workload was heavy. I appreciate that Dr. Burton encouraged me to apply the results of my research in the planning of actual HVDC schemes.

I would like to thank Mr. Erwin Dirks for providing me with much needed help in using tools and resources remotely, enabling me to work on my thesis while I was away from the campus.

The financial support from Manitoba Hydro and the Natural Sciences and Engineering Research Council (NSERC) of Canada, is greatly appreciated.

I am grateful for the support from the following individuals during the progress of this thesis:

- Professor Shaahin Filizadeh from the University of Manitoba.
- Dave Fletcher, Murray Bennett, Alfred Lee, Niraj Kshatriya, Thiromi Rajapakse, Amela Basic Bilic, Jenny Zhou, Helen Zhao, Daniel Weibe, Nick Kamenev, Jun Tan, Dr. Sameh Kodsi, Dr. Vajira Pathirana, and other colleagues and staff from Teshmont Consultants LP.
- Dr. Shan Jiang, Dr. Xi Lin, Dr. Bathiya Jayasekara, Dr. Chandana Karawita, and other friends and classmates at the University of Manitoba.
- Mr. Steve Heidt, Ms. Isabel Pana, and other colleagues from the Alberta Electric System Operator (AESO).
- Family members in Iran I left behind when I came to Canada to continue my education. I highly appreciate their support of my decision and their support for me throughout my studies.

Last, but not least, I would like to show my sincere gratitude towards my wife, Ms. Fereshteh Moradzadeh, for her unwavering support, kind words, and sound advice. Her encouragement gave me the strength to carry on with my research and finish my thesis. I would also like to thank my son Kian Rahimi for his patience during the times I had to take some of my family time to work on my thesis.

## **Abstract**

This research attempts to quantify the complex interactions between HVDC transmission schemes in a multi-infeed configuration, particularly with regard to the voltage interactions and the commutation failure phenomena.

The in-depth analysis of multi-infeed HVDC systems discussed in this research shows the application of several indices such as the MIIF, MIESCR, and CFII, that can provide researchers and planning engineers in the area of HVDC transmission with the necessary tools for their system studies. It shows that these indices are applicable in a multi-infeed system comprising HVDC schemes with different ratings.

The Multi-Infeed Interaction Factor (MIIF) quantifies the level of voltage interactions between converter ac buses. The Multi-Infeed Effective Short Circuit Ratio (MIESCR) index is an indicator of ac system strengths with regard to the assessment of the transient overvoltage (TOV) and the power-voltage stability of multi-infeed HVDC systems.

The Commutation Failure Immunity Index (CFII) utilizes electromagnetic transient simulation programs to evaluate the immunity of an HVDC converter to commutation failures. The CFII takes into account the ac system strength and the HVDC controls and evaluates their impact on the commutation process. The immunity of both single-infeed and multi-infeed systems to commutation failure phenomena are accurately evaluated and quantified by the CFII.

Using the CFII, it is shown that the current commutation in multi-infeed HVDC schemes could fail under circumstances in which the probability of failure had been perceived to be low. The causes of, the effects of, and the remedial actions needed to deal with such anomalous commutation failures are discussed in this thesis.

The capability of the new indices to provide an insight into the interactions phenomena in multi-infeed systems are clearly demonstrated by examples that show their application in the analysis of an actual multi-infeed HVDC system that is in the planning phase in the province of Alberta in Canada.

# Table of Contents

<b>Acknowledgments.....</b>	<b>ii</b>
<b>Abstract.....</b>	<b>iv</b>
<b>List of Figures .....</b>	<b>x</b>
<b>List of Tables.....</b>	<b>xii</b>
<b>List of Tables.....</b>	<b>xii</b>
<b>List of Symbols.....</b>	<b>xiii</b>
<b>List of Abbreviations .....</b>	<b>xiv</b>
<b>1. Introduction .....</b>	<b>1</b>
1.1. Multi-Infeed HVDC Systems.....	1
1.2. The Challenges of Multi-Infeed HVDC Systems .....	3
1.3. Voltage Interactions in an MIHVDC System .....	4
1.4. A Historical Perspective of Research on MIHVDC Systems.....	5
1.5. The Contributions of this Thesis.....	6
1.6. Thesis Organization.....	7
<b>2. Multi-Infeed Interaction Factor (MIIF).....</b>	<b>10</b>
2.1. Introduction .....	10
2.2. Definition of the MIIF Index .....	11
2.3. Features and Properties of the MIIF Index.....	13
2.3.1. Notation for the Interaction Factor ( $MIIF_{n,m}$ ) .....	13
2.3.2. Range of the MIIF.....	13
2.3.3. The Unsymmetrical Feature of the Index ( $MIIF_{2,1} \neq MIIF_{1,2}$ ) .....	14
2.4. Calculation of the MIIF .....	14
2.4.1. Dynamic Simulation Method.....	14
2.4.2. Network Admittance Matrix Method .....	15
2.4.3. Short Circuit Current Method .....	16
2.4.4. A Sample Case Study for MIIF Calculations .....	18

2.5.	Definition of SCR and ESCR Indices.....	21
2.6.	Parametric Studies on the MIIF.....	22
2.6.1.	Impact of the AC Systems Strengths.....	22
2.6.2.	MIIF <sub>2,1</sub> Based on Fault Currents.....	23
2.7.	MIIF Values in Multi-Infeed Systems with Different Ratings .....	25
2.8.	Threshold Values of the MIIF.....	26
2.8.1.	Threshold Values of the MIIF in an MI System with Different Ratings .....	27
2.9.	MIIF in Systems with more than Two HVDC Infeeds .....	27
2.10.	Summary and Conclusions of Chapter 2 .....	27
<b>3.</b>	<b>Multi-Infeed Effective Short Circuit Ratio (MIESCR) .....</b>	<b>29</b>
3.1.	Introduction .....	29
3.2.	Application of SCR and ESCR Indices in a Single-Infeed System.....	30
3.2.1.	ESCR Value as a Measure for Performance of an AC/DC System.....	30
3.2.2.	Problems with Low ESCR Systems .....	31
3.3.	Maximum Available Power (MAP) in a Single-Infeed System .....	32
3.3.1.	Critical Effective Short Circuit Ratio (CESCR) .....	34
3.4.	Transient Overvoltage (TOV) in Single-Infeed HVDC Systems .....	35
3.4.1.	Calculation of TOV in Single-Infeed HVDC Systems .....	37
3.5.	Definition of AC System Strength in Multi-Infeed Systems .....	38
3.5.1.	ESCR for Individual Converters in Multi-Infeed Systems.....	39
3.5.2.	Multi-Infeed Short Circuit Ratio (MSCR) and Effective Short Circuit Ratio (MESCR) .....	40
3.5.3.	Multi-Infeed Effective Short Circuit Ratio (MIESCR) .....	40
3.6.	Maximum Available Power (MAP) in Multi-Infeed Systems .....	42
3.6.1.	MAP of HVDC Link "n" when all the Other Links are Off.....	42
3.6.2.	MAP of the HVDC Link "n" when all the Other DC Links are Operating at Nominal Rating .....	43
3.6.3.	MAP of HVDC link "n" when all the HVDC Links are Simultaneously Increasing their Injected Power .....	43
3.6.4.	Parametric Study of MAP in a Multi-Infeed System.....	44
3.6.5.	Summary of MAP Analysis in a Multi-Infeed System .....	46
3.7.	Transient Overvoltage (TOV) in Multi-Infeed Systems .....	46
3.7.1.	TOV of the HVDC link "n" when all the Other Links are Off.....	46
3.7.2.	TOV of the HVDC link "n" when all the Other DC Links are Operating at Nominal Rating .....	46
3.7.3.	TOV of the HVDC link "n" when all the HVDC Schemes are Simultaneously	

Blocked.....	47
3.7.4. Summary of TOV Analysis in Multi-Infeed Systems.....	49
3.8. A Sample Case Study for the MIESCR Calculations .....	49
3.9. Range and Threshold Values of the MIESCR .....	51
3.10. Summary and Conclusions of Chapter 3 .....	52
<b>4. Commutation Failure Analysis in HVDC Systems .....</b>	<b>53</b>
4.1. Introduction .....	53
4.2. Normal Operation of a Line Commutated HVDC Inverter .....	54
4.3. Commutation Failure in an HVDC Inverter .....	55
4.3.1. Single and Successive Commutation Failure Phenomena .....	56
4.3.2. Effects of Commutation Failure on AC and DC Systems .....	57
4.3.3. Recovery from a Commutation Failure .....	58
4.4. Past Approaches in the Analysis of Commutation Failure .....	59
4.4.1. Calculation of Critical Voltage Drop ( $\Delta V_{Min}$ ).....	59
4.5. Analysis of Commutation Failure Using Detailed EMT Simulations.....	62
4.5.1. Detection of a Commutation Failure.....	63
4.5.2. Probability of a Commutation Failure .....	63
4.5.3. A Per-unit System for Fault Level in CF Studies.....	66
4.5.4. Selection of the Fault Type in Commutation Failure Studies .....	67
4.6. The Commutation Failure Immunity Index (CFII).....	69
4.7. Applications of the CFII in Commutation Failure Studies.....	70
4.7.1. CFII as a Function of Effective Short Circuit Ratio (ESCR).....	71
4.7.2. Impact of Increasing the Minimum Extinction Angle ( $\gamma_{min}$ ).....	71
4.7.3. Parameters of the Inverter Extinction Angle Controller .....	72
4.7.4. Parameters of the Rectifier Current Controller .....	73
4.7.5. Impedance of the AC System at Higher Frequencies .....	74
4.7.6. Impact of the X/R Ratio of the AC System Impedance.....	76
4.7.7. Impact of Increasing the Size of the Smoothing Reactor.....	77
4.8. Impact of the HVDC Rating on Commutation Failure .....	79
4.8.1. Case-Study 1: $V_{dc} = 500$ kV, Nominal $I_{dc}$ Varies .....	80
4.8.2. Case Study 2: $I_{dc} = 2000$ A, Nominal $V_{dc}$ Varies .....	81
4.8.3. Case Study 3: Both Nominal $I_{dc}$ and $V_{dc}$ Vary but $V_{dc}/I_{dc}$ is constant.....	81
4.9. Calculation Methodology for the CFII Index .....	83
4.9.1. Conventional Multiple-Run Method .....	83

4.9.2.	Optimization-Based Method .....	85
4.9.3.	Strategically Guided Multiple-Run Method .....	86
4.10.	Summary and Conclusions of Chapter 4 .....	89
<b>5.</b>	<b>Commutation Failure in Multi-Infeed HVDC Systems.....</b>	<b>90</b>
5.1.	Introduction .....	90
5.2.	Importance of the CF Phenomenon in MIHVDC systems.....	91
5.2.1.	Local and Concurrent Commutation Failure .....	92
5.3.	Local Commutation Failure .....	93
5.3.1.	Impact of System Parameters on the Local CFII .....	94
5.4.	Concurrent Commutation Failure.....	95
5.4.1.	Anomalous Commutation Failure in MIHVDC Systems .....	96
5.4.2.	Analysis of Anomalous Concurrent CF .....	103
5.4.3.	Correlation between the MIIF and Concurrent CF .....	105
5.4.4.	Region A: $MIIF_{2,1} \leq 0.06$ .....	106
5.4.5.	Region B: $0.06 < MIIF_{2,1} \leq 0.15$ .....	107
5.4.6.	Region C: $0.15 < MIIF_{2,1} \leq 0.6$ .....	107
5.4.7.	Region D: $MIIF_{2,1} > 0.6$ .....	107
5.4.8.	An Equation to Represent the MIIF-CFII Correlation.....	108
5.5.	CF Phenomena in Multi-Infeed Systems with Different Ratings.....	109
5.6.	CF Prevention and Remedial Actions in MI Systems.....	110
5.7.	Summary and Conclusions of Chapter 5 .....	111
<b>6.</b>	<b>Conclusions and Recommendations for Future Research .....</b>	<b>113</b>
6.1.	The Main Contributions of this Thesis.....	113
6.2.	Summary of the Conclusions.....	115
6.2.1.	MIIF Calculation Methods, Range, and Critical Values.....	115
6.2.2.	MIESCR Definition and Application in Multi-infeed Systems.....	116
6.2.3.	Commutation Failure in Single-Infeed Systems .....	117
6.2.4.	Commutation Failure in Multi-Infeed Systems.....	117
6.3.	Thesis Publications.....	118
6.3.1.	Technical Brochure (CIGRÉ publication).....	118
6.3.2.	Journal Paper .....	119
6.3.3.	Conference Papers.....	119
6.4.	Recommended Future Research.....	120
6.4.1.	Application of the Indices in Cases in which HVDC Links are in Parallel with	



AC Lines .....	120
6.4.2. Analysis of Multi-Infeed Schemes in which the Inverter and Rectifier of Independent Schemes are Connected to the same AC Network.....	121
6.4.3. Further Study to Evaluate the Impact of other HVDC Transmission Technologies on the Application of the Indices and the Validity of the Recommendations .....	122
6.4.4. Analytical Proof for the Value of Critical MIESCR (CMIESCR) for a General Case with n HVDC Infeeds.....	122
<b>References .....</b>	<b>124</b>
<b>Appendix A - HVDC Test System Data.....</b>	<b>129</b>
<b>Appendix B – Derivation of the MIIF Formula .....</b>	<b>131</b>
<b>Appendix C –TOV Formula in Single-Infeed Systems.....</b>	<b>134</b>
<b>Appendix D –TOV Formula in Multi-Infeed Systems .....</b>	<b>137</b>

## List of Figures

Figure 2-1: Multi-infeed HVDC test system .....	11
Figure 2-2: An example of dynamic voltage responses for calculation of MIIF <sub>2,1</sub> .....	12
Figure 2-3: MIIF calculation using the Y-Matrix .....	16
Figure 2-4: MIIF calculation using the Short Circuit Current Method.....	17
Figure 2-5: Approximate locations of the HVDC converters in southern Alberta .....	18
Figure 2-6: Dynamic simulation results for MIIF calculations .....	19
Figure 2-7: Schematic diagram of a single-infeed HVDC system .....	21
Figure 2-8: MIIF as a function of ac system strengths for a given tie-line length .....	23
Figure 2-9: MIIF <sub>2,1</sub> as a function of fault currents .....	24
Figure 3-1: Schematic diagram of a single-infeed HVDC system .....	30
Figure 3-2: Variation of terminal voltage and dc power with dc current .....	33
Figure 3-3: Schematic diagram of a single-infeed HVDC system .....	36
Figure 3-4: Magnitude of overvoltages at the inverter caused by blocking the HVDC .....	37
Figure 3-5: A system with two HVDC infeeds .....	39
Figure 3-6: Approximate locations of the HVDC converters in southern Alberta .....	50
Figure 4-1: Current commutation from valve 1 to valve 3 .....	55
Figure 4-2: Bridge voltage in a single commutation failure .....	57
Figure 4-3: Bridge voltage in a double commutation failure.....	57
Figure 4-4: Causing commutation failure in a single-infeed system .....	61
Figure 4-5: Effect of inductive fault on current and voltage (Fault level is 10% of the dc power)	62
Figure 4-6 : Dependence of CF occurrence on fault level (inductance) and point on wave.....	65
Figure 4-7 : Probability of a commutation failure for the CIGRÉ benchmark model .....	66
Figure 4-8: Threshold fault levels for three- and single-phase inductive, capacitive, and resistive faults .....	68
Figure 4-9: Commutation failure probability curve for the CIGRÉ Benchmark model. ....	70

Figure 4-10: Impact of the ESCR on the CFII.....	71
Figure 4-11: Impact of $\gamma$ on the reactive power and the CFII .....	72
Figure 4-12: Impact of inverter PI controller gains on the CFII.....	73
Figure 4-13: Impact of rectifier PI controller gains on the CFII .....	74
Figure 4-14: Source impedance ( $Z_s$ ), (a) original CIGRÉ model, (b) Series RL model.....	75
Figure 4-15: Comparison between the magnitude and the phase of the source impedance models.....	75
Figure 4-16: Schematic diagram of the inverter side.....	77
Figure 4-17: Impact of the X/R ratio on CFII .....	77
Figure 4-18: Impact of dc side inductance on the CFII.....	79
Figure 4-19: The CFII for systems with different ratings ( $V_{dc}=500$ kV, $200A < I_{dc} < 4000$ A ) ...	80
Figure 4-20: The CFII for systems with different ratings ( $I_{dc}=2000$ A, $50kV < V_{dc} < 1000$ kV )....	81
Figure 4-21: CFII for varying $I_{dc}$ and $V_{dc}$ ( $200$ A $< I_{dc} < 4000$ A, $50$ kV $< V_{dc} < 1000$ kV ) ....	82
Figure 4-22: Part of the grid of inductance and point on wave .....	84
Figure 4-23: Routine to find the $L_{min}$ with the desired accuracy.....	88
Figure 4-24: Part of PSCAD/EMTDC case for finding the $L_{min}$ .....	89
Figure 5-1: Multi-infeed HVDC test system .....	92
Figure 5-2: Probability of a commutation failure as a function of fault level .....	96
Figure 5-3: Test system for Case 1 .....	97
Figure 5-4: CF probability curve for Case 1 (Converter 1 is disconnected form the network) .....	98
Figure 5-5: Multi-infeed test system for Case 2 .....	99
Figure 5-6: Local and concurrent commutation failure probability curve for Case 2.....	100
Figure 5-7: Multi-infeed test system for Case 3 .....	102
Figure 5-8: Results for Case 3 (Converter 1 continues to operate regardless of CF1). .....	102
Figure 5-9: Commutating voltage of the off-going valve .....	103
Figure 5-10: Comparison of the voltage harmonics at low and high fault levels.....	104
Figure 5-11: Correlation between MIIF <sub>2,1</sub> and CF-causing ac faults .....	106
Figure 5-12: Impact of system ratings on concurrent commutation failure.....	110

List of Tables

Table 2.1: Interaction Factors between the Langdon and Brooks 240 kV buses.....	19
Table 2.2: MIIF Calculations Using Fault Currents .....	20
Table 2.3: Impact of System Ratings on MIIF .....	25
Table 2.4: Systems with extreme values of MIIF .....	27
Table 3.1: Critical MIESCR Values for a System with Two DC Infeeds.....	44
Table 3.2: MIESCR Values for Several Systems with Two DC Infeeds. System 1 is at the Point of PV Instability .....	45
Table 3.3: MIESCR Values for Several Systems with Three DC Infeeds. System 1 is at the Point of PV Instability .....	45
Table 3.4: TOV at the ac bus following its converter block in an MI system .....	47
Table 3.5: Comparison of TOV in single- and multi-infeed systems .....	48
Table 3.6: An Example of TOV and MIESCR Calculation in a Multi-infeed System .....	50
Table 4.1: Common Faults in AC Systems.....	67
Table 4.2: Parameters of the Gamma Controller at the Inverter.....	73
Table 4.3: Parameters of the Current Controller at the Rectifier.....	74
Table 4.4: Comparison between Various Source Models.....	76
Table 4.5: Impact of DC Voltage and Current on the CFII .....	82
Table 4.6: Details of the Example for Conventional Multiple-Run Methods .....	84
Table 4.7: Results of $L_{\min}$ Calculations using Guided Multiple-Run Methods .....	87
Table 5.1: Impact of System Parameters on the Local CFII .....	94

## List of Symbols

$I_f$	Fault Current
$Q_f$	Reactive Power Generated by Filter
$P_{dc}$	Rating of the HVDC Link
$Q_{dc}$	Reactive Power Consumed by a DC Converter
$\mu$	Overlap Angle
$\gamma$	Extinction Angle
$\alpha$	Valve firing angle
$X/R$	Ratio of the Inductance to the Resistance of an Impedance

## List of Abbreviations

CC	Constant Current
CEA	Constant Extinction Angle
CESCR	Critical Effective Short Circuit Ratio
CF	Commutation Failure
CFII	Commutation Failure Immunity Index
CIGRÉ	Conseil International des Grands Réseaux Électriques (International Council on Large Electric Systems)
CMIESCR	Critical Multi-Infeed Effective Short Circuit Ratio
EMT	Electromagnetic Transient
ESCR	Effective Short Circuit Ratio
FACTS	Flexible AC Transmission Systems
GA	Genetic Algorithm
HVDC	High Voltage Direct Current
MAP	Maximum Available Power
MESCR	Multi-Infeed Effective Short Circuit Ratio
MI	Multi-Infeed
MIESCR	Multi-Infeed Effective Short Circuit Ratio
MIHVDC	Multi-Infeed High Voltage Direct Current
MIIF	Multi-Infeed Interaction Factor
MISCR	Multi-Infeed Short Circuit Ratio
MPC	Maximum Power Curve
MR	Multiple Run
MSCR	Multiinfeed Short Circuit Ratio
PBR	Power Base Ratio
PI	Proportional-Integral
pu	Per-Unit
SC MVA	Short Circuit MVA
SCC	Short Circuit Capacity (Current)
SCL	Short Circuit Level
SCR	Short Circuit Ratio
TOV	Transient Overvoltage
VDCOL	Voltage Dependent Current Order Limit

## **1. Introduction**

The definition, application, and significance of multi-infeed HVDC (MIHVDC) systems are discussed in this chapter. The challenges to researchers and system planners in the analysis of MIHVDC systems are presented. The results of earlier research in this area and their recommendations to address the challenges are discussed. The objectives and the contributions of this thesis to this area are briefly discussed in this chapter.

New performance-indicative indices that could be used to predict the behaviour of an MIHVDC system with regard to different interaction phenomena are investigated. These indices would provide a valuable tool in the analysis and design of MIHVDC systems and will be discussed in detail in subsequent chapters.

### **1.1. Multi-Infeed HVDC Systems**

The first commercial high voltage direct current (HVDC) transmission system was commissioned in March 1954 [1]. Since then, HVDC transmission technology

has been chosen for electric power transmission in cases in which it has shown significant economical and technical advantages over ac transmission technology [2], [3].

Historically, HVDC transmission has been mainly used to do the following [4]-[5]:

- a) Transfer power over a very long distance (hundreds of kilometres)
- b) Interconnect asynchronous systems or networks with different frequencies
- c) Transmit power under large bodies of water using submarine cables

In recent years, the spread of deregulated electricity markets around the world, network security and reliability considerations, and power flow control requirements are triggering the use of HVDC technology rather than ac transmission and interconnection [3].

The demand for electricity in the developing world is rapidly increasing. In many cases, for example, in countries such as India and China, there is a significant distance between the generating plants and the load centres [6], a situation in which HVDC transmission has shown performance superior to that of ac transmission [5].

The aging infrastructure in the industrialized world and the increasing demand for renewable energy sources require a very reliable transmission system that maximizes the efficient usage of rights of way and provides greater control over power flow than ac transmission can provide. For such situations dc transmission technology has a proven advantage over ac transmission technology [7]-[8].



Because the number of HVDC transmission schemes in the world is rapidly increasing, it is becoming more common that several HVDC systems are connected to the same ac network within close electrical proximity [9]-[11]. Such a system configuration is referred to as a multi-infeed HVDC system (MIHVDC system) [12].

## **1.2. The Challenges of Multi-Infeed HVDC Systems**

For many years after the initial development of HVDC transmission technology HVDC schemes were relatively few in number, and the possible adverse interactions between adjacent HVDC systems were rarely a concern [3].

Prior to the introduction of MIHVDC systems, the focus of researchers, system planners, manufacturers, and others involved in dc transmission was the evaluation of the performance of the particular HVDC scheme under study and the determination of how it interacts with the ac system. Most of the literature, standards, industry norms, performance-indicating indices, and other guidelines were developed to give insight into the analysis and planning of a single HVDC scheme delivering power to an ac network (a single-infeed HVDC system).

The major challenges in the analysis and planning of MIHVDC systems are the lack of knowledge, experience, and tools for predicting possible interactions between dc converters and for predicting overall system performance under normal and contingency conditions. As shown in this thesis, a critical error would be to assume that the standards, norms, and indices that have been developed for single-infeed HVDC systems are applicable to MIHVDC systems.

Several interaction phenomena are investigated in this thesis, with voltage-related interactions being examined in detail.

### **1.3. Voltage Interactions in an MIHVDC System**

Proper operation of an HVDC converter, especially an inverter, largely depends on the quality of the ac voltage on the ac side of the converter [5]. Commutation failure (CF) is a severe dynamic event in an HVDC transmission system and its main cause is a sudden ac voltage drop (voltage dip) due to an ac fault [13]. During commutation failure, the dc voltage and power temporarily drop to zero [5]. For relatively weak ac systems at either side of the dc scheme, such an interruption of power (load rejection) can result in high overvoltages, component failure, and cascading outages of system elements. In severe cases it may result in power-voltage instability [13].

As the strength of the ac system increases, the likelihood of a sudden voltage drop decreases and, therefore, the rate of occurrence of commutation failure decreases. If a commutation failure occurs in a dc converter connected to a strong ac system, it generally has a smaller impact on the system as compared to a commutation failure that occurs in a dc converter connected to a weak ac system.

The effective short circuit ratio (ESCR) is a widely-used index in the assessment of the strength of an ac system [14]. Systems with high ESCR values are easier to control and experience fewer voltage fluctuations following a dynamic event such as commutation failure. However, systems with low ESCR

values may show poor performance that result in voltage instability and power curtailment.

Consequences of commutation failure could be more serious in multi-infeed systems than in single-infeed systems [15]. In an MIHVDC system, the commutation failure of one converter may cause a large enough disturbance of the ac voltage to precipitate a failure of commutation for another nearby converter and could even lead to system instability and blackouts.

#### **1.4. A Historical Perspective of Research on MIHVDC Systems**

An interesting pioneering reference is a paper titled “Aspects of Multiple Infeed of HVDC Inverter Stations into a Common AC System”, written in 1973 [16]. It investigates power frequency and harmonic issues in multi-infeed systems. The paper attempts to determine the amount of dc power an ac system can take and maintain satisfactory performance in a multi-infeed configuration. It also discusses the influence of ac system short circuit capacity (SCR) at inverter stations. One unresolved issue raised by the discussions that followed the paper is commutation failures at nearby inverter stations triggered by voltage distortion from a commutation failure in one station. This issue is discussed and addressed in this thesis.

An EPRI research project report titled “DC Multiinfeed Study” was published in 1995. A summary of the study was published in an IEEE paper [17]. The study was based on a realistic multi-infeed dc system and its focus was the control

interactions between HVDC schemes and how the HVDC controls could be coordinated to provide damping to the integrated ac/dc system [3].

“Coordination of Controls of Multiple FACTS/HVDC Links in the Same System,” published in 1999, was written by CIGRÉ Working Group 14.29. It investigates several control interactions and suggests that the end result of any undesired interaction between dc links will be to limit the transfer capability of the transmission system, a condition that is not acceptable in today’s systems when so much effort is being applied to utilize existing transmission systems to their fullest extent [3].

“Commutation failures in HVDC transmission systems,” was published by IEEE in 1996 [18]. The paper provides, for the first time, formulas for the calculation of the three-phase and single-phase ac voltage drops that will cause a commutation failure in the inverter. Although it uses quasi-steady-state equations in modeling the system, it still provides a good understanding of the commutation failure phenomena and the parameters that affect it. This thesis expands on this work and analyzes the commutation failure phenomena in single- and multi-infeed HVDC systems using more accurate modeling of the system.

### **1.5. The Contributions of this Thesis**

This thesis expands on the key elements mentioned in the previous section (Section 1.4). The authors of the papers mentioned earlier recognized the need for a multi-dimensional measure of interaction potential, somewhat analogous to the

concept of short circuit ratio (SCR) but applied to multiple inverters. This thesis investigates such an index: the multi infeed effective short circuit ratio (MIESCR). The author would like to acknowledge one of the members of his thesis advisory committee, Dr. Ioni Fernando, system planning department of Manitoba Hydro, who originally proposed this index. It indicates the ac system strength in a multi-infeed configuration using an intermediate index called the multi-infeed interaction factor (MIIF). The MIIF index [28] was originally proposed by the author's supervisor at Manitoba Hydro, Mr. J. Brett Davies and his team. Application of the MIESCR index in power-voltage stability and transient overvoltage calculations are presented in this thesis.

The commutation failure immunity index (CFII) is a new index proposed in this thesis. It quantifies the phenomena of commutation failure for a single-infeed system. The local commutation failure and concurrent commutation failure phenomena are introduced in this thesis. A local commutation failure occurs when an ac fault causes a commutation failure only on the nearby converter. A concurrent commutation failure occurs when there are failures of current commutation in local and remote converters following an ac fault. This thesis reveals, for the first time, the possibility of anomalous commutation failure in MIHVDC systems where commutation failure probability unexpectedly increases for less-severe faults [19].

### **1.6. Thesis Organization**

Chapter 1 (this chapter) provides an introduction to the thesis.

Chapter 2 introduces the multi-infeed interaction factor (MIIF) index that quantifies the voltage interactions between HVDC converters in a multi-infeed (MI) configuration. Several MIIF calculation methods are discussed and formulas for calculation of approximate MIIF are introduced. The approximate formulas are required to do parametric studies on MIIF for a wide range of ac and dc system parameters. Using such parametric studies, the sensitivity of MIIF to ac and dc system parameters is evaluated.

Chapter 3 reviews the power transfer capability of an HVDC scheme and its dependence on the ac system strength. In single-infeed systems, ESCR is a critical parameter in the calculation of the maximum available power (MAP). An analogous index, the MIESCR is proposed in this thesis to provide a similar indication of system performance in the multi-infeed context. A comparison between MIESCR and other similar indices is made as well.

Chapter 4 deals with the commutation failure phenomena in a single-infeed HVDC system and introduces the commutation failure immunity index (CFII). The methodology to calculate the CFII index using an electromagnetic transients simulation is discussed. The results of a parametric study on CFII that shows the impact of several factors such as the minimum extinction angle, the controller parameters, and the characteristics of the ac source impedance are presented.

Chapter 5 focuses on the commutation failure performance of multi-infeed HVDC systems. The local and concurrent commutation failure phenomena are introduced and examined for a range of system configurations with different system strengths. The research carried out in the course of this thesis showed

that multi-infeed HVDC systems sometimes show anomalous concurrent commutation failure behaviour where probability of commutation failure decreases by increasing the fault level. An explanation for this anomalous behaviour is provided.

Chapter 6 provides conclusions and directions for future research.

## **2. Multi-Infeed Interaction Factor (MIIF)**

### **2.1. Introduction**

The use of HVDC transmission is increasing, and it is becoming more common to have two or more dc converters from different transmission systems located in close mutual proximity [3]. It is likely that inter-converter interactions between dc converters will have a major impact on the performance of the dc converters in a multi-infeed configuration. The performance of a dc converter is largely dependent on the quality of the ac voltage at its terminal. HVDC converters connected to strong ac systems experience less voltage fluctuations under normal and contingency operating conditions than HVDC converters connected to weak ac systems, and have proven to be less problematic [14].

The multi-infeed interaction factor (MIIF) quantifies the level of voltage interactions between the commutating buses of the multi-infeed HVDC converters [3]. The definition and calculation methods for MIIF are described in



this chapter and the results of a parametric study to assess the impact of the ac system strengths on the MIIF are presented.

## 2.2. Definition of the MIIF Index

Figure 2-1 shows the schematic diagram of a multi-infeed system with two dc infeeds. The various impedances ( $Z_{S1}$ ,  $Z_{S2}$ ,  $Z_{tie}$ ), impedance angles ( $\phi_1$ ,  $\phi_2$ , and  $\phi_{tie}$ ), ac Thévenin voltages ( $E_1$  and  $E_2$ ), converter dc currents ( $I_{d1}$  and  $I_{d2}$ ), converter transformer impedances ( $X_{C1}$  and  $X_{C2}$ ), and extinction angles ( $\gamma_1$  and  $\gamma_2$ ) are indicated.

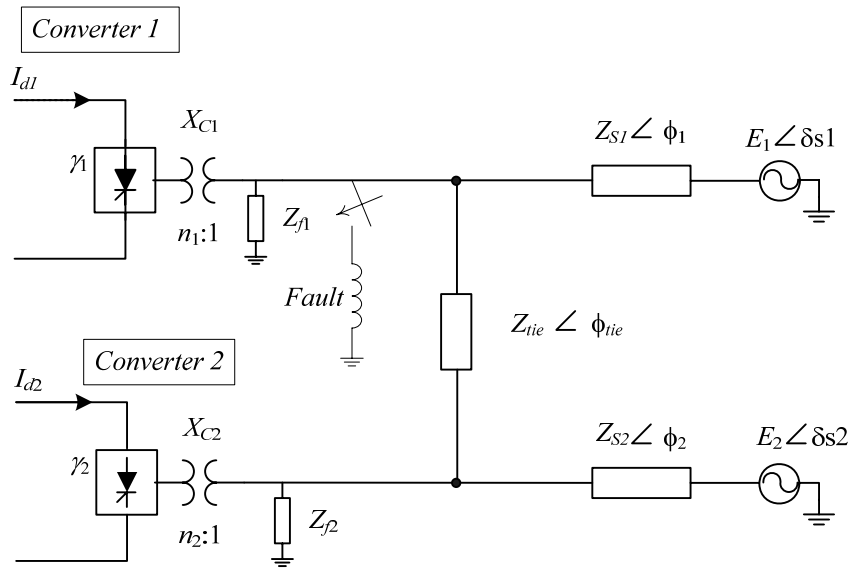


**Figure 2-1: Multi-infeed HVDC test system**

Equation (2-1) is the definition of MIIF [3], which is basically the ratio of the incremental voltage drops on bus 2 and bus 1 due to a fault at bus 1.

$$MIIF_{2,1} = \frac{\partial V_2}{\partial V_1} \equiv \frac{\Delta V_2 \%}{1\% \text{ voltage change in } V_1} \quad (2-1)$$

For practical reasons the voltage drop  $V_1$  should be small enough to prevent the system from showing non-linear characteristics; however,  $\Delta V_1$  should be large enough to have noise immunity. A value of  $\Delta V=1\%$  is recommended in [3].

For an arbitrary system, Figure 2-2 shows the time response of the voltages at bus 1 and bus 2 for an inductive fault at bus 1. An appropriately sized three-phase balanced inductor is switched on bus 1 to create a voltage drop of 1% on bus 1 and the resulting voltage drop on bus 2 shows the MIIF.

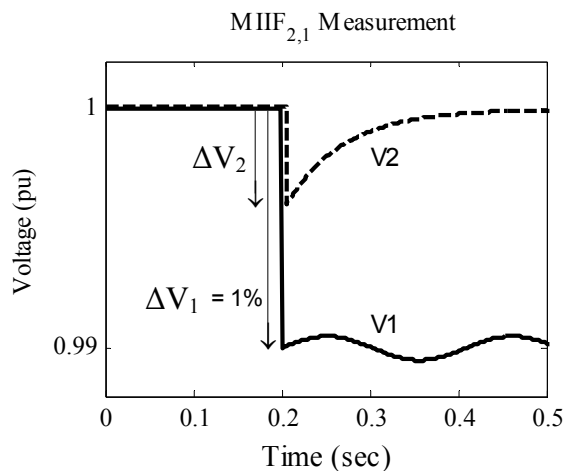


**Figure 2-2: An example of dynamic voltage responses for calculation of  $MIIF_{2,1}$**

To exclude the response of the system controls on the MIIF index, the voltage drop values ( $\Delta V_1$  and  $\Delta V_2$ ) are measured immediately after application of the fault (i.e., at  $t_{\text{fault}^+}$ ) [3].

When using power system simulation programs such as PSS/E, dynamic simulation can be used to measure the  $\Delta V_1$  and  $\Delta V_2$  at  $t_{\text{fault}^+}$  after the application of the inductive fault. As shown in Figure 2-2, due to different control actions the

magnitude of the ac voltages at bus 1 and bus 2 may vary differently after the application of the fault.

Although the above definition is given for a system with two dc infeeds, it can be generalized to systems with several infeeds. In such cases, the MIIF value from bus  $m$  to bus  $n$  ( $MIIF_{n,m}$ ) is calculated by dynamic simulation of the system following the connection of an inductor from bus  $m$  to the ground to cause a 1% drop, and then recording  $\Delta V_n$  [3], [12]. In that case:

$$MIIF_{n,m} = \frac{\Delta V_n}{\Delta V_m (=1\%)} \quad (2-2)$$

### 2.3. Features and Properties of the MIIF Index

#### 2.3.1. Notation for the Interaction Factor ( $MIIF_{n,m}$ )

In the calculation of  $MIIF_{n,m}$ , the inductive ac fault that causes a 1% drop is applied at converter “ $m$ ” and the voltage drop is measured at converter “ $n$ ”.

#### 2.3.2. Range of the MIIF

From the definition of the MIIF, it is clear that if two ac buses are infinitely far apart, then  $MIIF = 0.0$ , and if two inverters are connected to the same ac bus, then  $MIIF = 1.0$ .

### 2.3.3. The Unsymmetrical Feature of the Index ( $MIIF_{2,1} \neq MIIF_{1,2}$ )

In general,  $MIIF_{2,1} \neq MIIF_{1,2}$ . This feature will be proved in Section 2.4.2. Qualitatively, the MIIF from a weak ac system to a strong ac system would be low, while the MIIF from a strong system to a weak system would be high. This is because a 1% drop on a converter bus in a weak ac system will not cause a substantial voltage drop for another converter bus in a nearby strong system. Therefore,  $MIIF_{\text{strong system}, \text{weak system}}$  would be low. On the other hand, a voltage drop in a strong system brings the voltage down in neighbouring weak systems, and therefore  $MIIF_{\text{weak system}, \text{strong system}}$  would be high.

## 2.4. Calculation of the MIIF

Three methods for the calculation of the MIIF are given in this section:

- The dynamic simulation method
- The network admittance matrix method
- The short-circuit current method

### 2.4.1. Dynamic Simulation Method

In the dynamic simulation method, the system is modelled in a dynamic stability program such as PSS/E. A three-phase balance fault through a reactance is simulated at converter 1. The inductor is appropriately sized (usually through trial and error) to cause a 1% voltage drop at the converter 1 commutating bus. The voltage drop at the ac bus of converter 2 is measured.  $MIIF_{2,1}$  is then calculated using Equation (2-1). As Figure 2-2 shows, both voltage drop

measurements are carried out immediately after application of the fault (i.e., at  $t = t_{\text{fault}+}$ ).

This method gives an accurate value for the MIIF. However, planning studies are normally carried out at an early stage of a project, where the dynamic model of the system may not be available. The following simplified methods do not use dynamic simulation, and therefore the resulting MIIF may differ slightly from the standard definition of MIIF. The reason for that is that in the dynamic simulation method the full responses of system components, including the load models and the response of the fast acting elements, are taken into account whereas in simplified methods dynamic characteristics are ignored.

### 2.4.2. Network Admittance Matrix Method

In this approach, the impact of switching the inductor at bus  $m$  is represented as a small current source of  $\Delta I_m$  injected into bus  $m$ . Assuming that the superposition theorem is applicable, other sources in the system are set to zero and the system is reduced to a passive network of impedances ( $Y$  matrix). The resulting system is given in Figure 2-3. Equation (2-3) shows that the MIIF is readily calculated as the ratio of two entries in the impedance matrix  $Z$  (the inverse of the  $Y$  matrix).

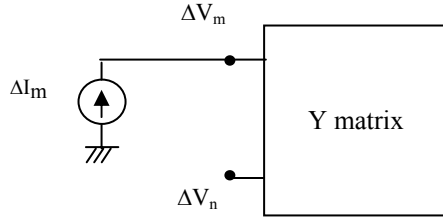


**Figure 2-3: MIIF calculation using the Y-Matrix**

$$Y \times \Delta V = \begin{bmatrix} 0 \\ \vdots \\ \Delta I_m \\ \vdots \\ 0 \end{bmatrix} \quad \begin{matrix} \Delta V_m = Z_{m,m} \times \Delta I_m \\ \Delta V_n = Z_{m,n} \times \Delta I_m \end{matrix} \quad \text{where} \quad Z = Y^{-1} \quad MIIF_{n,m} = \frac{\Delta V_n}{\Delta V_m} = \frac{Z_{m,n}}{Z_{m,m}} \quad (2-3)$$

As discussed earlier, due to the simplifying assumptions made in the Y matrix approach, the MIIF values calculated using this method are an approximation of the actual MIIF values. There is no need for dynamic simulation in this method, and all the MIIF values can be calculated from the inverse of the Y matrix. However, for large systems, inverting the Y matrix may require a large number of computations.

### 2.4.3. Short Circuit Current Method

The short circuit current method developed in this thesis provides an alternative to the dynamic simulation and network admittance matrix methods. The basic idea in this method is to utilize a standard power system analysis tool such as PSS/E to calculate the parameters of the two-port equivalent network for the entire ac system as seen from the ac terminals of the HVDC converters. Figure 2-4 shows the two-port equivalent network and the ac terminals of the HVDC converters for a two-infeed HVDC system.

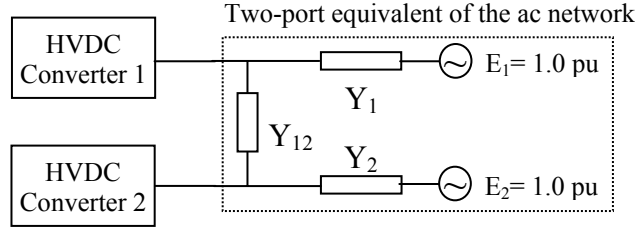


**Figure 2-4: MIIF calculation using the Short Circuit Current Method**

Assuming that the ac voltage is 1.0 pu and the impedances of the two-port network are purely inductive (no resistive component), Equation (2-4) can be used to calculate the value of  $MIIF_{2,1}$ . Derivation of the Equation is given in Appendix B.

$$MIIF_{2,1} = If_1 - \sqrt{\frac{If_1}{If_2} \cdot (1 - If_1) \cdot (1 - If_2)}$$

In which:

$If_1$  : Fault current at bus 1 in per unit of  $If_{1\&2}$

$If_2$  : Fault current at bus 2 in per unit of  $If_{1\&2}$

$If_{1\&2}$  : Fault current for simultaneous faults at bus 1 and bus 2

(2-4)

It should be noted that  $If_{1\&2}$  is not the sum of  $If_1$  and  $If_2$ .

To calculate the MIIF by using fault currents, three fault current calculations should be done using an ac fault current analysis program such as PSS/E:

- Three-phase fault current at bus 1 ( $If_1$ )
- Three-phase fault current at bus 2 ( $If_2$ )
- Total three-phase fault current for simultaneous faults at bus 1 and bus 2 ( $If_{1\&2}$ )

After these three measurements, the per-unitized values of  $If_1$  and  $If_2$  based on  $If_{1\&2}$  should be substituted in Equation (2-4) to calculate  $MIIF_{2,1}$ . The reciprocal  $MIIF_{1,2}$  can be obtained in a similar manner.

A case study for the MIIF calculations is discussed in the following section.

#### 2.4.4. A Sample Case Study for MIIF Calculations

To provide a practical example of MIIF calculation, the multi-infeed HVDC system in the province of Alberta, Canada is considered. Figure 2-5 shows the possible converter locations for a multi-infeed HVDC system being planned for the province.

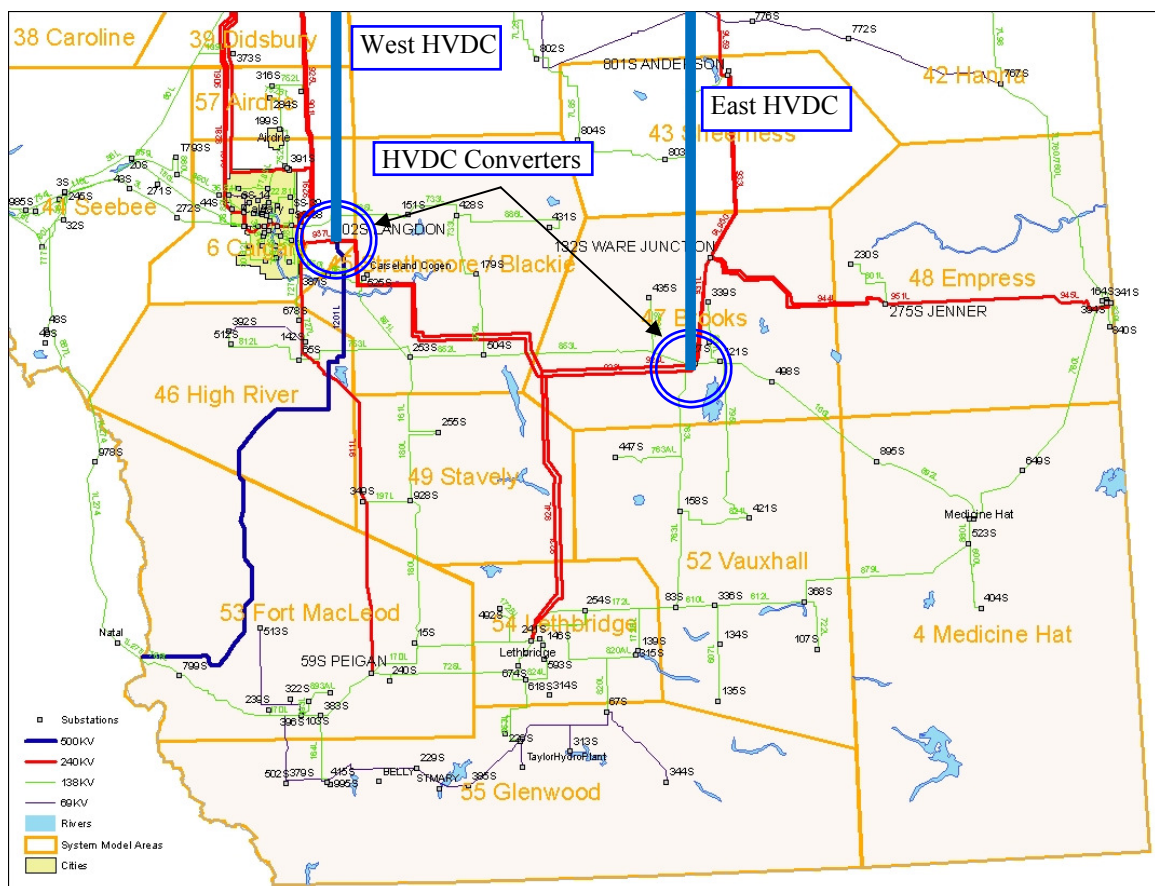


**Figure 2-5: Approximate locations of the HVDC converters in southern Alberta**

The figure and system data were obtained from the Alberta Electric System Operator (the AESO) website. As shown in Figure 2-5, one of the converters will



be located close to Langdon and one will be located close to Brooks. Langdon and Brooks are approximately 140 km apart.

The MIIF values between the 240 kV buses at Langdon and Brooks are calculated using the load flow and dynamic data of the system. Figure 2-6 shows the dynamic responses of the voltages at the Langdon and Brooks 240 kV buses for a 1% drop at either Langdon or Brooks. The MIIF values from Langdon to Brooks and from Brooks to Langdon are calculated using the plots in Figure 2-6 and the results are given in Table 2.1.

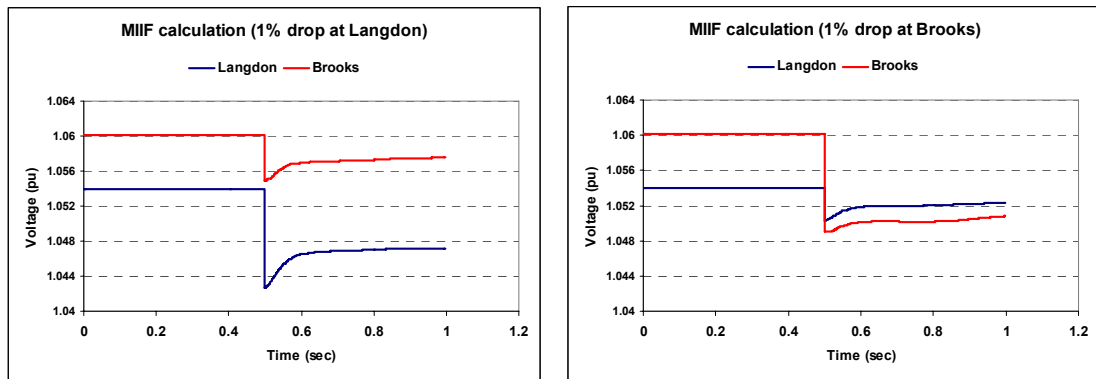


**Figure 2-6: Dynamic simulation results for MIIF calculations**

Table 2.1 shows that the MIIF from Langdon to Brooks is higher than the MIIF from Brooks to Langdon.

**Table 2.1: Interaction Factors between the Langdon and Brooks 240 kV buses**

Fault At bus	Langdon	Brooks
Inductive Fault MVA	60	42
Pre-fault voltage at Langdon (pu)	1.0540	1.0540
Post-fault voltage at Langdon (pu)	1.0435	1.0507
Pre-fault voltage at Brooks (pu)	1.0601	1.0601
Post-fault voltage at Brooks (pu)	1.0556	1.0495
<b>MIIF<sub>Brooks, Langdon</sub></b>	<b>0.456</b>	-
<b>MIIF<sub>Langdon, Brooks</sub></b>	-	<b>0.330</b>

This is also clear from the MVA of the fault required to cause a 1% drop at the ac buses. A higher fault MVA is required at Langdon to cause a 1% voltage drop. Therefore, the ac system at Langdon is stronger than the ac system at Brooks.

To verify the validity of utilizing an approximate calculation of the MIIF using Equation (2-1), the fault currents at Langdon and Brooks and the MIIF values are calculated and given in Table 2.2.

**Table 2.2: MIIF Calculations Using Fault Currents**

Three-phase fault current at Langdon	15.45 kA	= 0.7707 pu
Three-phase fault current at Brooks	11.29 kA	= 0.5632 pu
Simultaneous fault at Langdon and Brooks	20.05 kA	= 1.0000 pu
<b>MIIF</b> Brooks, Langdon	<b>0.400</b>	
<b>MIIF</b> Langdon, Brooks	<b>0.293</b>	

A comparison of the results of the dynamic simulation and short circuit current methods shows that the simplifying assumptions in fault current calculation cause approximately a 12% error in the MIIF value. Since the MIIF is meant to provide a general insight in the planning of multi-infeed systems it is acceptable at the initial study phase to use the fault current method, which is faster, and therefore makes parametric studies and sensitivity studies practical. As the study progresses and a dynamic model of the system becomes available, the dynamic simulation method should be used for the MIIF calculation. At the final stages of the studies every phenomena should be studied in detail using the appropriate tools.

## 2.5. Definition of SCR and ESCR Indices

One of the widely-used parameters in the analysis of HVDC systems is the short circuit ratio (SCR); another is the closely related index called the effective short circuit ratio (ESCR) [4], [5], [14]. A schematic diagram of the inverter side of an HVDC link is shown in Figure 2-7.

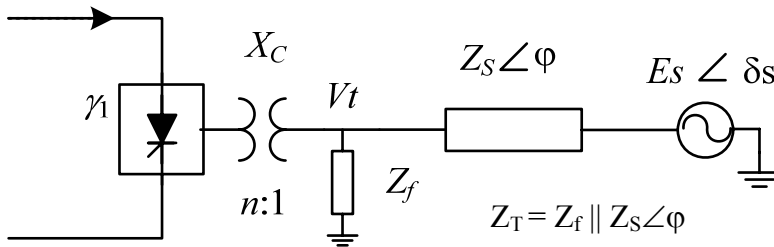


**Figure 2-7: Schematic diagram of a single-infeed HVDC system**

The definition of SCR and ESCR are given in the following formulas [14]:

$$\text{SCR} = \frac{\text{SC MVA (Short Circuit MVA of the ac system at the convert ac bus)}}{\text{Pdc (MW rating of the HVDC converter)}} \quad (2-5)$$

In which:

$$\text{SC MVA} = \frac{V_t^2}{Z_s}$$

As per the definition of the SCR, the impedance of the filters at the ac terminal of the converter ( $Z_f$ ) is not considered in the SCR definition. However,  $Z_f$  does affect the Thévenin impedance as seen from the converter bus looking into the ac network ( $Z_T = Z_s \angle \varphi \parallel Z_f$ ).  $Z_T$  plays an important role in the operation of the HVDC converter, especially during the recovery from faults.

The effective short circuit ratio (ESCR) is essentially the SCR calculated with  $Z_s$  replaced by the Thévenin impedance  $Z_T$  at the fundamental frequency taking into account the filter impedance. As the filter impedance is purely capacitive and the network impedance is almost purely inductive, Equation (2-6) gives the definition of ESCR.

$$\text{ESCR} \approx \frac{\left| \frac{V_t^2}{Z_T} \right|}{P_{dc}} \approx \frac{V_t^2 \cdot (Y_s - Y_f)}{P_{dc}} = \frac{\text{SC MVA} - Q_f}{P_{dc}} \quad (2-6)$$

## 2.6. Parametric Studies on the MIIF

The results of several parametric studies of the MIIF are given in this section.

### 2.6.1. Impact of the AC Systems Strengths

Figure 2-8 shows the variation of  $\text{MIIF}_{2,1}$  for a given tie-line length ( $Z_{\text{tie}}$  in Figure 2-1) with the strength of the ac systems ( $\text{ESCR}_1$  and  $\text{ESCR}_2$ ) seen at the ac terminal of the corresponding HVDC converters. It shows that  $\text{ESCR}_1$  has a very marginal impact on  $\text{MIIF}_{2,1}$ , while  $\text{ESCR}_2$  has a strong impact on  $\text{MIIF}_{2,1}$ .

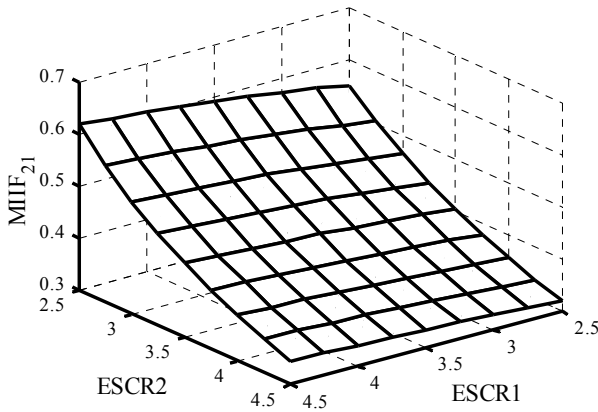


**Figure 2-8: MIIF as a function of ac system strengths for a given tie-line length**

The reason for this type of correlation between  $MIIF_{2,1}$ ,  $ESCR_1$ , and  $ESCR_2$  is as follows: As per the definition of  $MIIF_{2,1}$ , the ac fault is applied on bus 1 to cause a 1% voltage drop on bus 1. The stronger the ac system at converter 1 (higher  $ESCR_1$ ), the higher the fault level required to cause a 1% voltage drop should be. However, the corresponding voltage drop that appears on the remote bus (bus 2), highly depends on the strength of the remote system ( $ESCR_2$ ) [20].

In Figure 2-8 the correlation between ESCRs and MIIF is clearly visible. Note that the plots in Figure 2-8 are valid only for a given tie-line length. For example, Figure 2-8 suggests that for  $ESCR_1 = 2$  and  $ESCR_2 = 3$ ,  $MIIF_{2,1} = 0.45$ . However, this is correct only for a given system configuration. Theoretically, there are infinite system configurations with varying MIIF values that could result in  $ESCR_1 = 2$  and  $ESCR_2 = 3$ . This issue is addressed in the following section.

### 2.6.2. $MIIF_{2,1}$ Based on Fault Currents

From Equation (2-4) in Section 2.4.3, the MIIF value can be calculated using the fault currents at the converter ac buses. The family of plots shown in

Figure 2-9 help to determine the MIIF values based on the measured fault currents. For any given system configuration, after calculating the fault currents the plots in Figure 2-9 can be utilized to calculate the MIIF index. This is an easy, practical way to calculate MIIF.

There is no clear indication of the correlation between the ac system strengths and MIIF value in Figure 2-9. However, stronger ac systems always result in higher fault currents.

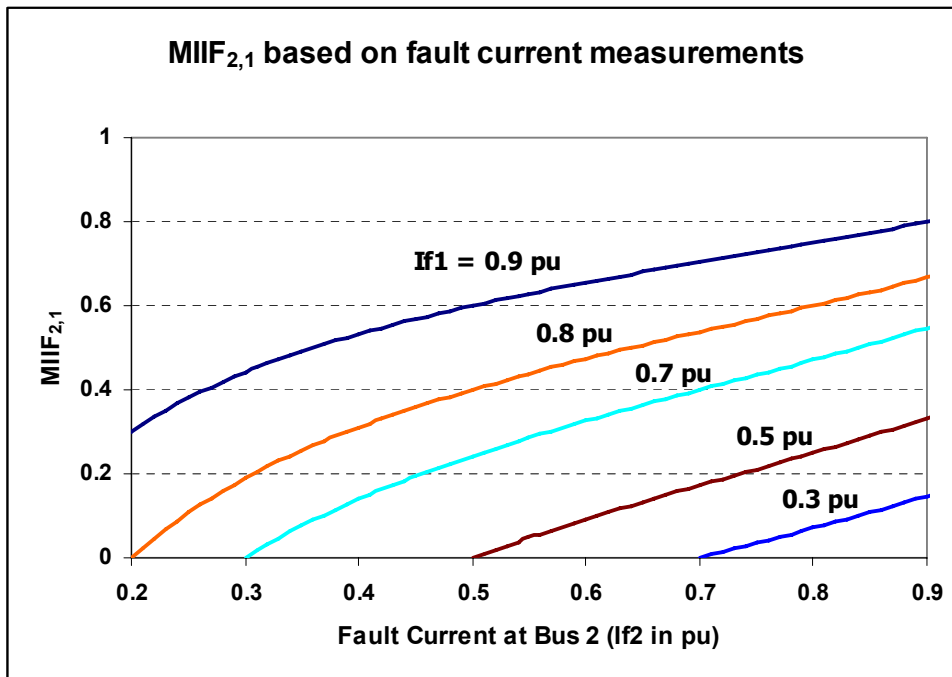


Figure 2-9: MIIF<sub>2,1</sub> as a function of fault currents

It can be observed from Figure 2-9 that if  $I_{f1} + I_{f2} = 1.0$  pu, then MIIF<sub>2,1</sub> is equal to zero. The condition  $I_{f1} + I_{f2} = 1.0$  pu means that  $I_{f1} + I_{f2} = I_{f1\&2}$ , i.e., the total fault current for a simultaneous fault at bus 1 and bus 2 is equal to the sum of fault currents for individual faults at bus 1 and bus 2. In other words, the three-phase-

to-ground fault on one bus does not have any impact on the fault current of the other bus. This could only happen for buses that are infinitely far apart, for which MIIF = 0.0.

### 2.7. MIIF Values in Multi-Infeed Systems with Different Ratings

For MIIF to be a universally useful index for the estimation of the voltage interaction level, it should be applicable in cases of multi-infeed systems with different dc ratings. The ratio of the dc power of the two converters is referred to as the power base ratio (PBR) [9]. The equation for the PBR is given in (2-7).

$$PBR_{j,i} = \frac{P_{dcj}}{P_{dci}} \quad (2-7)$$

To verify the validity of using the MIIF for the estimation of voltage interactions, several multi-infeed configurations with PBR<sub>2,1</sub> ranging from 0.1 to 2.0 were studied. The results given in Table 2.3 show that the MIIF is not significantly affected by the ratio of the ratings of the HVDC schemes.

**Table 2.3: Impact of System Ratings on MIIF**

SCL <sub>1</sub> (MVA)	SCL <sub>2</sub> (MVA)	PBR <sub>2,1</sub>	MIIF <sub>2,1</sub>
3000	3000	0.1	0.5099
“	“	0.2	0.5120
“	“	0.4	0.5159
“	“	0.7	0.5215
“	“	1.0	0.5265
“	“	1.5	0.5342
“	“	2.0	0.5409

This could be proved further by analyzing Equation (2-4), which shows that MIIF is only a function of the fault currents. However, it should be noted that

due to the reactive power generated by the HVDC filters, the ac voltages and, as a result, the fault current would be slightly different, but the impact would be negligible.

## **2.8. Threshold Values of the MIIF**

In Section 2.3.2 it was noted that the MIIF varies between 0 and 1 ( $0.0 \leq \text{MIIF} \leq 1.0$ ). If two systems are infinitely far apart then  $\text{MIIF} = 0$ , and the HVDC schemes could be analyzed as two single-infeed systems. If the HVDC converters are connected to the same ac bus then  $\text{MIIF} = 1.0$ , and it is essentially a single-infeed system.

For practical purposes, it should be determined at what MIIF value the two ac buses can be considered totally independent, and at what MIIF value the two ac buses can be considered to be on the same bus.

The study results of this thesis reported in [3] show that systems could be considered to be of a multi-infeed configuration if the MIIF index greater than 0.15. Systems with  $\text{MIIF} < 0.15$  could be analyzed as two systems without any interactions. It is shown later in Chapter 5 that this criteria is applicable in the commutation failure analysis of multi-infeed HVDC systems.

Table 2.4 shows the parameters of a system with the MIIF of 0.15. In this example, the  $\text{MIIF} = 0.15$  occurs if typical 230 kV commutating buses are 330 km apart. For practical purposes the dc converters at such a distance can be assumed to be independent single infeed systems.



**Table 2.4: Systems with extreme values of MIIF**

ESCR <sub>1</sub>	3.0
ESCR <sub>2</sub>	3.0
Tie-line length (230 kV line)	330 km
<b>MIIF<sub>2,1</sub></b>	<b>0.15</b>

### 2.8.1. Threshold Values of the MIIF in an MI System with Different Ratings

Reference [3] recommends that in the analysis of a dc link in a multi-infeed system the presence of a remote converter can be ignored if  $MIIF_{2,1} \times PBR_{2,1} < 0.15$ .

For example, in the analysis of a local 1000 MW dc link, a 500 MW remote dc link with  $MIIF = 0.25$  could be ignored ( $0.25 \times 500/1000 = 0.125 < 0.15$ ).

## 2.9. MIIF in Systems with more than Two HVDC Infeeds

Up to this point, all the analysis in this chapter have been carried out based on the test system shown in Figure 2-1, which represents a two infeed scheme. However, as discussed in Section 2.4, the MIIF definition and procedures are applicable to schemes with three or more infeeds.

## 2.10. Summary and Conclusions of Chapter 2

The multi-infeed interaction factor (MIIF) was introduced in this chapter, and the definition and calculation procedures for the MIIF were discussed.

The MIIF is a simple-to-calculate index that gives reasonable insight into the performance of a given multi-infeed HVDC system.

The MIIF index is not meant to replace detailed analysis of the system with regard to dynamic overvoltage, commutation failure, harmonic interactions, and power-voltage stability studies. However, it would be a good practice to calculate the MIIF for use as a screening index and use the value of the MIIF to determine the level of detailed analysis of different phenomena is required.

Reference [3], which the candidate is a contributing author of, recommends a threshold value of  $MIIF = 0.15$ , below which interactions between the two HVDC converters could be ignored, and a system could be analyzed as two single-infeed schemes.

### **3. Multi-Infeed Effective Short Circuit Ratio (MIESCR)**

#### **3.1. Introduction**

Effective short circuit ratio (ESCR) is an indicator of the relative strengths of ac and dc systems. Phenomena such as transient overvoltage, maximum available power [13], and harmonic interactions [21] are analyzed based on the value of the ESCR.

In this chapter, the application of the ESCR and related indices in the analysis of a single-infeed HVDC system with regard to transient overvoltage and power-voltage stability are briefly discussed.

The main objective of this chapter is to provide an index similar to ESCR that can be used in multi-infeed systems to provide information similar to that which ESCR provides about single infeed systems. Multi-infeed effective short circuit ratio (MIESCR) is introduced and shown to have applications similar to those of ESCR.

### 3.2. Application of SCR and ESCR Indices in a Single-Infeed System

For a single-infeed system, the short circuit ratio (SCR) and the effective short circuit ratio (ESCR) are defined in Section 2.5. These indices quantify the relative strength of the ac and dc systems. The following examples show the calculation of these indices. Assume that the system in Figure 3-1 is the inverter end of a 1000 MW HVDC link with a 550 Mvar capacitor bank connected to the ac bus.

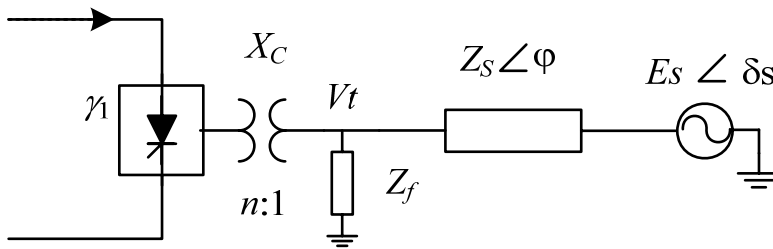


**Figure 3-1: Schematic diagram of a single-infeed HVDC system**

Consider that the above HVDC link is delivering power to a 230 kV ac system with source impedance of 20 Ω. In this case, the short circuit MVA is 2645 MVA and the SCR = 2.65.

With 550 Mvar of reactive power the ESCR value is 2.1, as opposed to SCR = 2.65.

The following section shows how the ESCR value could be used to categorize the relative strengths of the ac and dc systems.

#### 3.2.1. ESCR Value as a Measure for Performance of an AC/DC System

The nature of the ac/dc system interactions and the associated problems are very much dependent on the strength of the ac system relative to the capacity of

the dc link. Modern HVDC systems are categorized based on the value of the ESCR parameter [14]:

- The ac system is strong if the ESCR is greater than 3
- The ac system is moderately strong (or weak) if the ESCR is between 2 and 3
- The ac system is very weak if the ESCR is less than 2

It should be noted that the above classification of ac system strength provides only a means for preliminary assessment of potential ac/dc interaction issues.

Detailed studies are necessary for the proper evaluation of problems.

In addition to the ESCR, the angle of the source impedance ( $\phi$  in Figure 3-1) has an impact on the ac/dc system interactions as well. The impedance angle is called the “damping angle” and could improve the damping of the system oscillation. Typical values of the damping angle are in the range of  $75^\circ$  to  $85^\circ$  [14].

### 3.2.2. Problems with Low ESCR Systems

Operating HVDC systems in an ac network with low ESCR values increases the magnitude of dynamic overvoltages and makes the system susceptible to voltage instability [4]-[5]. These issues are discussed in the following sections.

#### 3.2.2.1. High Transient Overvoltages

When the dc converter is blocked, it no longer absorbs reactive power from the system. However, the shunt capacitors and harmonic filters are connected to the system and continue to generate reactive power. The excessive reactive power in a low ESCR system results in high overvoltages. This would require a

high insulation level for the terminal equipment, thus imposing an economic penalty. As well, special schemes may be necessary to protect the thyristors [14].

#### 3.2.2.2. Voltage Instability

In dc systems connected to weak ac systems the ac and dc voltages are very sensitive to changes in loading, particularly on the inverter side [20]. An increase in dc current is accompanied by a fall of the ac voltage. Consequently, the actual increase in power may be small or negligible. Control of voltage and recovery from disturbances become difficult [22]. The sensitivity increases if there are a large number of shunt capacitors [23]. In such a system, the dc controls may contribute to voltage instability by responding to a reduction in ac voltage by increasing the dc current. Higher dc current increases the reactive power demand by the converter, which, for weak ac systems will reduce the voltage even further, thereby aggravating the situation, and possibly leading to total voltage collapse [14].

### 3.3. Maximum Available Power (MAP) in a Single-Infeed System

In this section, the impact of the ESCR on the maximum amount of power that could be delivered to an ac system by an HVDC link is discussed.

The dc power transmitted by an HVDC link can be controlled by changing the dc current order. However, if the dc current is increased, the ac voltage of the converter bus drops. The formula for calculation of the dc power, given in Equation (3-1), shows that  $P_{dc}$  is a function of the dc current and the ac voltage.

$$P_{dc} = \frac{3 \cdot \sqrt{2}}{\pi} \cdot n \cdot V_{ac} \cdot \cos(\gamma) \cdot I_{dc} - \frac{3}{\pi} \cdot X_c \cdot I_{dc}^2 \quad (3-1)$$

In (3-1),  $V_{ac}$  is the magnitude of the system ac voltage,  $n$  is the turns ratio of the converter transformer,  $I_{dc}$  is the dc current,  $X_c$  is the impedance of the converter transformer, and  $\gamma$  is the extinction angle.

In this section, the maximum available power from a single-infeed HVDC test system with similar topology to the CIGRÉ Benchmark is calculated. The ESCR of the test system is 2.5. The dc current is varied from 0 to 1.5 pu and corresponding  $P_{dc}$  and  $V_{ac}$  are calculated by solving power flow equations. The results are shown in Figure 3-3. The  $P_{dc}$  curve in Figure 3-2 is often referred to as the maximum power curve (MPC), and it shows the variation of dc power as a function of dc current. The maximum power on the MPC is called the maximum available power (MAP). For the test system in this example MAP is 1.07 pu and occurs at  $I_{dc}=1.27$  pu.

Figure 3-2 shows that as dc current increases the ac voltage drops due to larger reactive power consumption by the converter.

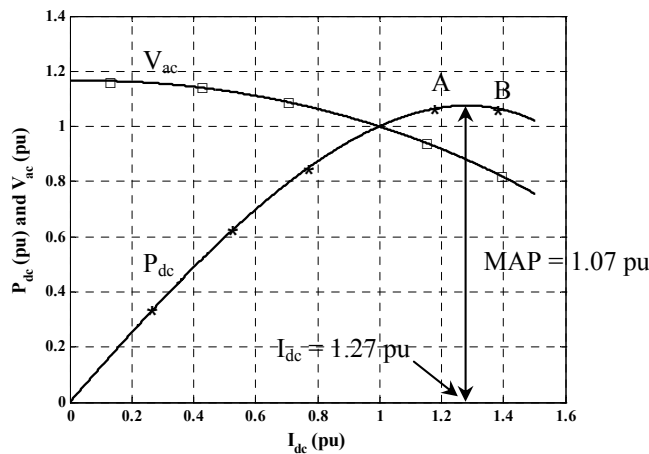


**Figure 3-2: Variation of terminal voltage and dc power with dc current**

When an HVDC system is operating near the MAP (point A in Figure 3-2) a small increase in power demand will result in power-voltage instability. For example, if the ac voltage drops due to a remote ac fault, the  $P_{dc}$  drops according to Equation (3-1). In this situation, if the dc link is in power control mode, the converter controls attempt to compensate for the drop in  $P_{dc}$  by increasing the dc current. However, since the system is operating near the MAP point, the increased dc current possibly pushes the system into the unstable region beyond the MAP (for example, point B in Figure 3-2) and worsens the situation by further decrease in dc power. References [24] and [25] detail the dynamic voltage stability of ac/dc systems.

### 3.3.1. Critical Effective Short Circuit Ratio (CESCR)

The critical effective short circuit ratio (CESCR) is the ESCR of a system in which the maximum dc power transfer occurs at dc current equal to 1.0 pu (MAP = 1.0 pu) [11], [12], [26]. Such a system is marginally stable and a small disturbance may cause instability. It is shown in [11] that CESCR can be approximated by Equation (3-2).

$$CESCR = \frac{P_{dc} \cdot \cot(\phi/2) - Q_{dc}}{V_t^2}$$

$$\phi = 90^\circ - \gamma - \mu$$

$\gamma$  : inverter extinction angle ( $^\circ$ )

$\mu$  : overlap angle ( $^\circ$ )

$P_{dc}$  : dc power injected to the ac system (pu)

$Q_{dc}$  : reactive power consumed by the HVDC converter (pu)

$V_t$  : ac terminal voltage (pu)

(3-2)



The parametric studies performed in this thesis show that the extinction angle of the inverter has almost no impact on the CESSCR. The reason the CESSCR is not affected by the extinction angle can be explained using Equation (3-2). Increasing the extinction angle will increase the  $\cot(\phi/2)$  term, but at the same time doing so will increase the  $Q_{dc}$ , and the net effect on the CESSCR will be very small. Study results show that the CESSCR is approximately 1.5 for typical converter transformer impedances (15% to 18%). In the case studies in this thesis the extinction angle,  $\gamma$ , is  $15^\circ$ .

This result is in line with the general guidelines regarding ac system strength that consider systems with  $ESCR < 2$  as “very weak” systems. As shown in this section, there is a theoretical limit of  $ESCR = 1.5$  below which the system shows power-voltage instability. Hence, the  $ESCR$  of the network should be larger than 1.5. Therefore, to allow for some flexibility in the operation of the system, it is recommended to have an  $ESCR$  in the 2.0 – 2.5 range or larger [14].

### **3.4. Transient Overvoltage (TOV) in Single-Infeed HVDC Systems**

An important criterion in the design of an HVDC link is the permissible transient overvoltage (TOV) at the ac terminals of the converter station [13]. The overvoltage influences the ratings of the station equipment on both the ac and dc sides and affects the ac network. The overvoltage at the ac terminals of a converter station can occur due to disturbances on either the ac system or the dc system. The worst case overvoltages at most inverter buses are caused by a sudden and complete loss of transmitted dc power [27],[28]. The reason for an

overvoltage following the blocking of the dc converter is the elimination of the reactive power consumption of the inverter, which suddenly increases the reactive power generated by filters and by other shunt capacitor banks that are still connected to the ac system [20],[29]. Figure 3-3 shows the schematic diagram of a single-infeed HVDC system at the inverter end. The highest overvoltage for  $V_t$  occurs when the inverter is operating at nominal power and is blocked suddenly while the filters ( $Z_f$ ) are still connected to the ac bus.

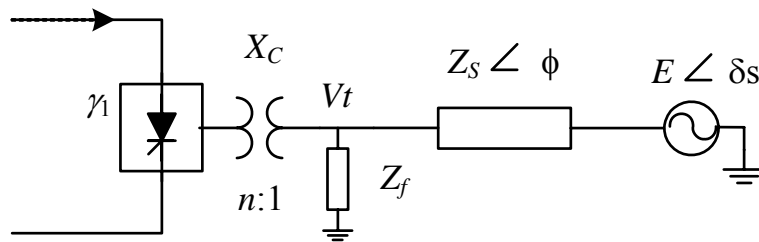


**Figure 3-3: Schematic diagram of a single-infeed HVDC system**

The TOV values resulting from converter blocking are plotted in Figure 3-4 for the ESCR varying between 1.5 and 5. The plot is given for three impedance angles. It is evident in Figure 3-4 that for systems with  $ESCR < 2$  the overvoltage starts to rise very rapidly. Typically, a 30% overvoltage is considered very high and special protection schemes are required to prevent damage to the equipment [13].

These results also show that in systems with the same ESCR, the TOV is lower for systems with a lower impedance angle (higher resistive component in the ac source Thévenin impedance).

A closed-form formula for TOV calculation is developed in the following section.

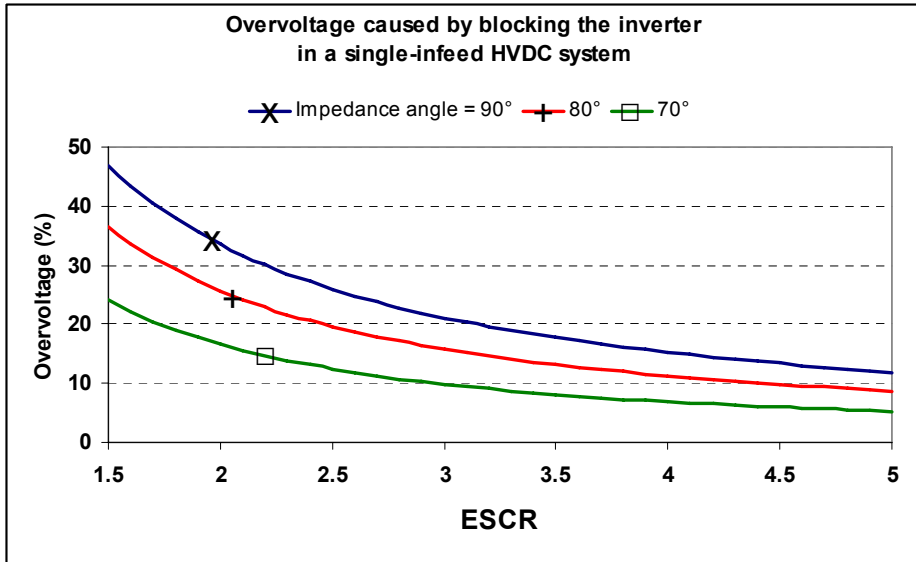


Figure 3-4: Magnitude of overvoltages at the inverter caused by blocking the HVDC

### 3.4.1. Calculation of TOV in Single-Infeed HVDC Systems

A power system studies program such as PSS/E could be used to calculate the TOV, or simple programs could be developed to calculate the transient overvoltage for different ESCRs and for different damping of the ac network.

In this thesis it is shown that a formula can also be developed for calculation of the TOV, assuming that the angle of the ac system impedance is 90°. Equation (3-3) can be used to calculate the TOV based on the  $Q_{dc}$  and the ESCR value.

$$TOV = \sqrt{1.0 + \frac{2 \cdot Q_{dc}}{ESCR} + \frac{1 + Q_{dc}^2}{ESCR^2}} - 1.0 \quad (3-3)$$

The derivation of the formula above is given in Appendix C.

The assumption of a  $90^\circ$  angle for the ac source impedance is conservative. The impedance angles are normally in the range of  $75^\circ$  to  $85^\circ$  [14] and therefore the TOV values would be smaller than what is calculated using formula (3-3).

Definition of multi-infeed ESCR and analysis of maximum transient overvoltage and power-voltage stability in multi-infeed systems are presented in the following sections.

### **3.5. Definition of AC System Strength in Multi-Infeed Systems**

As discussed in Sections 3.2 to 3.4, the ESCR parameter is a very helpful index in the preliminary analysis of single-infeed HVDC systems. It was shown that the transient overvoltage and power and voltage stability (PV stability) could be assessed at a high level using the ESCR index.

A schematic diagram of a multi-infeed HVDC system with two dc infeeds is shown in Figure 3-5.  $Z_{s1}\angle\varphi_1$ ,  $Z_{s2}\angle\varphi_2$ , and  $Z_{tie}\angle\varphi_{tie}$  are the impedances of the two-port equivalent of the ac system.  $E_1\angle\delta_{s1}$  and  $E_2\angle\delta_{s2}$  represent the ac voltage of the system.  $Z_{f1}$  and  $Z_{f2}$  represent the impedance of the ac filters and capacitor banks at the converter buses.  $X_{c1}$  and  $X_{c2}$  are the impedance of the converter transformers.  $\gamma_1$  and  $\gamma_2$  are the extinction angle of converter 1 and converter 2 respectively.

An index similar to the ESCR in single-infeed systems is required for multi-infeed HVDC systems to provide similar information [3]. Several indices are discussed in the following sections.

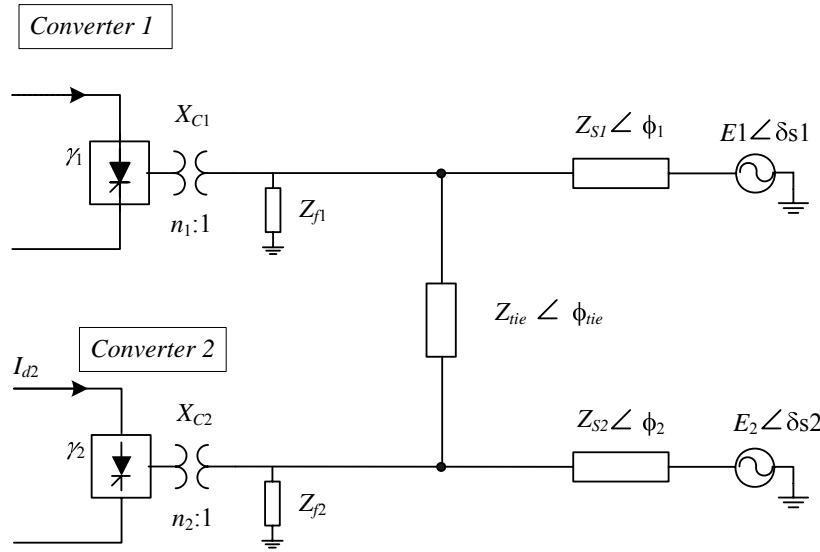


**Figure 3-5: A system with two HVDC infeeds**

### 3.5.1. ESCR for Individual Converters in Multi-Infeed Systems

Care must be taken in calculating the effective short circuit ratio in multi-infeed configurations. Because the effective short circuit ratio is an indicator of the performance of a given converter without any other converter in operation, the Thévenin impedance  $Z_{tie}$  is measured looking into the ac network from the converter's ac bus [30]. The other converter is considered to be blocked in this calculation. Thus, the ESCR for the  $i^{\text{th}}$  converter is given by Equation (3-4).

$$ESCR_i = \frac{SCL_i - Q_{fi}}{P_{dci}} \quad (3-4)$$

In the calculation of the ESCR for converter  $i$ , all other HVDC converters are assumed to be blocked (a standard practice in most short circuit study tools). It will be shown later in this thesis that for some phenomena in MI systems the ESCR is a still a useful index.

### 3.5.2. Multi-Infeed Short Circuit Ratio (MSCR) and Multi-Infeed Effective Short Circuit Ratio (MESCR)

Reference [31] introduces two new indices called multi-infeed short circuit ratio (MSCR) and Multi-infeed effective short circuit ratio (MESCR). The application of these indices in the analysis of multi-infeed systems is shown in [31], [32]. MSCR and MESCR are defined by equations (3-5) and (3-6).

$$MSCR_n = \frac{1}{\sum_{m=1}^k Pdc_m \times Z_{n,m}} \quad (3-5)$$

$$MESCR_n = \frac{1}{\sum_{m=1}^k Pdc_m \times Z_{en,m}} \quad (3-6)$$

The power and impedance parameters in the above equations are per-unitized based on the power rating of converter “n”. Hence, the  $Pdc_n$  is equal to 1.0 pu.  $Pdc_m$  is the rating of the HVDC link “m” and  $Z_{n,m}$  are the elements of the inverse of the Y matrix. In the calculation of the MSCR the filters and capacitor banks are ignored (in a similar manner as in the calculation of the SCR in single-infeed systems). The  $Z_{en,m}$  parameter in the MESCR definition is the equivalent impedance when the filter impedances are considered in the calculation. To calculate the MESCR, the inverse of the admittance matrix of the entire system is needed, which for large systems requires a significant amount of calculations.

### 3.5.3. Multi-Infeed Effective Short Circuit Ratio (MIESCR)

Dr. Ioni Fernando, the author’s colleague in the CIGRÉ B4-41 group, suggested a formula for calculation of the ac system strength in multi-infeed

HVDC schemes [3]. In collaboration with Dr. Fernando, the final form of the formula was developed in this thesis. The index is called multi-infeed effective short circuit ratio (MIESCR). The definition of MIESCR is given by Equation (3-7).

$$MIESCR_i = \frac{SCL_i - Qf_i}{\sum_{j=1}^n MIIF_{j,i} \cdot Pdc_j} \quad (3-7)$$

In (3-7),  $SCL_i$  is the short circuit level at the converter  $i$ ,  $Qf_i$  is the Mvar rating of the capacitor and filters connected to the ac bus at converter  $i$ ,  $Pdc_j$  is the nominal rating of the HVDC links, and  $MIIF_{j,i}$  is the multi-infeed interaction factor from converter  $i$  to converter  $j$ .

Note that if the MIESCR definition in (3-7) is applied to a single-infeed system, it yields the same value as the ESCR (for single-infeed systems  $MIIF_{i,i}=1.0$ ).

Calculation of the MIESCR index is simpler than calculation of the MESCR index. The MIIF, and consequently, the MIESCR values, could be calculated using dynamic simulation or using fault current calculations, which could be easily conducted using typical power system analysis tools.

Using the approximate definition of MIIF given in Section 2.4.2, it is easy to show, as in (3-8), that the MIESCR as defined by Formula (3-7) and the MESCR index as defined by (3-6) give approximately the same results.

$$MIESCR_i = \frac{SCL_i - Qf_i}{\sum_{j=1}^n MIIF_{j,i} \cdot Pdc_j} \approx \frac{\frac{1}{Z_{i,i}}}{\sum_{j=1}^n \frac{Z_{i,j}}{Z_{i,i}} \cdot Pdc_j} = \frac{1}{\sum_{j=1}^n Z_{i,j} \cdot Pdc_j} = MESCR_i \quad (3-8)$$

In the following sections, the application of the above indices in the calculation of the transient overvoltage and the calculation of the maximum available power is discussed.

### 3.6. Maximum Available Power (MAP) in Multi-Infeed Systems

The following three MI scenarios with varying levels of interdependency in the operation of the HVDC links are selected for calculation of the MAP. The test system for these cases has the configuration shown in Figure 3-5.

#### 3.6.1. MAP of HVDC Link "n" when all the Other Links are Off

Consider an MI system in which only converter 1 is operating and the other converters are off. This is basically a single-infeed system, and therefore the ESCR is calculated in a manner similar to (3-4) using the Thévenin equivalent impedance of the entire ac network. Hence, the CESCO formula given for single-infeed systems could be used directly. Assuming a 15% impedance for the converter transformer, the CESCO value for this scenario is 1.48.



### 3.6.2. MAP of the HVDC Link “n” when all the Other DC Links are Operating at Nominal Rating

Deriving a closed-form formula similar to (3-4) for a multi-infeed system is difficult and has not been attempted in this thesis. Instead, parametric studies were performed on several system configurations using computer modelling.

For each system configuration, the MAP of one dc link is calculated by increasing the current order of that dc link while the other dc links are operating at their nominal ratings.

Simulation results showed that the power peaked at 1.0 per-unit current when the ESCR was 1.54. For the single-infeed analysis in Section 3.6.1, the CESCR was 1.48. In other words, the stability margin of a dc link in a multi-infeed system is essentially the same (slightly less) as for a single-infeed system with the same ESCR.

### 3.6.3. MAP of HVDC link “n” when all the HVDC Links are Simultaneously Increasing their Injected Power

This scenario represents a system condition in which all the HVDC links participate proportionally to a change in power order. In other words, the step change of the per-unit dc current ( $\Delta I_{dc}$ ) of each converter is the same for all the HVDC links.

The simulation-based method is adopted in this thesis for calculation of the MAP. In this study, a two-infeed test system with the same configuration as the configuration in Figure 3-5 was used.  $ESCR_2$  was maintained constant at 2 while

$ESCR_1$  was varied so that the MAP for dc link 1 occurs at  $I_{dc1} = I_{dc2} = 1.0$  pu. Table 3.1 gives the  $ESCR_1$  and  $ESCR_2$  values of the test system for the critical MIESCR<sub>1</sub> (CMIESCR) value of 1.45.

This example shows that although the individual  $ESCR_1$  and  $ESCR_2$  are well above the critical value of 1.5 for single-infeed systems, the multi-infeed system as a whole is on the edge of PV instability. Hence, MIESCR is the appropriate index to be used in the PV analysis of MI systems in this scenario, and the CMIESCR is around 1.5.

**Table 3.1: Critical MIESCR Values for a System with Two DC Infeeds**

$ESCR_1$	$ESCR_2$	$MIIF_{2,1}$	CMIESCR <sub>1</sub>
2.23	2.0	0.534	1.45

#### 3.6.4. Parametric Study of MAP in a Multi-Infeed System

The MIESCR values for many different test systems are reported in Table 3.2. To calculate CMIESCR<sub>1</sub>, for each given value of  $ESCR_1$  and  $ESCR_2$ , the length of the tie-line is varied so that MAP<sub>1</sub> occurs at  $I_{dc}=1.0$  pu for all converters. As the results in Table 3.2 show, while system 1 is PV stable, the other dc link could be operating at a PV stable (high MIESCR<sub>2</sub>) or a PV unstable (low MIESCR<sub>2</sub>) point.

As shown in Table 3.2, for many system configurations with varying  $ESCR_1$  and  $ESCR_2$ , the CMIESCR is always around 1.5 [29].

The investigation is extended to a three-inverter multi-infeed HVDC test system. The results in Table 3.3 show that system 1 is marginally stable, and has its MIESCR<sub>1</sub> value around approximately 1.4 for all the different system configurations.

This example shows that for a MI system with three infeeds the MIESCR is also expected to be around 1.5 [29].

**Table 3.2: MIESCR Values for Several Systems with Two DC Infeeds. System 1 is at the Point of PV Instability**

ESCR <sub>1</sub>	ESCR <sub>2</sub>	Tie line Length (km)	MIF <sub>2,1</sub>	MIF <sub>1,2</sub>	MIESCR <sub>1</sub>	MIESCR <sub>2</sub>
2	1	513	0.392	0.151	1.44	0.87
2	1.5	266	0.400	0.278	1.43	1.17
2	2	178	0.395	0.395	1.43	1.43
2	2.5	128	0.398	0.518	1.43	1.65
2	3	97	0.401	0.641	1.43	1.83
2	3.5	77	0.401	0.757	1.43	1.99
2	4	62	0.402	0.875	1.43	2.13
2	4.5	52	0.398	0.980	1.43	2.27
2	5	43	0.400	1.093	1.43	2.39
2.5	1	251	0.720	0.219	1.45	0.82
2.5	1.5	126	0.708	0.383	1.46	1.08
2.5	2	74	0.711	0.551	1.46	1.29
2.5	2.5	46	0.715	0.715	1.46	1.46
2.5	3	29	0.717	0.873	1.46	1.60
3	1	166	0.978	0.249	1.52	0.80
3	1.5	72	0.978	0.442	1.52	1.04
3	2	34	0.984	0.633	1.51	1.23
3	2.5	14	0.986	0.814	1.51	1.38
3	3	2	0.983	0.983	1.51	1.51

**Table 3.3: MIESCR Values for Several Systems with Three DC Infeeds. System 1 is at the Point of PV Instability**

ESCR <sub>1</sub>	ESCR <sub>2</sub>	ESCR <sub>3</sub>	MIESCR <sub>1</sub>	MIESCR <sub>2</sub>	MIESCR <sub>3</sub>
2.60	4.23	3.64	<b>1.38</b>	1.80	1.69
2.69	3.78	3.58	<b>1.38</b>	1.65	1.64
2.84	3.53	3.39	<b>1.40</b>	1.52	1.59
3.03	2.90	3.45	<b>1.41</b>	1.35	1.52

### 3.6.5. Summary of MAP Analysis in a Multi-Infeed System

The conclusion of this section is that in the PV analysis of multi-infeed systems, if only the dc current of one converter varies the ESCR index is a good indication of the stability margin.

When several converters are simultaneously responding to a change in power order, the MIESCR index should be used. For proper operation of an MI system the MIESCR of any given dc link should be around 1.5 or higher.

## 3.7. Transient Overvoltage (TOV) in Multi-Infeed Systems

### 3.7.1. TOV of the HVDC link "n" when all the Other Links are Off

Such a system is essentially a single-infeed system, and therefore the ESCR index as defined in (3-4) could be used to directly estimate the TOV level using the Equation (3-3).

### 3.7.2. TOV of the HVDC link "n" when all the Other DC Links are Operating at Nominal Rating

The results of a parametric study conducted in this thesis show that the TOV resulting from blocking one of the HVDC links in a multi-infeed system is slightly higher than the TOV for a single-infeed system with the same ESCR. In this study the  $ESCR_2$  was kept constant at 2.0 and  $ESCR_1$  was varied from 1.5 to 4.0. The two systems have the same ratings. The results of the study are given in Table 3.4.

**Table 3.4: TOV at the ac bus following its converter block in an MI system**

ESCR <sub>1</sub>	Impedance Angle	Single Infeed TOV (pu)	ESCR <sub>2</sub>	Multi-Infeed TOV (pu) (only converter one blocked)
1.5	90°	1.51	2.0	1.58
2.0	90°	1.36	2.0	1.42
2.5	90°	1.28	2.0	1.32
3.0	90°	1.23	2.0	1.26
3.5	90°	1.19	2.0	1.22
4.0	90°	1.16	2.0	1.19

Table 3.4 shows that the difference between the TOV values is insignificant, and it could be assumed that the ESCR of a converter is a reasonable index for the calculation of the TOV in the event of only one converter block.

### 3.7.3. TOV of the HVDC link “n” when all the HVDC Schemes are Simultaneously Blocked

Assume a multi-infeed system with two dc links delivering power to an ac network. Also assume that the rectifiers of the dc links are located in very close proximity. Under these conditions, an ac fault at the rectifier side could cause both dc links to block the power transfer. The maximum TOV occurs in the inverters ac system in this worst-case scenario. The reason for large the TOV values is the huge surplus of reactive power generated by the capacitors and filter banks still connected to the system while no reactive power is absorbed by the converters.

Initial study results show that using Equation (3-3) gives inaccurate and optimistic results, and therefore the ESCR is not a proper index for calculation of the TOV in this scenario. Hence, in this thesis Equation (3-9) is derived to

calculate the amount of TOV at a given bus in multi-infeed systems. The derivation of (3-9) is shown in Appendix D.

$$TOV_i = \sqrt{1.0 + \frac{2 \cdot Q_{dci}}{MIESCR_i} + \frac{1 + Q_{dci}^2}{MIESCR_i^2}} - 1.0 \quad (3-9)$$

Comparison of Equation (3-3) and (3-9) shows that the MIESCR index has the exact same application in TOV calculation as the ESCR index has in single-infeed systems. Table 3.5 shows the results of two studies:

- i) TOV resulting from blocking a single-infeed system with ESCR varying from 1.5 to 4.0,
- ii) TOV on bus 1 of a multi-infeed system with  $ESCR_1$  varying from 1.5 to 4.0 while  $ESCR_2$  is kept constant at 2.0

Analysis of results in Table 3.5 shows that the MIESCR has the same application in multi-infeed system as ESCR has in single-infeed system. For example, for a single infeed system with  $ESCR_1=2.5$ , TOV is 28% where as in a multi-infeed system with  $MIESCR_1 = 2.53$ , the TOV on bus 1 resulting from blocking all converters is 27%.

**Table 3.5: Comparison of TOV in single- and multi-infeed systems**

ESCR <sub>1</sub>	Single Infeed TOV (pu)	ESCR <sub>2</sub>	MIIF <sub>2,1</sub>	MIESCR <sub>1</sub>	Multi-Infeed TOV (pu) (both converters blocked)
1.5	1.51	2.0	0.48	1.01	1.80
2.0	1.36	2.0	0.51	1.32	1.58
<b>2.5</b>	<b>1.28</b>	2.0	0.54	1.62	1.46
3.0	1.23	2.0	0.55	1.94	1.38
3.5	1.19	2.0	0.57	2.23	1.32
4.0	1.16	2.0	0.58	<b>2.53</b>	<b>1.27</b>

#### 3.7.4. Summary of TOV Analysis in Multi-Infeed Systems

When a dc link in a multi-infeed system is blocked while all other links are operating at their nominal ratings the overvoltage can be calculated using the ESCR.

In the case of simultaneous blocking of all the dc links, the MIESCR is the appropriate index for TOV calculations. Under these conditions, the MIESCR plays exactly the same role as the ESCR does in single-infeed systems.

### 3.8. A Sample Case Study for the MIESCR Calculations

In a similar manner as in the MIIF example in Section 2.4.4, the planned HVDC systems in Alberta are used to provide an example for MIESCR calculations. The MIIF values between the 240 kV buses at Langdon and Brooks are given in Chapter 2. Table 3.6 shows the single-infeed and multi-infeed TOV for converter blocking at Langdon and Brooks.

The study results show that the calculated TOV is around 25% higher than the TOV measured using the dynamic simulation method. One of the reasons for this is the angle of system impedance. In the derivation of the TOV formulas it was assumed that the impedance angle of the ac system is  $90^\circ$ ; whereas, in the case study the angle is around  $80^\circ$ . In addition to that, the dynamic response of the system load, which is also ignored in the formula, has an impact on the TOV value as well.

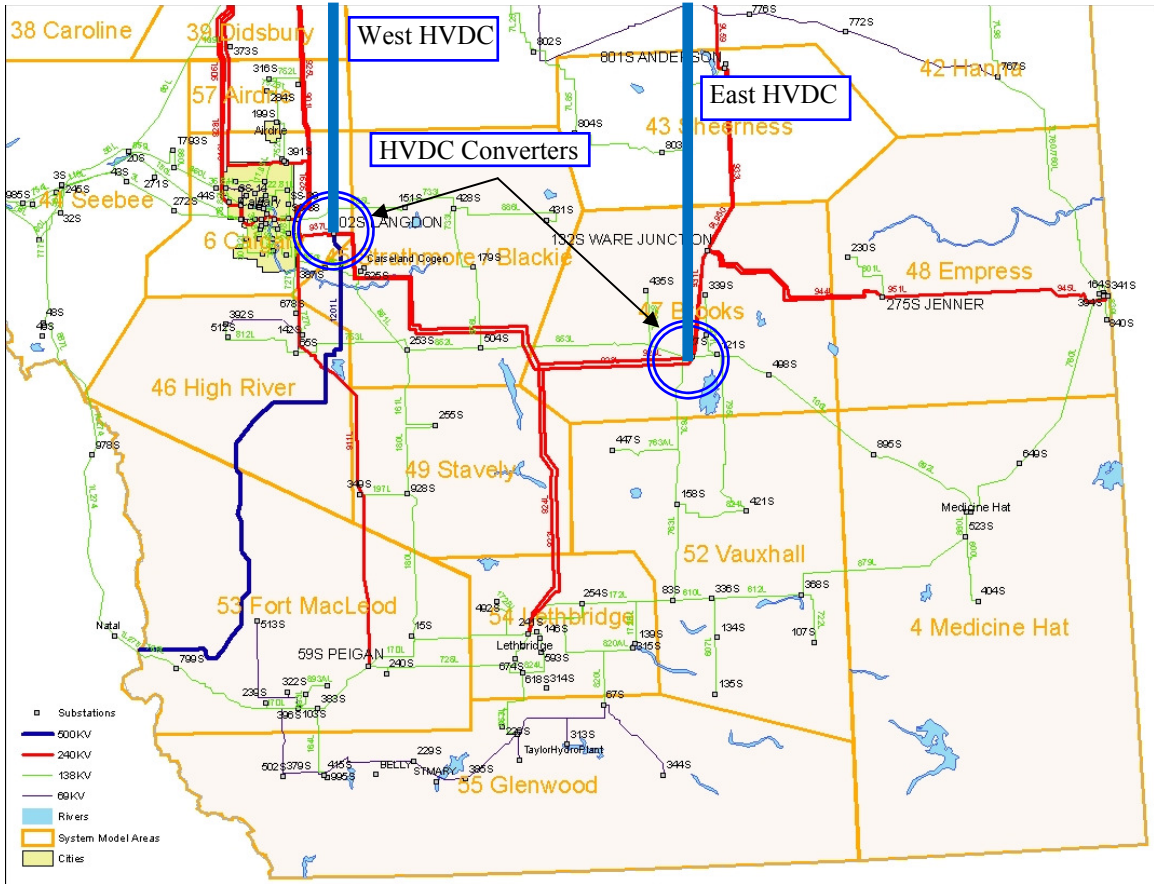


Figure 3-6: Approximate locations of the HVDC converters in southern Alberta

Table 3.6: An Example of TOV and MIESCR Calculation in a Multi-infeed System

System Parameters	Langdon	Brooks
Rated Pdc	1000 MW	1000 MW
Rated Qdc = Rated Qfilter	550 Mvar	550 Mvar
Short Circuit Level	6422 MVA	4693 MVA
ESCR	5.87	4.14
Calculated TOV (single-infeed)	10.7%	15.8%
MIIF <sub>Brooks, Langdon</sub>	0.456	-
MIIF <sub>Langdon, Brooks</sub>	-	0.330
MIESCR	4.03	3.11
Calculated TOV (multi-infeed)	16.3%	22.0%
Measured TOV by simulation multi-infeed	13.1%	17.2 %
Measured TOV by simulation single-infeed	7.0 %	11.9%



The conclusion is that the simplified TOV formulas give a conservative estimate for the worst case overvoltage. The actual TOV of any practical system (single-infeed or multi-infeed) due to damping angles less than  $90^\circ$  would be smaller than the TOV calculated using equations (3-3) and (3-9).

### 3.9. Range and Threshold Values of the MIESCR

Maximum MIESCR occurs when the MIIF indices between the converter ac buses are 0.0. In this case, the MIESCR is the same as the ESCR.

Minimum MIESCR occurs when all the dc links are delivering power to the same ac bus, and therefore the MIIF indices between the converter ac buses are 1.0. The range of the MIESCR is given by Equation (3-10).

$$\frac{ESCR_i}{\sum P_{dc_j}} \leq MIESCR_i \leq ESCR_i \quad (3-10)$$

Similar to the ESCR index, the MIESCR index has several threshold values for classification of the strength of the ac system. The following guideline is applicable for an HVDC link in a multi-infeed configuration:

- $MIESCR_i > 3$  : Converter i is connected to a strong ac system
- $2 < MIESCR_i < 3$  : Converter i is connected to a moderate (or weak) system
- $MIESCR_i < 2$  : Converter i is connected to a weak ac system
- It is recommended that MIESCR should be at least 2.5 [3]
- The critical MIESCR with regards to power-voltage stability is around 1.5, as in the case for the critical ESCR in single-infeed systems.

Note that since the MIESCR varies from one link to another, an ac system classified as strong for a particular dc scheme might be classified as weak for another scheme within the same multi-infeed system.

### **3.10. Summary and Conclusions of Chapter 3**

For multi-infeed systems, ESCR and MIESCR both play a role in the analysis of the system.

If only one dc link is considered in the study while other dc links are operating at normal rating, the ESCR index should be used in the analysis. Under these conditions the maximum available power (MAP) and the transient overvoltage (TOV) are primarily a function of ESCR. For this operating scenario the CESC value for each link is around 1.5.

If all the dc links in the multi-infeed system are participating in the response to the power order change, the MIESCR index should be used in the studies. The MIESCR index of a dc link determines the maximum available power (MAP) from that dc link and determines the maximum TOV. For this operating scenario the CMIESCR value for each link is around 1.5.

## **4. Commutation Failure Analysis in HVDC Systems**

### **4.1. Introduction**

In a normally operating conventional HVDC converter the current will “commutate” from one valve to another valve by triggering a thyristor valve in the firing sequence [5]. However, because of a fault on the ac system, a control circuit malfunction, or a phase shift in the voltage, the process of current commutation may not be completed successfully and a “commutation failure” occurs. During a commutation failure, the dc voltage, and therefore, the dc power that is injected to the ac system, drops to zero. Depending on the strength of the ac system, a commutation failure could be a severe dynamic event that may cause unacceptable voltage fluctuations. Especially in weak ac systems, successive commutation failures can occur resulting in prolonged energy loss. Most commutation failures are caused by voltage disturbances due to ac system faults, and they can never be completely avoided [16].

In this chapter, the commutation process is briefly discussed followed by a review of past approaches to the analysis of commutation failure. A new approach that utilizes electromagnetic transient (EMT) simulation to assess the immunity of an HVDC converter to commutation failure is introduced. The results of a parametric study on the immunity of a converter in a single-infeed system to commutation failure are also presented.

#### **4.2. Normal Operation of a Line Commutated HVDC Inverter**

A schematic diagram of the converter valves involved in a current commutation process are shown in Figure 4-1. In this circuit, valves 1 and 2 are conducting and valve 3 is triggered in the firing sequence so that the dc current will be transferred from valve 1 to valve 3. Following the triggering of valve 3, its current ( $i_3$ ) starts to ramp up and the current of valve 1 ( $i_1$ ) starts to ramp down, and after an overlap angle of  $\mu$ , valve currents  $i_3$  and  $i_1$  reach their final values of  $I_d$  and zero, respectively, and the commutation process from valve 1 to valve 3 is over. After a period of  $60^\circ$ , similar current commutation from valve 2 to valve 4 will occur, and so on.

As shown in Figure 4-1, for a period of time ( $\gamma$ ) the voltage across valve 1 ( $V_{T1}$ ) will be negative. The valve going off must remain reversed biased for a minimum time. This period is normally 300 - 400 $\mu$ s (around  $7^\circ$ -  $8^\circ$  in 60 Hz systems) [13]; however, it is larger for higher dc currents. During this period, the stored charges in the thyristor valve produced during a forward conduction interval are completely removed and the valve can establish a forward voltage

blocking capability [5]. If the voltage across the valve becomes positive before removal of all the charges, the valve will start conducting without a trigger and a commutation failure occurs. Hence, the reverse bias time, also represented by the electrical angle  $\gamma$  (called the extinction angle) in Figure 4-1 must be greater than the critical value of  $\gamma_{\min} \approx 7^\circ - 8^\circ$

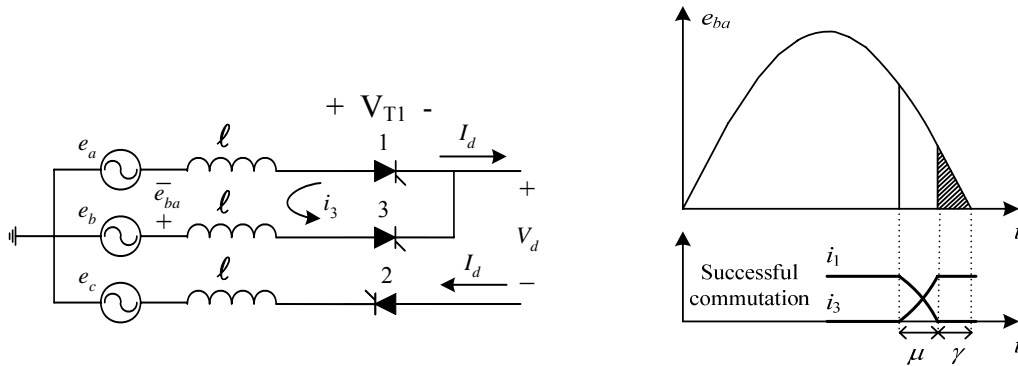


Figure 4-1: Current commutation from valve 1 to valve 3

### 4.3. Commutation Failure in an HVDC Inverter

As discussed in the previous section, to prevent uncontrolled re-ignition of the valves, the extinction angle  $\gamma$  shown in Figure 4-1 should be larger than a minimum value of  $\gamma_{\min}$ . Both the magnitude and the duration of the negative voltage across the valve play a role in the extinction process. In other words, for a successful commutation the volt-second area under the commutating voltage for the duration of  $\gamma$  should also be above a threshold value [16] indicated by the shaded portion in Figure 4-1.

If the magnitude of the commutating voltage drops due to an ac fault or if the zero crossing of the commutating voltage moves to the left because of a

phase shift in ac voltage, the area under the voltage may not be sufficient, and if it is not, a commutation failure will occur [33].

The sudden drop of the inverter's ac voltage causes a dip in the dc voltage. This results in a temporary increase of dc current until the rectifier current control has time to react. As the dc current increases, more charges have to be removed from the thyristor to turn it off, and therefore, the area under the commutating voltage needs to be higher, which could be a challenge due to the lower ac voltage magnitude.

A single commutation failure is not usually a very critical event in an HVDC system; however, if several successive commutation failures occur the converter must be blocked [13]. The following section discusses the definitions of single and successive commutation failures.

### 4.3.1. Single and Successive Commutation Failure Phenomena

If the causes that led to a commutation failure in a valve in the first instance have disappeared, the bridge operation returns to the normal state in the next firing of the failed valve. Thus, a single commutation failure is said to be self-clearing [34]. The waveforms of the bridge voltage are shown in Figure 4-2. The failure of two successive commutations in the same cycle is called a double commutation failure. The bridge voltage waveform for this case is shown in Figure 4-3, and it can be seen that for close to half a cycle the dc voltage at the converter reverses. Therefore, in a double commutation failure the dc current

rapidly increases, which may result in the failure of subsequent current commutations [34].

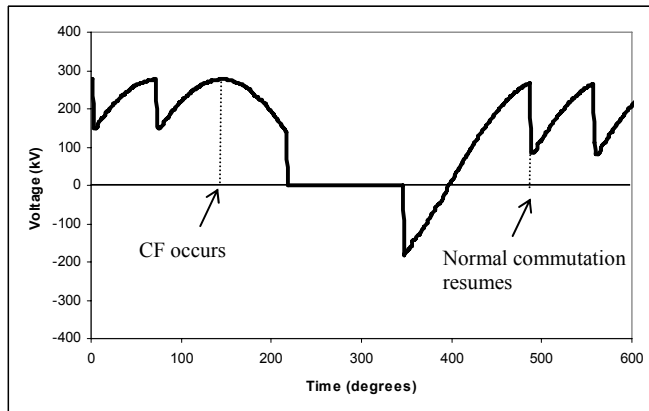


**Figure 4-2: Bridge voltage in a single commutation failure**

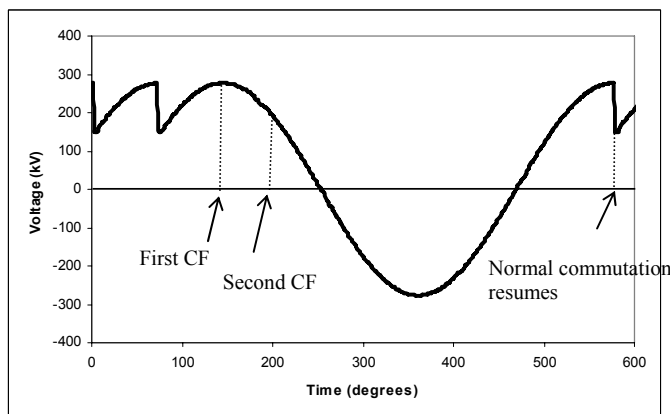


**Figure 4-3: Bridge voltage in a double commutation failure**

#### 4.3.2. Effects of Commutation Failure on AC and DC Systems

The following are the effects of a single commutation failure:

1. The bridge voltage remains zero for a period exceeding 1/3 of a cycle, during which time the dc current tends to increase
2. There is no ac current for the period in which the two valves in an arm are left conducting

In most cases, commutation failures are self clearing, but in the case of successive commutation failures the converter protection helps to take the converter out of service. During commutation failures in which the two valves in an arm of a bridge are left conducting, the ac current goes to zero while the dc current continues to flow. The commutation failure in a bridge can lead to consequential commutation failure in the series-connected bridges unless the rate of rise of the current is sufficiently limited by the series connected smoothing reactors.

### 4.3.3. Recovery from a Commutation Failure

The recovery from a commutation failure depends on the following factors [13]:

- The response of the extinction angle ( $\gamma$ ) controller at the inverter
- The current control in the link
- The magnitude of the ac voltage

If, after detection of a commutation failure, the firing angle,  $\alpha$ , is rapidly reduced, there is a good chance that subsequent commutation failures will be prevented. However, the prevention of subsequent commutation failures also depends on the control of the dc current and the magnitude of the ac voltage. The initial rate of rise of the current in the inverter is limited by the smoothing reactor, and the current controller at the rectifier helps to limit the current in the case of persistent commutation failures. It may even be necessary to reduce the current reference to limit the overlap angle in the case of low voltages caused by



faults in the ac system. In most HVDC schemes, a voltage dependent current order limit (VDCOL), which reduces the rectifier current order for low inverter ac voltage, is present. This reduction in current reduces the overlap angle and the required minimum extinction angle, and hence helps to prevent a commutation failure and aids in the recovery from a commutation failure.

#### **4.4. Past Approaches in the Analysis of Commutation Failure**

As discussed in earlier sections, although a commutation failure can be due to many causes, the most common cause of a commutation failure in HVDC systems is ac-fault-induced voltage drop at the inverter terminal. Therefore, numerous studies have been conducted in the past to calculate the amount of voltage drop that causes commutation failure in a converter. The level of voltage drop that could occur on the ac terminal of an HVDC converter without causing a commutation failure has been used in the assessment of the immunity of an HVDC system to commutation failure.

In this section, a quasi-steady-state method for the calculation of the voltage drop that causes a commutation failure introduced in [16] is discussed.

##### **4.4.1. Calculation of Critical Voltage Drop ( $\Delta V_{\text{Min}}$ )**

Reference [16] proposes Formula (4-1) for calculating the maximum permissible balanced voltage drop  $\Delta V$  that can be tolerated (i.e., the drop that does not result in a CF) on the converter's ac busbar. If the voltage dropped by more than this amount commutation failure was presumed to occur. This

equation is derived using the quasi-steady-state converter equations. It calculates the voltage drop  $\Delta V$  that yields the critical value  $\gamma = \gamma_{\min}$  of the extinction angle.

$$\Delta V = 1 - \frac{I'_d}{I_d} \frac{(I_d / I_{dFL}) \cdot X_{cpu}}{(I_d / I_{dFL}) \cdot X_{cpu} + \cos \gamma_{\min} - \cos \gamma} \quad (4-1)$$

In which:

$I_d$  : Pre-fault dc current,

$I'_d$  : Post-fault dc current,

$I_{dFL}$  : Nominal dc current,

$X_{cpu}$  : Transformer per-unit impedance

$\gamma$  : Minimum extinction angle setting

$\gamma_{\min}$  : Extinction angle below which commutation fails

Reference [16] assumes an ideal ac voltage source (not a Thévenin equivalent).  $\Delta V$  is a step drop in the magnitude of this voltage source. It also discusses other simplifying assumptions in deriving the Formula (4-1).

This thesis assesses the validity of this approach in a more realistic situation. A widely-used HVDC test system in the literature is the “First CIGRÉ Benchmark HVDC Test System” [35] that was adopted in this thesis. The test system considers a monopolar, 500 kV, 1000 MW dc transmission scheme. The rectifier end is connected to a 345 kV system with an SCR of 2.5 @ 84°. The inverter end is connected to a 230 kV system with an SCR of 2.5 @ 75°. (See Appendix A for the data.) The nominal control modes were constant current (CC) at the rectifier and constant extinction angle (CEA) at the inverter.

A model of the CIGRÉ Benchmark system was developed on the PSCAD/EMTDC electromagnetic transient simulation program [36]. The

program models the turn-on and turn-off process of the valves, and hence can be used to model the current commutation process in detail.

Using the benchmark model in PSCAD, a three-phase balanced fault was applied on the inverter ac terminal. The fault level (fault current times pre-fault voltage) was equal to 10% of the rated dc power. The system and the fault branch are shown in Figure 4-4, and the simulated ac voltage and dc current plots are given in Figure 4-5. Analysis of the ac voltage and dc current waveforms in Figure 4-5 shows that there is no occurrence of a CF, while a transient dc current rise of 12% and a voltage drop of 13.5% for one phase are observed. However, Equation (4-1) incorrectly predicts that a CF should occur for a voltage drop  $\Delta V$  of only 5.8% for this condition. The reason for this error is that the steady state calculation does not take into account other factors such as phase shifts in the voltage and the transient response of the firing circuits. This example shows that quasi-steady-state equations cannot be accurately used to determine the occurrence of a commutation failure. Hence, detailed electromagnetic transient simulation is recommended to properly consider the CF phenomenon.

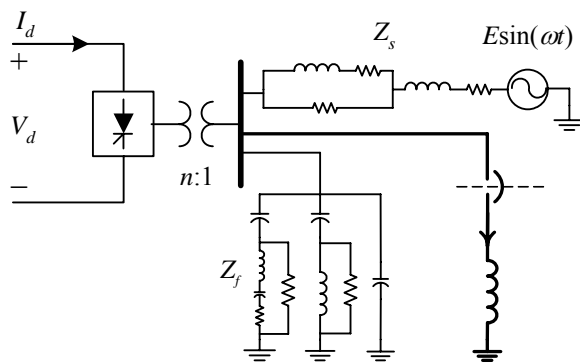


**Figure 4-4: Causing commutation failure in a single-infeed system**

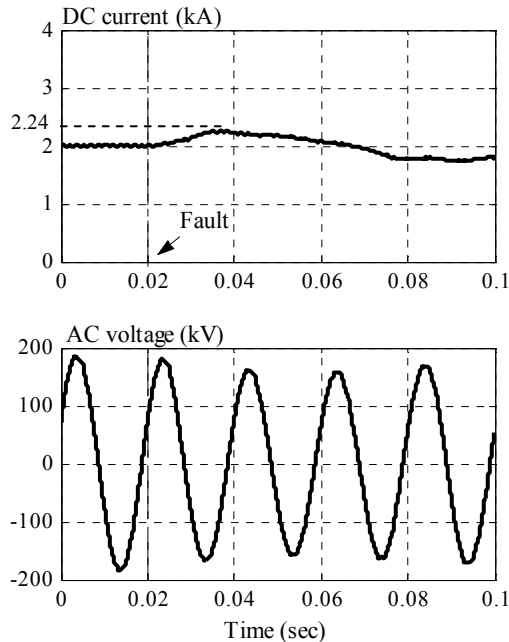


**Figure 4-5: Effect of inductive fault on current and voltage (Fault level is 10% of the dc power)**

An alternative method for analysis of commutation failure developed in this thesis as discussed in the next section.

#### **4.5. Analysis of Commutation Failure Using Detailed EMT Simulations**

As seen in the previous section, the steady-state method could give a poor estimation of the susceptibility of the system to a commutation failure. It only considers the voltage drop aspect of switching the inductance and ignores issues, such as phase shift, which have a significant role in the commutation process. A more accurate analysis of the commutation failure phenomenon is only possible with electromagnetic transient simulation.

One of the major contributions of this thesis is the proposal of an approach for quantifying the commutation failure immunity of an HVDC converter [30]. The details of this study methodology are discussed in this section.

#### 4.5.1. Detection of a Commutation Failure

There are different methods for the detection of a commutation failure in an HVDC converter. In some systems, commutation failures are detected directly from measured valve conduction status. After a valve is gated, valve monitoring signals normally indicate valve conduction. A commutation failure is detected when current is flowing in an inappropriate combination of valves with respect to the valve gating sequence [13]. The approach selected in this thesis is described in [13]; it is based on comparison of the dc current with the valve side ac currents: In the normal operation of a dc converter, Equation (4-2) applies to the currents.

$$|I_A| + |I_B| + |I_C| = 2 \cdot I_{dc} \quad (4-2)$$

During a commutation failure, the ac current on all phases will go to zero and the sum of the absolute values of the ac currents becomes smaller than  $2 \times I_{dc}$ , giving an indication that a CF has occurred.

#### 4.5.2. Probability of a Commutation Failure

This section shows, through the use of an example, that not only the fault level, but also the point on wave (time instant) at which the fault is applied, plays a role in the occurrence of a CF. In this example, a balanced three-phase-to-

ground fault through an inductance on the ac terminal of the CIGRÉ benchmark model is considered (see Figure 4-4). The procedure is as follows.

The CIGRÉ Benchmark model in PSCAD/EMTDC is used as the base case for this analysis. Additional components are added to the case to simulate the application of the inductive faults and to monitor the ac and dc current for detection of a commutation failure. CF detection is performed based on the methodology described earlier in this chapter.

Fifty uniformly distributed fault inductances are selected in the 1.15 H to 1.3 H range and 200 uniformly distributed points on wave are selected within an ac cycle of 20 ms.

Using the multiple-run feature of the PSCAD/EMTDC program, the occurrence of CF is checked for all the combinations of fault inductances and points on wave in the abovementioned range. The results are given in Figure 4-6. The Z-axis in Figure 4-6 shows whether a fault has caused commutation failure or not (0 means no CF and 1 means a CF). The plot in Figure 4-6 shows that for the same value of inductance, a CF may or may not occur depending on the point-on-wave. The reason for dependency of commutation failure on the point on wave switching time is the discrete nature of the triggering of the thyristor valves, occurring at specific time instances. For example if the fault occurs just before a thyristor is triggered, there would not be sufficient time for the valve firing control system to adjust the firing angle. On the other hand if the fault occurs right after switching of a valve, a period of time would be available for the control circuit to make some level of adjustments. The available time depends

on the converter configuration. For a 12-pulse converter, there is a  $360^\circ/12=60^\circ$  period available for adjustment. This is the probable reason for the 12 peaks in the plot in Figure 4-6.

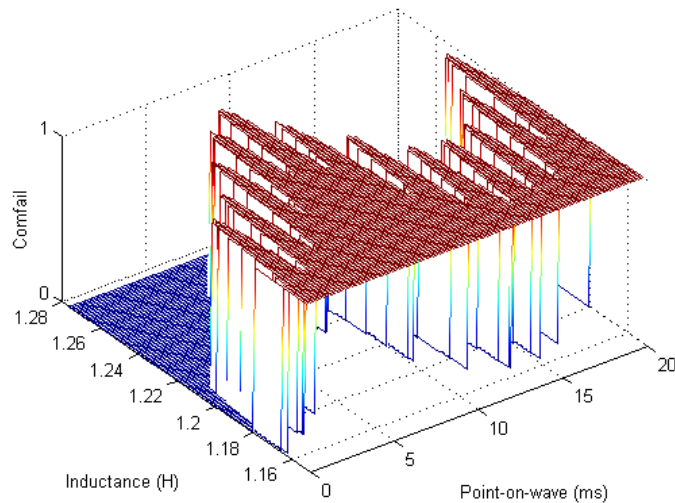


**Figure 4-6 : Dependence of CF occurrence on fault level (inductance) and point on wave**

The dependency of CF on point on wave allows the definition of a CF-probability for any given fault level. Practically, such a probability can be calculated by taking the ratio of the number of points on wave where a CF occurs to the total number of points on wave considered.

Using the above methodology, the probability of a commutation failure occurring for any given three-phase inductive fault on the CIGRÉ benchmark system was calculated, and is shown in Figure 4-7.

- For  $L_{\text{fault}} > 1.27$  H, a CF does not occur for any point on wave (Probability = 0%);
- For  $L_{\text{fault}} < 1.18$  H, a CF occurs for all points on wave (Probability = 100%);
- For  $1.18 \text{ H} < L_{\text{fault}} < 1.27$  H, the probability varies between 0 and 100%.

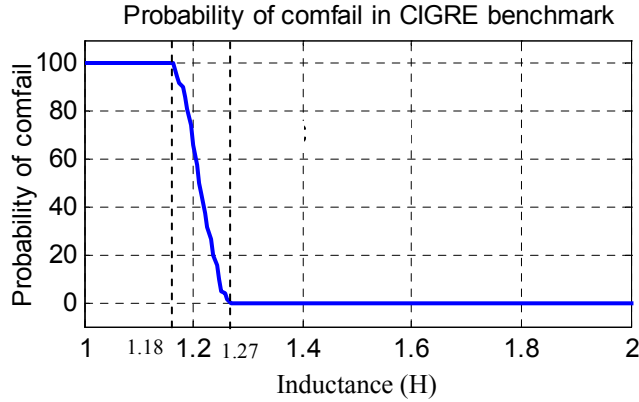


**Figure 4-7 : Probability of a commutation failure for the CIGRÉ benchmark model**

#### 4.5.3. A Per-unit System for Fault Level in CF Studies

In the previous section, the severity of a fault was determined by the size of the inductor, which was expressed in henries. However to generalize the results to different systems, a per-unitization approach is recommended. One approach is to use the fault MVA rather than the fault inductance. Hence, instead of 1.2 H, one can say that the fault level is  $(V_{ac}^2 / (\omega \cdot L_{fault})) = 140$  MVA. However, a 140 MVA fault in a 500 MW dc system is more severe than a 140 MVA fault in a 2000 MW system. Hence, the fault level can be per-unitized by dividing it by the rated dc power. In this thesis, Formula (4-3) is proposed for per-unitizing the CF fault level.

$$CF \text{ Fault Level}(\%) = \frac{CF \text{ Fault level in MVA}}{\text{Rated dc power}} \cdot 100 = \left( \frac{V_{ac}^2}{Z_{fault} \cdot P_{dc}} \right) \cdot 100 \quad (4-3)$$

In Equation (4-3),  $V_{ac}$  is the line voltage,  $Z_{fault}$  is the fault impedance, and  $P_{dc}$  is the rated dc power. The multiplying factor of 100 is used to express the fault



level as a percentage. Using (4-3), the fault through a 1.2 H inductance is the equivalent of a 14% fault level for the CIGRÉ benchmark model.

#### 4.5.4. Selection of the Fault Type in Commutation Failure Studies

As mentioned in the introductory remarks of Section 4.5, the objective of EMT-simulation-based CF analysis is to calculate the critical fault level for the occurrence of a commutation failure. One issue in this context is what type of fault should be applied on the system. Table 4.1 shows a variety of faults that could be selected for this purpose. Among these faults, the two types of commonly used faults were considered: the most severe three-phase fault, and the more common single-phase fault. In the previous section, a three-phase balanced inductive fault was assumed. This section justifies that selection.

**Table 4.1: Common Faults in AC Systems**

No. of Phases in the Fault	Impedance Type
- Three-phase to ground	- Inductive (to model remote faults)
- Line to line to ground	- Capacitive (to simulate filter switching)
- Line to line	- Resistive (to model load switching)
- Single-phase to ground	

The test setup and methodology used in the example in Section 4.5.2 is adopted in this section. The threshold fault level beyond which commutation failure occurs is calculated for each point on wave. The simulations were conducted for all the impedance types and for both single-phase and three-phase faults. The results of this study are given in Figure 4-8. As an example, consider point A on the three-phase inductive fault curve in Figure 4-8. Point A shows

that the maximum three-phase inductive fault level that does not cause commutation failure for a point on wave at 10 ms, is 14.2%.

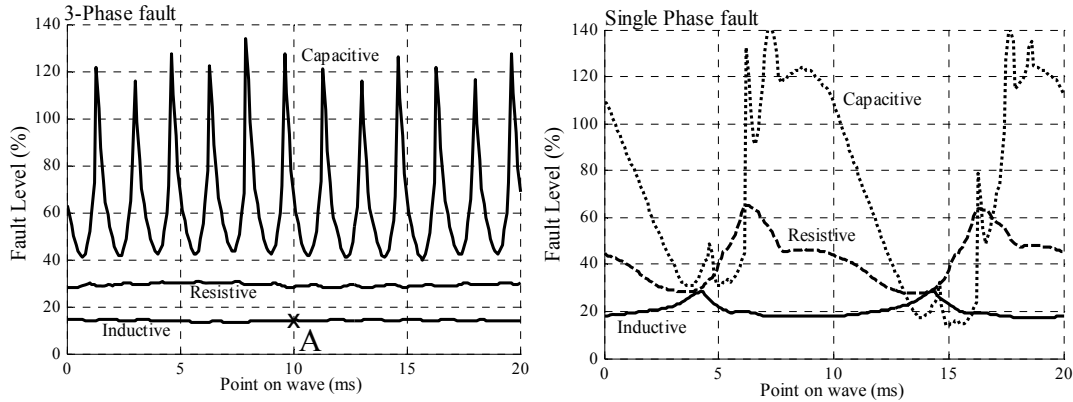


**Figure 4-8: Threshold fault levels for three- and single-phase inductive, capacitive, and resistive faults**

The results show a lower immunity (higher susceptibility) to inductive faults than to resistive faults and capacitive faults. The capacitive fault is applied by connecting an initially discharged capacitor at the busbar, and in contrast to the other two fault impedance categories, the immunity is seen to be more sensitive to the point on wave at which the fault is applied. A fact worth noting is that in the design of an HVDC converter station one of the requirements is that switching a filter/capacitor bank should not cause commutation failure [13]; therefore, the capacitive components are designed accordingly.

Study results show that among the faults listed in Table 4.1, the most severe fault is the three-phase-to-ground fault through a balanced three-phase inductor. Inductive faults are more representative of most actual faults in the system. Therefore, the three-phase inductive fault was selected for the CF studies in this thesis, as it gives the most conservative immunity assessment.

#### 4.6. The Commutation Failure Immunity Index (CFII)

One of the major contributions of this thesis is proposing the commutation failure immunity index (CFII). Basically, the CFII shows the immunity of an HVDC inverter to a commutation failure caused by an ac fault. As discussed in the previous section, the immunity against a commutation failure is generally the lowest for three-phase inductive faults. The inductive fault is representative of the most common situation for voltage depressions, i.e., a fault located on a transmission line that terminates close to the inverter busbar. Therefore, the minimum of the three-phase inductive fault curve in Figure 4-8 can be selected as a single worst-case representative index for CF susceptibility. The CFII is defined in Equation (4-4) by re-stating Equation (4-3) with the fault level replaced by the worst case fault level.

$$CFII = \frac{\text{Worst Critical Fault MVA}}{P_{dc}} \cdot 100 = \frac{V_{ac}^2}{\omega \cdot L_{\min} \cdot P_{dc}} \cdot 100 \quad (4-4)$$

The inductance  $L_{\min}$  is the smallest possible fault inductance that never results in a commutation failure, regardless of whether the fault is single-phase or three-phase, or at what point on wave it is applied. With this definition, the CFII for the example CIGRÉ benchmark system is calculated to be 13.3%. The CFII could also be derived from the commutation failure probability curve: the CFII would be the maximum fault level for which the probability of a CF is zero. Figure 4-9 shows the CF probability curve and the CFII for the CIGRÉ benchmark model.

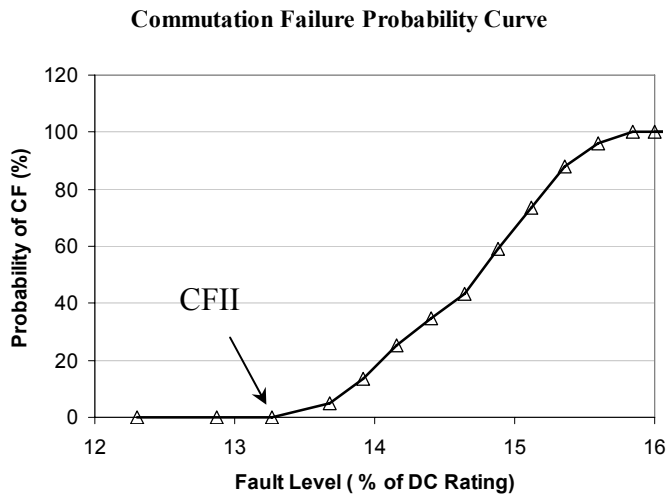


**Figure 4-9: Commutation failure probability curve for the CIGRÉ Benchmark model.**

#### **4.7. Applications of the CFII in Commutation Failure Studies**

In this section, a few examples of the application of the CFII in quantifying the impact of different factors on the commutation failure phenomenon are presented. All of these factors are known to have an impact on commutation failure; however, CFII will give insight into the extent of their impact. The impact of the following factors has been considered:

- Effective short circuit ratio (ESCR)
- Extinction angle order
- Parameters of the inverter PI controller
- Parameters of the rectifier PI controller
- X/R ratio of the ac system
- Impedance of the ac system at higher frequencies
- Size of the smoothing reactor

The application of the CFII is not limited to these factors and could be used for any study related to commutation failure.

#### 4.7.1. CFII as a Function of Effective Short Circuit Ratio (ESCR)

One of the most widely used indices in the analysis of HVDC systems is the effective short circuit ratio (ESCR) index. The definition of ESCR is given in Chapter 2 and is repeated in (4-5) for convenience.

$$\text{ESCR} = \frac{\text{Short Circuit Level at converter ac terminal} - \text{Filter ratings}}{\text{Rated dc power}} = \frac{SCL - Q_f}{P_{dc}} \quad (4-5)$$

In this section, the CFII values for systems with ESCRs ranging from 1.5 to 5.0 are calculated and shown in Figure 4-10. These results show that there is a linear correlation between the ESCR and the CFII indices; systems with higher ESCRs have more immunity to commutation failure.

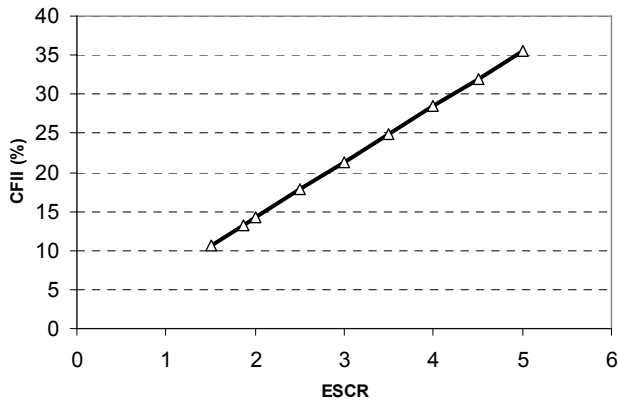


**Figure 4-10: Impact of the ESCR on the CFII**

#### 4.7.2. Impact of Increasing the Minimum Extinction Angle ( $\gamma_{\min}$ )

In the CIGRÉ benchmark model, the design value for the minimum extinction angle ( $\gamma$ ) in the inverter controller is  $15^\circ$ . From the point of view of reducing reactive power demand, a lower  $\gamma$  value is preferred. A lower  $\gamma$  also reduces the harmonic current and the stress on the thyristor valves [14]. Higher  $\gamma$  values are better when CF is considered. To assess the impact of  $\gamma$  on the probability of a

commutation failure, the CFII for varying  $\gamma$  values are calculated for the CIGRÉ Benchmark model and plotted in Figure 4-11. It shows that by increasing  $\gamma$  from  $15^\circ$  to  $20^\circ$ , the CFII goes up from 13.3 % to 23.0%. However, with the  $5^\circ$  increase in  $\gamma$ , the converter reactive power demand goes up from 577 Mvar to 689 Mvar, a 19% increase which the ac system may not be capable of supplying.

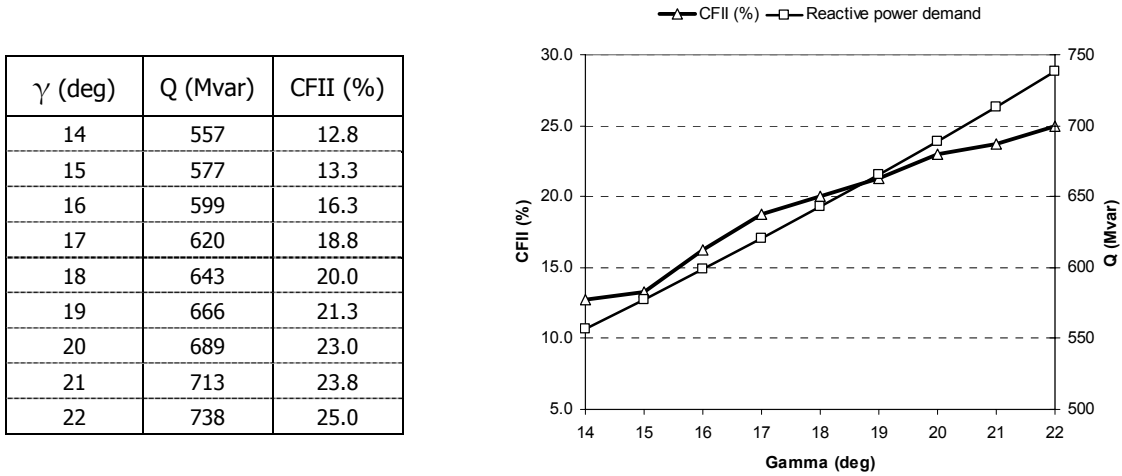


**Figure 4-11: Impact of  $\gamma$  on the reactive power and the CFII**

#### 4.7.3. Parameters of the Inverter Extinction Angle Controller

In the CIGRÉ benchmark model, the rectifier controls the dc current and the inverter operates with constant extinction angle  $\gamma$ . To assess the impact of the inverter controller parameters on commutation failure susceptibility, the gains of the  $\gamma$  controller were multiplied by numbers ranging from 0.1 to 2.5. The proportional-integral (PI) controller parameters of the original CIGRÉ Benchmark model are given in Table 4.2 and the values of the CFII for a range of PI controller gains are shown in Figure 4-12.

**Table 4.2: Parameters of the Gamma Controller at the Inverter**

Parameter	CIGRÉ Model
Proportional gain	0.7506
Integral time constant (sec)	0.0544
Maximum output (deg)	90.0
Minimum output (deg)	29.8

The results indicate that the correlation between the controller gains and the CFII is nonlinear and the immunity to commutation failure varies between 11.4% and 18%. Further research is needed to examine the high sensitivity of the CFII to the PI controller gains when the values are multiplied by two.

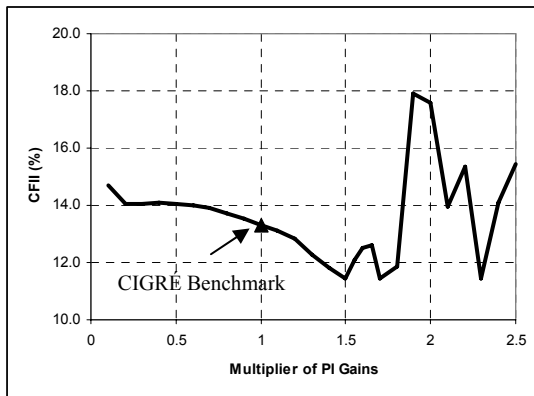


**Figure 4-12: Impact of inverter PI controller gains on the CFII**

#### 4.7.4. Parameters of the Rectifier Current Controller

In this section, in order to assess the impact of the rectifier controller parameters on commutation failure performance the gains of the current controller were multiplied by numbers ranging from 0.1 to 2.5. The PI controller parameters of the original CIGRÉ benchmark model are given in Table 4.3, and the values of the CFII for the range of PI controller gains are shown in Figure 4-13. The results indicate that the correlation between the controller gains and the

CFII is nonlinear and the immunity to commutation failure varies between 13.0% and 19.9%. The higher immunity with controller gains multiplied by 2 is probably due to the tighter control of dc current resulting from the higher gains. It should be noted that in the design of the HVDC control systems, the controller gains are selected based on a range of operating conditions and their values should not be changed without full consideration of the effects on overall system performance.

**Table 4.3: Parameters of the Current Controller at the Rectifier**

Parameter	CIGRÉ model
Proportional gain	1.0989
Integral time constant (sec)	0.01092
Maximum output (deg)	175
Minimum output (deg)	29.8

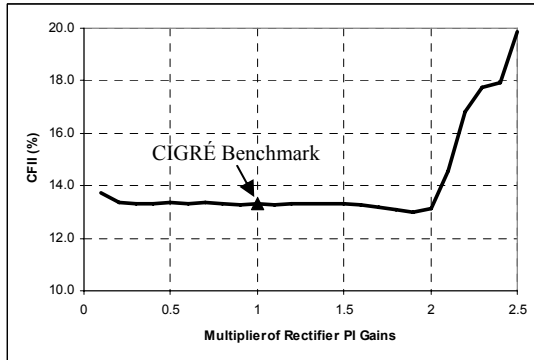


**Figure 4-13: Impact of rectifier PI controller gains on the CFII**

#### 4.7.5. Impedance of the AC System at Higher Frequencies

In the CIGRÉ benchmark model, the impedance of the inverter’s ac system,  $Z_s$ , at the fundamental frequency is  $21.16 \angle 75^\circ \Omega$ . The equivalent circuit originally used in the CIGRÉ benchmark model is shown in Figure 4-14.a. To investigate the impact of the source impedance model and its high-frequency characteristics on the CFII value, an alternative representation based on a series RL combination



(see Figure 4-14.b) is also considered. The R and L elements were selected to yield the same  $Z_s$  at the fundamental frequency (i.e., the same SCR); however, the frequency response of the two representations is distinctly different, as shown in Figure 4-15.

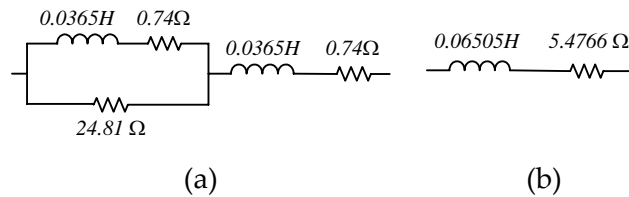


**Figure 4-14: Source impedance ( $Z_s$ ), (a) original CIGRÉ model, (b) Series RL model**

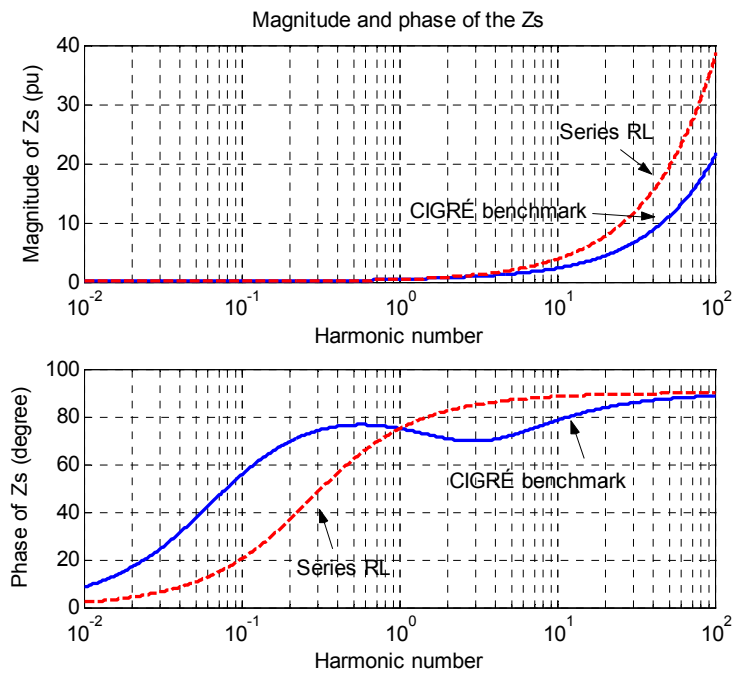


**Figure 4-15: Comparison between the magnitude and the phase of the source impedance models**

The  $L_{min}$  and CFII values were calculated for both representations and the results are given in Table 4.4. Although the SCR of the system does not change with either of the  $Z_s$  models, the higher CFII associated with the original CIGRÉ

model (about 19% higher) indicates that the system is more immune to commutation failure than the system with a simple RL equivalent representing the ac system.

**Table 4.4: Comparison between Various Source Models**

Parameter	CIGRÉ model	Series RL model
SCR	2.5	2.5
Zs (at 50 Hz)	$0.4 \angle 75^\circ$ pu	$0.4 \angle 75^\circ$ pu
Lmin (H)	1.26	1.55
CFII (%)	13.3	10.9

The CFII analysis shows that the frequency dependence of the ac system impedance plays an important role in commutation failure susceptibility. A simple 60 Hz impedance and phase angle as is used in the SCR definition cannot give accurate results.

#### 4.7.6. Impact of the X/R Ratio of the AC System Impedance

In this example, the effect of the X/R ratio of the ac system's Thévenin impedance on the CFII is studied. The test system is the CIGRÉ benchmark model with a different ac source impedance. The model of the ac source impedance in the CIGRÉ benchmark is more detailed, but for the purposes of this study it was replaced with a simple series RL model. For this parametric study the value of Zs in Figure 4-16 is kept constant at its value in the CIGRÉ benchmark model (21.16  $\Omega$ ), while the impedance angle,  $\phi$ , which is  $75^\circ$  in the benchmark model, is varied so that it creates X/R ratios between 1 and 20. The results are shown in Figure 4-17. In all cases the system has the same short circuit ratio magnitude. The CFII

analysis shows that the value of  $X/R$  plays a role in commutation failure susceptibility and the value of CFII.

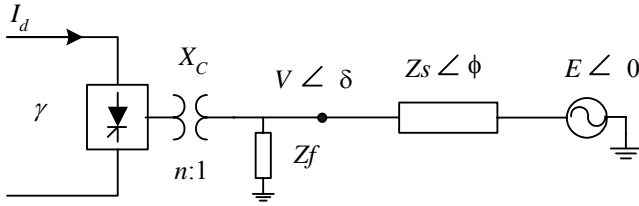


**Figure 4-16: Schematic diagram of the inverter side**

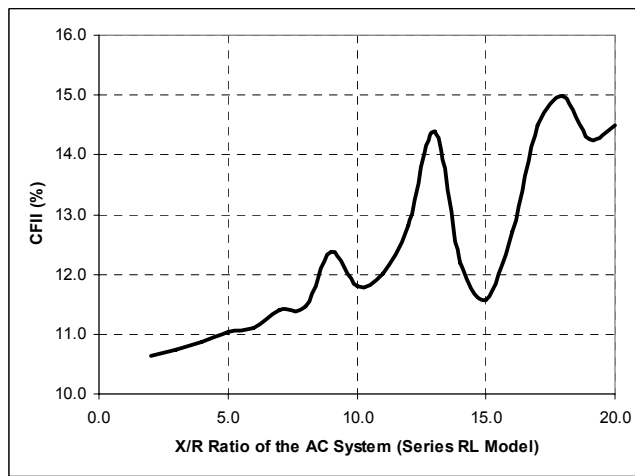


**Figure 4-17: Impact of the X/R ratio on CFII**

#### 4.7.7. Impact of Increasing the Size of the Smoothing Reactor

Any ac fault at the inverter end of a dc link transiently drops both the ac and the dc voltages. Because of the dc voltage drop at the inverter side, the voltage across the dc line will increase, and subsequently, the dc current will increase. The lower commutating voltage caused by the ac fault, combined with the higher dc current, increases the probability of a commutation failure. The dc smoothing reactor, which plays a variety of other roles, also limits the rate of change of the dc current. In the CIGRÉ benchmark model, a total of 1.194 H reactor is

represented in the dc line equivalent [35]. The total inductance includes the dc line inductance and the smoothing reactor.

As a sensitivity study, the inductance at each end of the line was varied to assess its impact on the CFII. The simulation results given in Figure 4-18 show that the dependence of the CFII on the size of the smoothing reactor can be divided into two regions. In region 1, shown in Figure 4-18, increasing the size of the smoothing reactor increases the CFII. The reason is that the larger smoothing reactor limits the rate of rise of the current and therefore reduces the probability of commutation failure.

In region 2 diminishing returns are obtained because any increase in the inductor size reduces the CFII. The reason for the higher CFII for the larger smoothing reactor in region 2 is probably the mismatch between the smoothing reactor size and the parameters of the converter controllers. These results show that increasing the size of the smoothing reactor without coordination with the ac system and the HVDC control could result in deterioration of the commutation failure susceptibility.

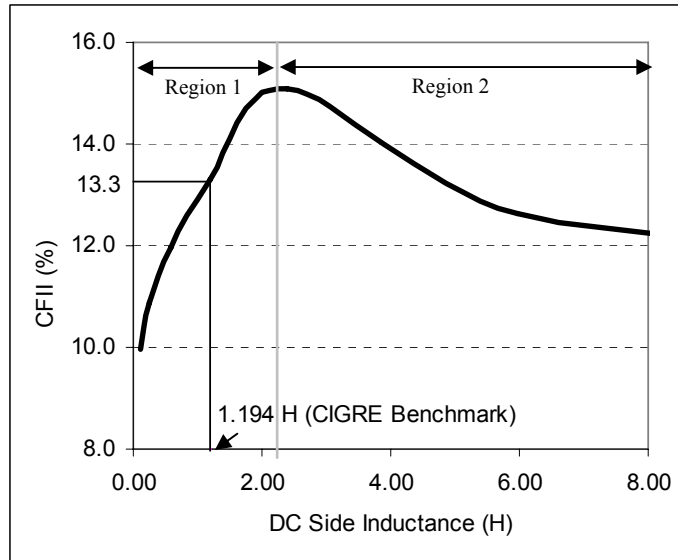


**Figure 4-18: Impact of dc side inductance on the CFII**

#### **4.8. Impact of the HVDC Rating on Commutation Failure**

In the simulations performed in this report so far, the rating of the dc system is equal to the 1000 MW nominal rating of the CIGRÉ benchmark model. To develop a dc system with different nominal ratings one or more of the following parameters should change at both the inverter and the rectifier to keep the per-unit values constant:

- The ratings of the ac filters
- The MVA rating of the converter transformer
- The nominal current and voltage (both dc and ac)
- The impedances at the dc side

The study results show that if all the above parameters are adjusted according to the ratings of the dc system the CFII value will remain constant. However, to examine the impact of the dc voltage and the dc current ratings on the commutation failure performance three case studies have been considered.

The test system has the same configuration as the CIGRÉ Benchmark model but the ESCR is 3.0 ( In CIGRÉ model ESCR = 1.87). Details of the cases are discussed in the following three subsections.

#### 4.8.1. Case-Study 1: $V_{dc} = 500$ kV, Nominal $I_{dc}$ Varies

In Case Study 1, the dc voltage is kept constant at 500 kV while the nominal dc current varies between 200 A and 4000 A to create systems with different power ratings. The ac filters, the converter transformers MVA, and the ac system are modified to represent ac/dc systems with different ratings but with the same effective short circuit ratio of 3.0. The values of the CFII are calculated for the above systems and shown in Figure 4-19. This case study shows that although ESCR is constant, the CFII value increases as the nominal dc power (and hence nominal dc current) increases. The reason is that at higher nominal dc currents while nominal dc voltages are kept constant the per-unit value of the smoothing reactor is higher ( $Z_L$  in per unit =  $Z_L/Z_{base}$ ,  $Z_{base} = V_{dc}^2/I_{dc}$ ). Therefore, as shown in region 1 in Figure 4-18, the CFII is higher for systems with a larger smoothing reactor.

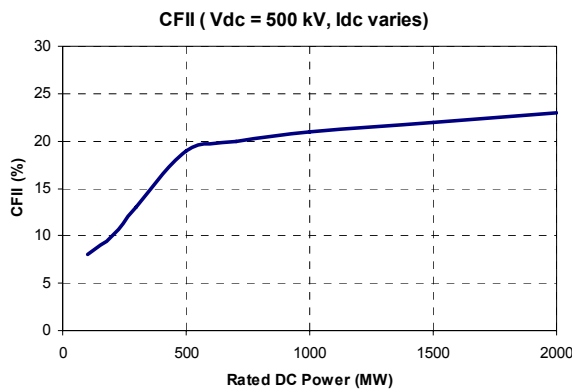


**Figure 4-19: The CFII for systems with different ratings (  $V_{dc} = 500$  kV,  $200$  A <  $I_{dc}$  <  $4000$  A )**

#### 4.8.2. Case Study 2: $I_{dc} = 2000$ A, Nominal $V_{dc}$ Varies

In Case Study 2, the nominal dc current is kept constant at 2000 A while the nominal dc voltage varies. The results are given in Figure 4-20, and they show that in this case the immunity to commutation failure is lower for higher dc voltages. The reason for the higher CFII at lower nominal dc voltage is the same as discussed regarding Case Study 1. At higher nominal dc voltages, while nominal dc currents are kept constant the per-unit value of the smoothing reactor is lower ( $Z_L$  in per unit =  $Z_L/Z_{base}$ ,  $Z_{base} = V_{dc}^2/I_{dc}$ ) and so is the CFII (region 1 in Figure 4-18).

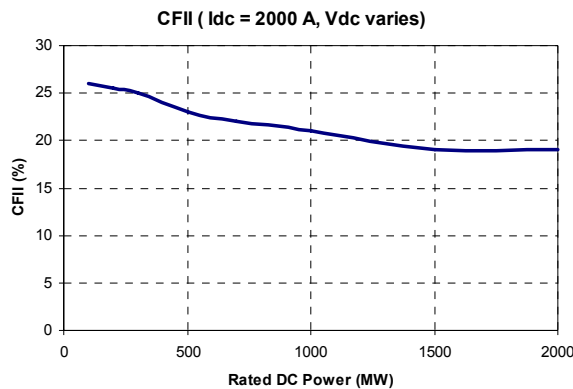


**Figure 4-20: The CFII for systems with different ratings ( $I_{dc} = 2000$  A,  $50$  kV  $< V_{dc} < 1000$  kV )**

#### 4.8.3. Case Study 3: Both Nominal $I_{dc}$ and $V_{dc}$ Vary but $V_{dc}/I_{dc}$ is constant

In Case Study 3, both the nominal dc current and the nominal dc voltage are varied to create systems with different ratings. The ratio of dc voltage to dc current is kept constant. The study results given in Table 4.5 and Figure 4-21 show that the immunity to commutation failure is the same for all the ratings.

The explanation for this is that keeping the nominal  $V_{dc}$  and  $I_{dc}$  constant means that the  $Z_{base}$  for the per-unitization of the dc side parameters remains unchanged, and as a result the per-unit values of the smoothing reactor and the dc line resistance remains the same for different ratings. These results show an important feature of the CFII, which is its applicability for systems with different ratings as long as the per-unit values of the dc side impedances are the same.

These results show that the CFII is a probability-based index and is useful in assessing the CF performance of different ac systems on a comparative basis.

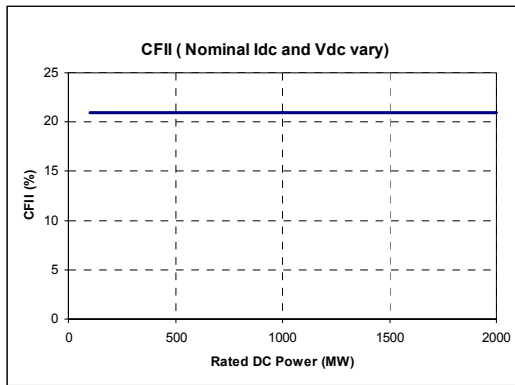


**Figure 4-21: CFII for varying Idc and Vdc (200 A < Idc <4000 A, 50 kV < Vdc <1000 kV )**

**Table 4.5: Impact of DC Voltage and Current on the CFII**

DC Power (MW)	Idc (A)	Vdc (kV)	ESCR	CFII (%)
100	632	158	<b>3.0</b>	21
200	894	224		21
300	1095	274		21
500	1414	354		21
700	1673	418		21
<b>1000</b>	<b>2000</b>	<b>500</b>		<b>21</b>
1500	2449	612		21
2000	2828	707		21



## 4.9. Calculation Methodology for the CFII Index

As discussed in the previous sections, due to the complexity of the commutation failure phenomena  $L_{\min}$  could only be calculated using digital simulation. The value of  $L_{\min}$  is required for the calculation of the CFII and can be determined by repeatedly simulating several cases with varying values of inductance. The multiple-run feature available in many emtp-type programs allows the user to conduct parametric studies by consecutively running a simulation case with a series of sequentially or randomly generated parameter sets. It was shown previously that the occurrence of commutation failure is affected by point on wave as well as by the size of the inductance.

The multiple-run feature of the PSCAD/EMTDC program [36] was used in this study to automatically run the simulations varying both the point on wave switching and the inductor size to find the value of  $L_{\min}$ . Three multiple-run (MR) based approaches have been tested for this purpose and are detailed in the following three subsections:

- The conventional multiple-run method
- The optimization-based method
- The strategically guided multiple-run method

### 4.9.1. Conventional Multiple-Run Method

This method is the same as the method discussed in Section 4.5.2. In this method, a two-dimensional grid is formed from inductances and points on wave as is partially shown in Figure 4-22.

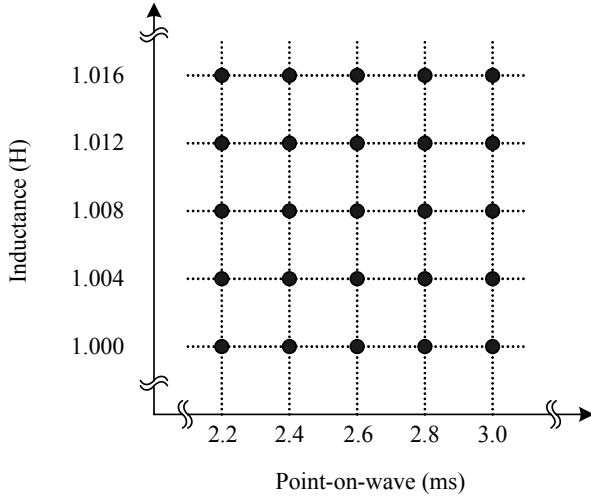


**Figure 4-22: Part of the grid of inductance and point on wave**

For each point on the grid a simulation is carried out and it is observed if a commutation failure occurs. When all the “runs” are finished,  $L_{min}$  is directly obtained as the smallest inductor that does not cause a commutation failure on any point on wave. Equation (4-4) could then be used to calculate the CFII. Table 4.6 shows an example of the range of variables and the required number of simulations in the conventional multiple-run method.

**Table 4.6: Details of the Example for Conventional Multiple-Run Methods**

Conventional Multiple Run				
Range for $L$	Range for $T$	$\Delta T$ (ms)	$\Delta L$ (H)	Number of runs
[1.0,1.4] H	[0,20] ms	0.2	0.004	10000

The main drawback of the conventional multiple run approach is the excessively large number of simulations required, which is caused by the fact that the search is unintelligent and cannot be easily confined or terminated within an arbitrary feasible region [37]. Simulations are conducted over areas that could be eliminated through the use of enhanced methodologies. For

example, if a certain value of inductance does not cause a commutation failure at a given instant of time, then there is no need for trying larger inductances at that point. Such knowledge cannot be incorporated in the conventional method and simulations are performed on all the predefined values of inductor and point on wave. It should, however, be stated that the multiple run is a powerful method when parametric studies are required as it makes no pre-assumptions of the interdependencies in complicated networks.

Indeed, for MI systems considered in Chapter 5, the above assumptions proved not to be always true. For example, contrary to expectations, decreasing the fault level increased the probability of commutation failure [19].

### 4.9.2. Optimization-Based Method

PSCAD/EMTDC has a feature that allows for multiple runs to be modified by non-linear optimization algorithms [36]. Several optimization methods are possible [38]; of these, the genetic algorithm method was selected in this thesis due to the non-linearity of the CF phenomena. The calculation of  $L_{min}$  was formulated as an objective function and genetic algorithm was attempted to calculate the  $L_{min}$ . Although it created a reduction in the number of runs compared to the conventional multiple run method, the reduction was not significant [37]. Hence, this approach was not pursued further in this thesis. Details of the optimization-based method for CFII calculations are discussed in [37].

### 4.9.3. Strategically Guided Multiple-Run Method

The conventional multiple-run method, described previously, is capable of finding the value of  $L_{min}$ , but requires a large number of simulations. This is due to the lack of the ability to intelligently eliminate regions that do not contain the solution. To address this issue, an enhanced search methodology has been developed and coupled with the transient simulation so that the MR simulations are intelligently supervised. The underlying assumption in this method is that for a given instant of time, finding an inductor size that does not cause commutation failure means that larger inductors will not cause a commutation failure for the same point. The method is schematically represented in the flowchart in Figure 4-23. As shown, the approach is to do a quick search with large steps in the inductor size and testing it only on a few points on wave to get an estimate of the value of  $L_{min}$ . This is accomplished by the execution of two loops following the initialization. At the end of the execution of the first two loops, the value of  $L_{min}$  is recorded. This procedure will be repeated several times with smaller increments in inductor size to obtain the  $L_{min}$  with sufficient accuracy. As the time-step ( $\Delta T$ ) decreases at each stage, the final  $L_{min}$  will be tested on many points on wave.

The procedure shown in Figure 4-23 is implemented in the PSCAD/EMTDC transient simulation program as a component supervising and steering the MR simulations. Part of the designed component is shown in Figure 4-24.

The component was tested to find the  $L_{min}$  for the CIGRÉ benchmark model. The successive refined values of  $L_{min}$  are shown in Table 4.7. The final value of

$L_{min}$  has a tolerance of 0.004 H, which is obtained after only 385 simulations. The conventional multiple-run requires 10000 simulations.

The tolerance of the calculated  $L_{min}$  can be arbitrarily small, resulting in a very accurate solution, albeit obtained at the expense of more simulations.

**Table 4.7: Results of  $L_{min}$  Calculations using Guided Multiple-Run Methods**

<b>Strategically Guided Multiple Run</b>				
Stage	$\Delta T$ (ms)	$\Delta L$ (H)	$L_{min}$	Number of runs (cumulative)
1	6.4	0.256	1.312	6
2	3.2	0.128	1.312	15
3	1.6	0.064	1.312	34
4	0.8	0.032	1.280	59
5	0.4	0.016	1.264	109
6	0.2	0.008	1.264	247
7	0.2	0.004	1.264	385

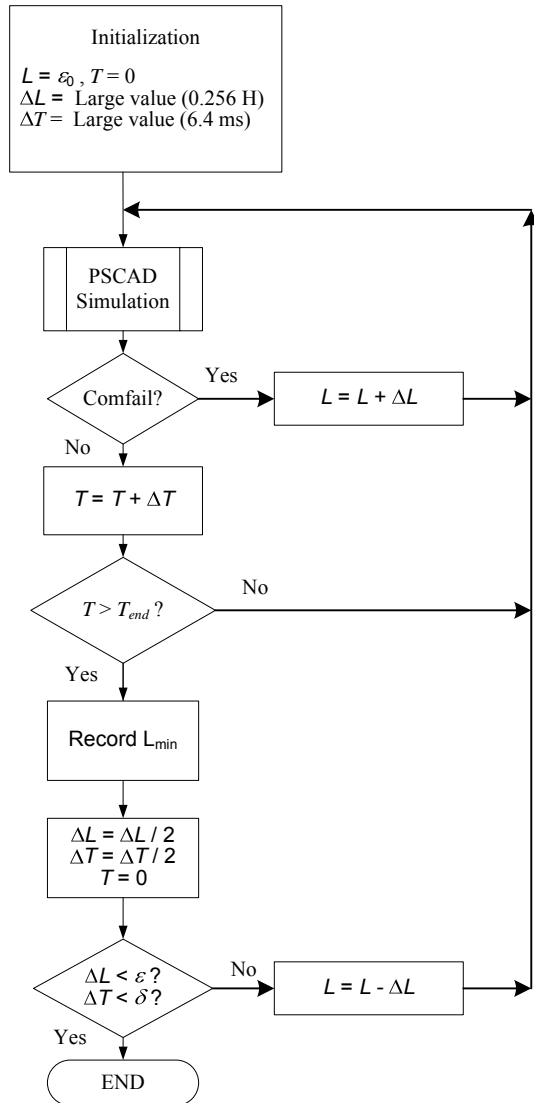


Figure 4-23: Routine to find the  $L_{\min}$  with the desired accuracy

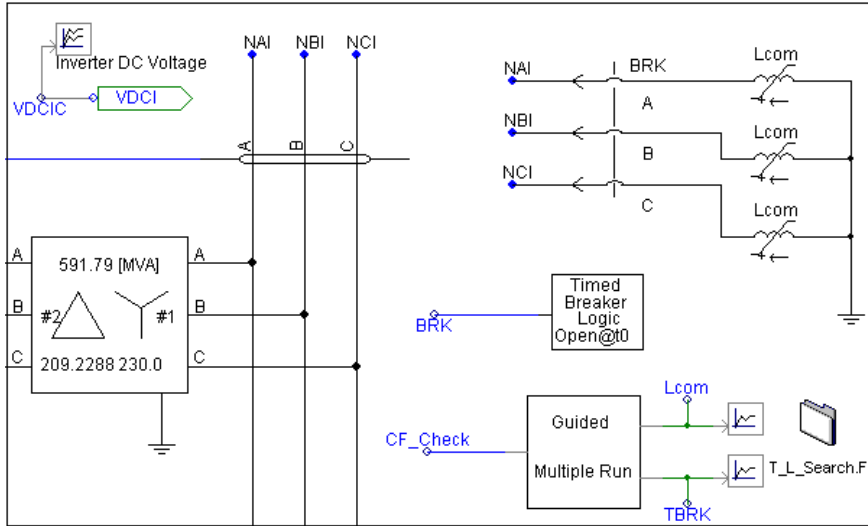


Figure 4-24: Part of PSCAD/EMTDC case for finding the  $L_{min}$

#### 4.10. Summary and Conclusions of Chapter 4

The first conclusion of this chapter is that the simple deterministic formulas given previously in the literature are not accurate enough to be used to determine the susceptibility of realistic HVDC systems to commutation failure. Simulation-based methods give more accurate results.

A newly defined index called the commutation failure immunity index (CFII) is determined by calculating the largest inductive fault the system can tolerate without a commutation failure. Using this index, the impacts of several system parameters such as ESCR, HVDC controller gains, and the damping of the ac systems on commutation failure are parameterized.

The strategically guided multiple run method is recommended for the calculation of the CFII. The computational burden is significantly reduced using this method.

## **5. Commutation Failure in Multi-Infeed HVDC Systems**

### **5.1. Introduction**

The commutation failure phenomenon in single-infeed systems was discussed in Chapter 4. The inter-converter interactions in multi-infeed systems can potentially affect the CF behaviour of the converters [19]. In this chapter, the impact of a multi-infeed configuration on the commutation failure phenomenon is analyzed. In MI systems, a local fault can cause a commutation failure on only the local converter or concurrently on local and remote converters. The former is called a local commutation failure and the latter is called a concurrent commutation failure. The local and concurrent CF phenomena are analyzed in this chapter.



This chapter also examines CF in the case of having the MI configuration that consists of systems with different power ratings. Results of a parametric study to evaluate the impact of MIIF on the immunity of the converters to an ac fault are also presented.

## **5.2. Importance of the CF Phenomenon in MIHVDC systems**

The commutation failure phenomenon in a single HVDC scheme and its consequences were discussed in Chapter 4. It was concluded that for any HVDC system, especially in the case of a weak ac system, it is critical to identify, evaluate, and mitigate any possible issue with regard to commutation failure. Due to the inter-converter interactions, commutation failure is a more complex phenomenon when several converters are operating in close proximity [13],[39].

To investigate the commutation failure performance of multi-infeed HVDC systems, a multi-infeed test system with two dc infeeds was used (Figure 5-1). Each HVDC scheme has a voltage rating of 500 kV and a power rating of 1000 MW. The detail data for the test system including the parameters of the impedances ( $Z_{S1}$ ,  $Z_{S2}$ , and  $Z_{tie}$ ) are given in Appendix A. The two ac sources ( $E_1$  and  $E_2$ ) along with  $Z_{S1}$ ,  $Z_{S2}$ , and  $Z_{tie}$  represent a two port equivalent network for the ac system to which the two HVDC schemes are connected.

Application and detection of commutation failures was carried out using similar methodology to that used for single-infeed systems, which was described in Chapter 4. A balanced three-phase inductive fault was applied on bus 1 and both converters were monitored for the occurrence of a commutation failure.

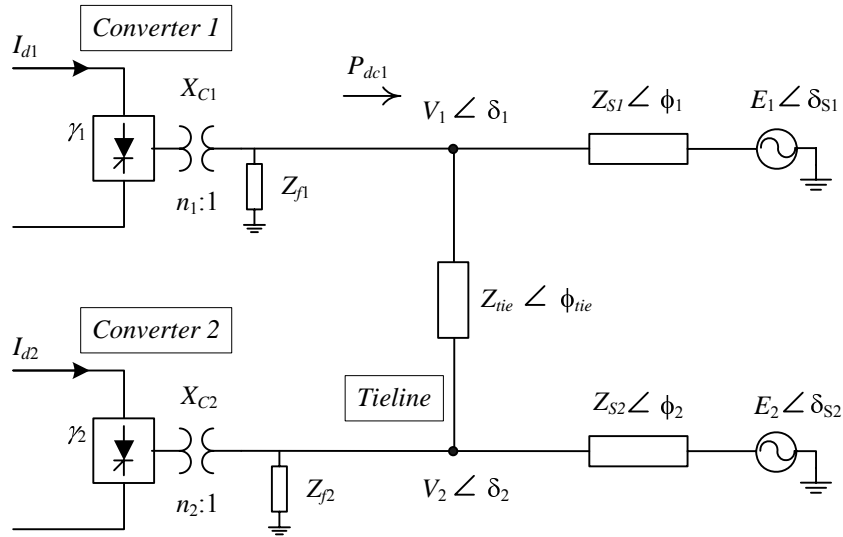


**Figure 5-1: Multi-infeed HVDC test system**

### 5.2.1. Local and Concurrent Commutation Failure

The study results showed that, depending on the severity of fault, the system configuration, and the operating conditions, an ac fault could result in a commutation failure for only the nearby dc converter or it could concurrently cause commutation failure(s) for nearby and remote dc converters. Hence, the commutation failures caused by an ac fault are divided into two categories: local commutation failure and concurrent commutation failure. For example, in a typical MI system such as the one shown in Figure 5-1, if an ac fault on bus 1 causes a commutation failure only for converter 1, the phenomenon is called a local commutation failure; whereas, if a fault on bus 1 causes commutation failure(s) for the local and remote converters, the event is called a concurrent commutation failure.

Both local and concurrent CFs cause interruption of the power delivered to the receiving ac system. However, with a concurrent CF several converters suffer commutation failure at the same time, which has more serious consequences, especially in weak ac systems.

Given the above reasons, it is imperative that the commutation failure phenomenon in multi-infeed HVDC systems be examined. The following sections will discuss local and concurrent commutation failures.

### 5.3. Local Commutation Failure

This section analyses how the severity of a fault can result in a commutation failure only for the local converter. The methodology for this study, which is described in [19], is to apply a CF-inducing fault at the converter 1 ac bus, as shown in Figure 5-1. The CF of converter 1 due to such fault is classified as a local commutation failure.

In a manner similar to that used for single-infeed HVDC systems, the commutation failure immunity index (CFII) could be defined to quantify the immunity of the system to local commutation failure. The definition of the local CFII, given in (5-1), is that it is the largest fault level (smallest three-phase inductor) that could be switched on the ac bus 1 without causing a CF for the converter 1 at any point on wave.

$$\text{Local CFII} = \frac{\text{Critical Fault MVA on Bus 1}}{P_{dc1}} \cdot 100 = \frac{V_{ac1}^2}{\omega \cdot L_{min1} \cdot P_{dc1}} \cdot 100 \quad (5-1)$$

The results of a parametric study carried out for this thesis in order to evaluate the impact of different parameters on the local CFII is given in the following section.

### 5.3.1. Impact of System Parameters on the Local CFII

As described in Chapter 3, the ESCR parameter for each of the converters in an MIHVDC system is determined by the equivalent impedance seen at the ac bus of that converter looking into the entire ac system.

In this parametric study, the tie-line impedance ( $Z_{tie}$  in Figure 5-1) is kept constant while the  $Z_{S1}$  and  $Z_{S2}$  parameters are varied to create different system configurations. The local CFII values for several test systems with the ESCR1 maintained at a value of 2.0 are given in Table 5.1. Both converters operate at the rated conditions prior to the fault application.

**Table 5.1: Impact of System Parameters on the Local CFII**

ESCR1	ESCR2	MIIF <sub>2,1</sub>	Local CFII (%)
2.0	2.0	0.64	13.3
2.0	3.0	0.45	13.7
2.0	4.0	0.35	13.9
2.0	5.0	0.28	13.7
2.0	6.0	0.24	13.5
2.0	7.0	0.21	13.4
2.0	10.0	0.15	13.6
SINGLE INFEED SYSTEM			
2.0	-	-	13.6

The results show that, although there is a considerable change in the MIIF<sub>2,1</sub> and ESCR<sub>2</sub> values, the immunity index is almost constant as long as the local ESCR is constant. Similar tests were carried out on systems with different ESCR<sub>1</sub> values, and the conclusion is that the local CFII is affected mainly by the local

short circuit ratio, not by the inter-converter interactions. The local CFII is also very close to that of a corresponding single-infeed system, which shows an immunity index of 13.6%.

#### **5.4. Concurrent Commutation Failure**

As discussed in the introductory remarks of this chapter, a concurrent commutation failure in an MIHVDC system could have serious consequences and the possibility of this phenomena occurring should be analyzed when the system is designed. One of the major contributions of this thesis is demonstrating that multi-infeed HVDC systems could have an anomalous behaviour with regard to concurrent commutation failure. In summary, the anomalous behaviour is the occurrence of a commutation failure for strong systems under circumstances in which the probability of commutation failure is perceived to be low. This anomalous behaviour could only be detected by detailed electromagnetic transient simulations. Note that due to this anomalous behaviour the strategically guided multiple-run method is not applicable for analysis of concurrent commutation failure because it always assumes the probability of commutation failure increases as the fault level increases [37]. This assumption is not always valid in multi-infeed system.

The anomalous behaviour and its cause are discussed in detail in the following section.

### 5.4.1. Anomalous Commutation Failure in MIHVDC Systems

A typical commutation failure probability curve for a single-infeed system is shown in Figure 5-2. The curve is generated by simulating the application of an inductive fault on many points on wave and calculating the ratio of the number of the points for which the commutation failure occurs. It is expected that no commutation failure occurs at very low fault MVA. As the fault level increases, the probability of CF increases and eventually reaches 100% at high fault MVAs.

To demonstrate the occurrence of an anomalous commutation failure in this thesis, the commutation failure probability curves were calculated for three case studies.

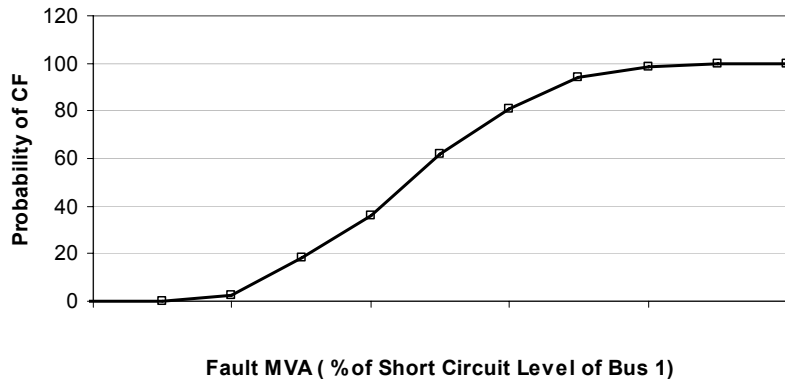


**Figure 5-2: Probability of a commutation failure as a function of fault level**

The following case studies, which have varying levels of interactions, were considered in order to investigate the impact of mutual interactions on concurrent CF. In all three cases the following parameters are constant:  $ESCR_1=2$ ,  $ESCR_2=5$ , and tie line length is 80 km. Each HVDC link has the same configuration as the CIGRÉ Benchmark model and is operating at nominal

operating conditions ( $V_{dc} = 500$  kV and  $P_{dc} = 1000$  MW) prior to application of the fault.

### Case 1: A System Similar to a Single-Infeed Configuration

The test system for this case is shown in Figure 5-3. Only one HVDC converter is connected to the ac system and an ac fault is applied on a remote bus. In other words, this case represents a multi-infeed system in which the local converter is disconnected from the network, creating a single-infeed configuration with a remote fault (Figure 5-3). Three-phase balanced inductive faults are then applied at bus 1, and converter 2 is monitored for the occurrence of a commutation failure.

The reason for this case study is to provide a baseline for comparison of the system performance after adding another HVDC system to create a multi-infeed configuration.

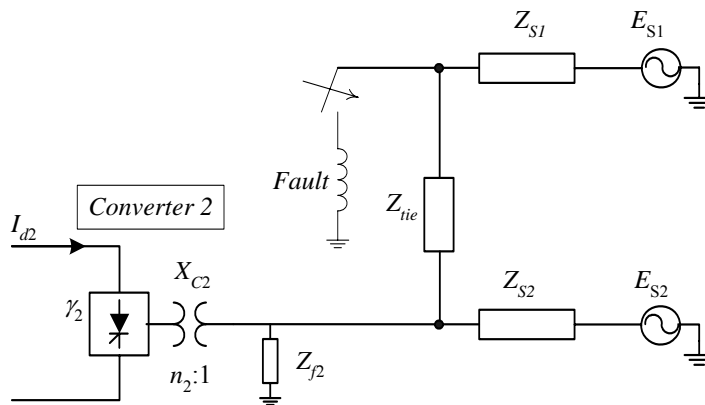


**Figure 5-3: Test system for Case 1**

The commutation failure probability curve for this case is shown in Figure 5-4. As expected, at low fault MVA (up to 35% of the short circuit capacity

at bus 1) no commutation failure occurs. The probability of a CF occurring increases with the increase in the severity of the faults, so that for fault levels above 55% of the short circuit capacity at bus 1, a commutation failure occurs for all points on wave (probability = 100%). No anomalous behaviour is observed in this case.

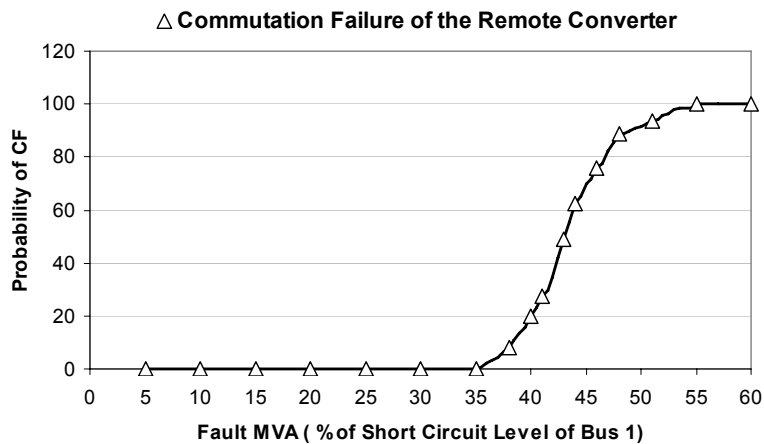


**Figure 5-4: CF probability curve for Case 1 (Converter 1 is disconnected from the network)**

### Case 2: Two Converters in Operation (Multi-Infeed System), Limited Interactions

In this case study, initially, both HVDC converters are operating at nominal power and, in a manner similar to Case 1, faults of different severity are applied at bus 1. The probabilities of a CF for the local converter connected at bus 1 and for the remote converter connected at bus 2 are calculated. One feature intentionally introduced in this case study is blocking the local converter upon detection of a commutation failure in the converter. This was done to limit the post-CF interactions between the converters in order to be able to investigate the



onset of the commutation failure in the remote converter, rather than analyzing the impact of the recovery of one converter from a commutation failure on the performance of the remote converter. Another reason to block the local converter after a CF is that in many actual HVDC schemes after detection of a CF the control system makes the necessary adjustments in the valve firing signals to prevent multiple commutation failures and substantial energy loss [13]. The CIGRÉ benchmark model lacks such provisions in the control circuit, and in this study it is not intended to include a remedial action in the controls for commutation failure. Examples of such provisions are discussed in [40], [41]. However, to somewhat limit the inter-converter interactions in this case, converter 1 was intentionally blocked after detection of the CF in the valves. The test setup for this case is shown in Figure 5-5, and the dotted line used for converter 1 is meant to show it being blocked after CF detection.

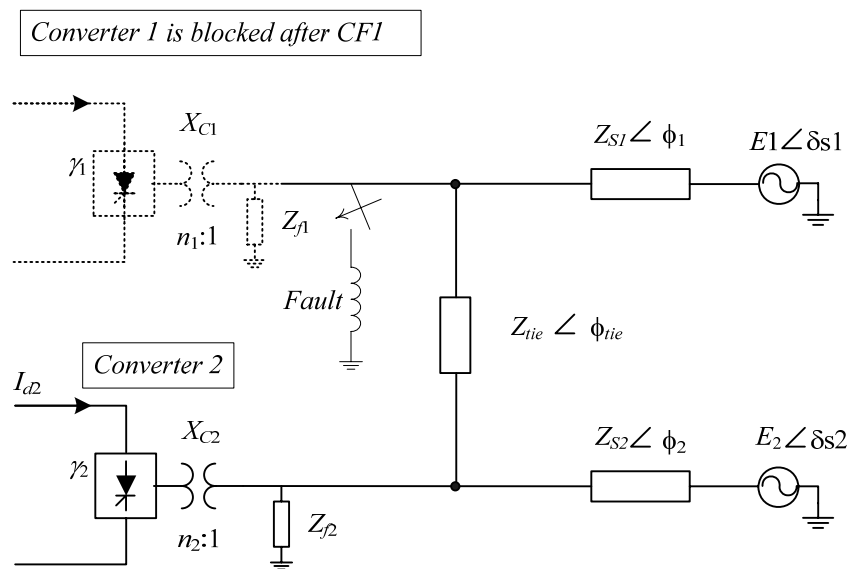
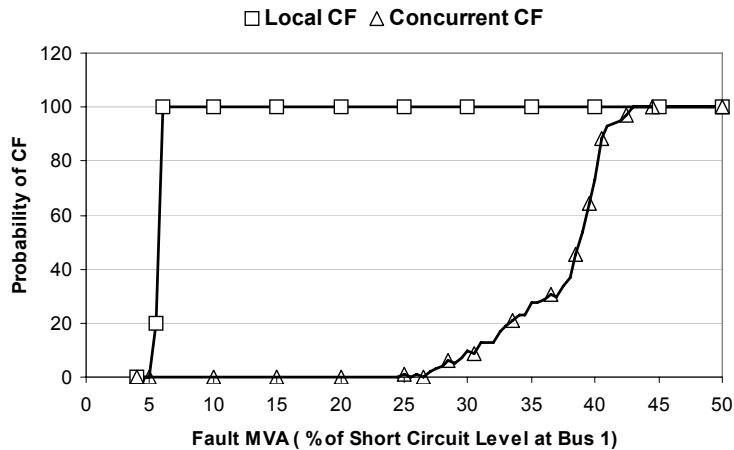


Figure 5-5: Multi-infeed test system for Case 2

The results of this case study for both local and concurrent commutation failures are given in Figure 5-6.



**Figure 5-6: Local and concurrent commutation failure probability curve for Case 2**

Based on the severity of fault, the plot can be divided into the following regions. As before, the fault level is pre unitized as a fraction of the system short circuit capacity (SCC) at that bus.

- i) Fault level  $< 5\%$  : no commutation failure occurs
- ii)  $5\% < \text{Fault level} < 25\%$ : commutation failure only occurs for the local converter
- iii)  $25\% < \text{Fault level} < 42\%$ : probability of commutation failure in the remote converter is no longer zero
- iv) Fault level  $> 42\%$ : commutation failure definitely occurs in the remote converter

Note that in Case 1, in which the converter 1 was not in operation, the non-zero probability of a commutation failure started at fault levels around 35% (see Figure 5-4). Hence, the susceptibility of the remote converter to commutation failure due to a fault at a local converter is higher when both converters are

operating. This is an important conclusion that should be considered in the planning of MIHVDC systems.

The system performance in this case is as expected and there is no anomalous behaviour: the higher the fault level, the higher the probability of commutation failure.

### Case 3: Two Converters in Operation (Multi-Infeed System), No Change in Controls

This is a re-simulation of Case 2. The only difference is that there is no converter blocking of the local converter upon the occurrence of a commutation failure and converter 1 continues to operate regardless of any CF. The probabilities of local and concurrent CF for different fault levels at bus 1 are plotted in Figure 5-8. It shows that concurrent CF occurs not only for relatively severe faults, as expected based on earlier results, but also for very minor faults, which is rather unexpected. Additionally, there is no concurrent commutation failure for many intermediate values of faults.

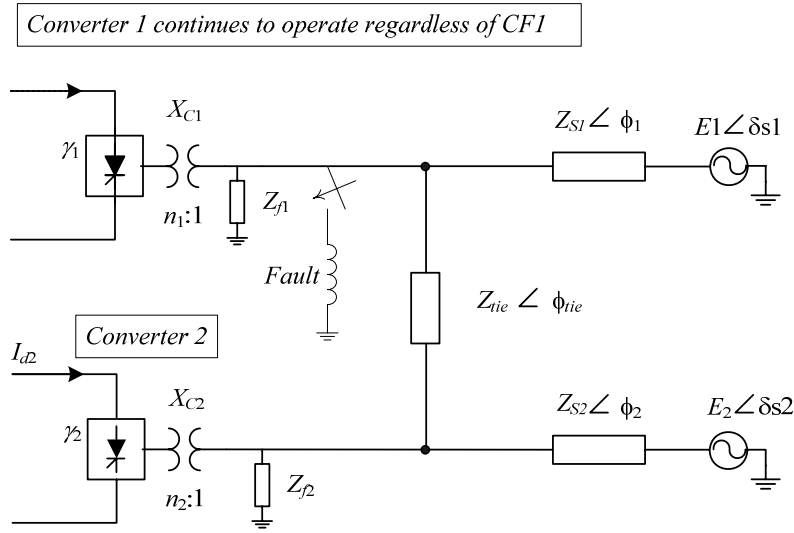


**Figure 5-7: Multi-infeed test system for Case 3**

The cause of such unexpected behaviour is examined in the following section by analyzing the shape of the voltage waveforms at the ac terminals of the HVDC converters.

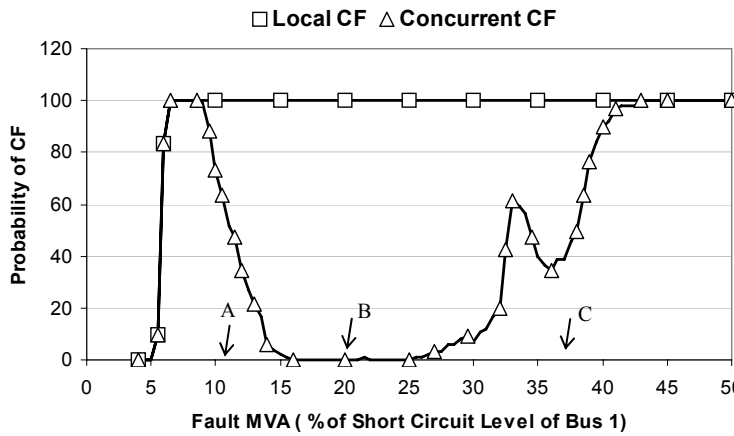


**Figure 5-8: Results for Case 3 (Converter 1 continues to operate regardless of CF1).**

### 5.4.2. Analysis of Anomalous Concurrent CF

To investigate the cause of anomalous behaviour, the ac commutating voltage of an off-going valve is recorded for the following cases. As before, the fault level is pre unitized as a fraction of the system short circuit capacity (SCC) at that bus.

- i) Normal operation of the converter without fault
- ii) Following a fault with 12% fault levels (Point A in Figure 5-8)
- iii) Following a fault with 20% fault levels (Point B in Figure 5-8)
- iv) Following a fault with 37% fault levels (Point C in Figure 5-8)

These fault levels are applied at a point on wave at which converter 2 does not suffer a CF, but is on the borderline of doing so for 12% and 37% fault levels. The commutating voltage waveforms are plotted in Figure 5-9. The reason for the above anomalous behaviour becomes apparent on inspecting the respective commutation waveforms, as shown in Figure 5-9.

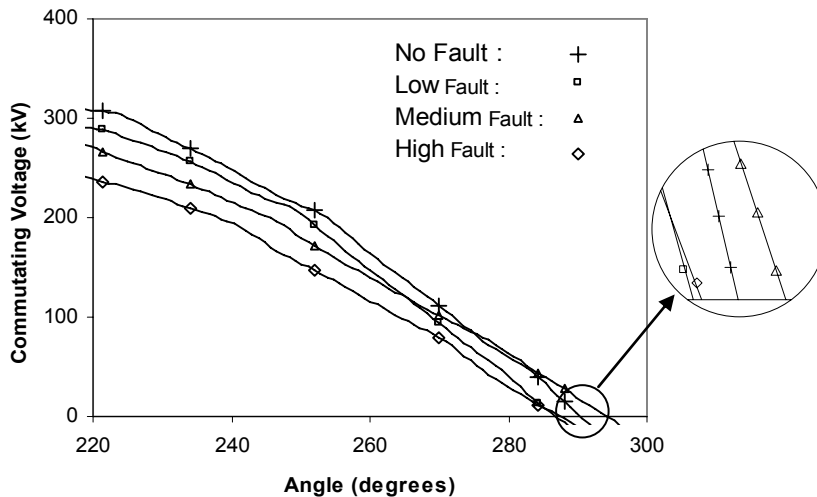


**Figure 5-9: Commutating voltage of the off-going valve**

For the more severe fault, the ac voltage reduction is larger than for the no fault case or the less severe fault cases, as expected. However, for the less severe faults, the zero crossing of the voltage is advanced as compared to the other cases. This shows that although the commutation voltage is less depressed for the weaker fault case, the commutation margin is reduced because of the advancement of the valve voltage bringing the valve to the precipice of commutation failure. Note that the intermediate fault level has the voltage zero crossing much later, allowing a greater commutation margin.

Note also that the stronger fault effectively temporarily improves the short circuit ratio as it decreases the total Thévenin impedance, in comparison to the weaker fault. Hence, the waveform for the weaker fault is more distorted, and this is the chief reason for its zero crossing to be advanced. The distortion is evident from a spectral plot of the harmonic distribution of Figure 5-10, which shows that the harmonic content for the low fault level case is considerably higher than other cases, especially at lower harmonics.

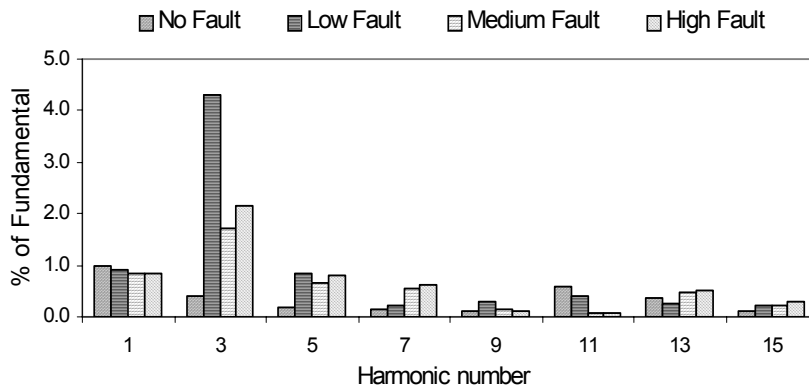


**Figure 5-10: Comparison of the voltage harmonics at low and high fault levels**

This analysis shows that the dominant cause of CF for the remote converter at low local fault levels is the distortion of the voltage waveform. However, for more severe faults, although the distortion is less, sudden reduction in the magnitude of the fundamental voltage is the primary cause of CF.

#### 5.4.3. Correlation between the MIIF and Concurrent CF

In a concurrent commutation failure, a fault at a local converter causes a commutation failure for the remote converter. Since the MIIF quantifies the level of inter-converter interactions, it would be expected that the concurrent commutation failure would be mainly a function of the MIIF.

In order to check this theory, several different system configurations with local and remote ESCR ranging from 2 to 10 were considered. For each of these systems, the MIIF was calculated. Transient simulations were also carried out on the systems, in the same manner as described in Section 4.5.2, to calculate the threshold fault levels at bus 1 that do not cause concurrent commutation failure on converter 2 for any point on wave. In these simulations, converter 1 is blocked after detection of a CF to prevent a CF in the remote converter caused by voltage distortion. The results are given in Figure 5-11. For each of the circles shown in the plot, the simulation has been carried out to calculate the MIIF and the threshold fault level. For example, point X in Figure 5-11 represents a system for which  $MIIF_{2,1} = 0.21$ . The fault level equal to 40% of the short circuit level at bus 1 is the maximum fault level that does not cause a concurrent commutation failure.

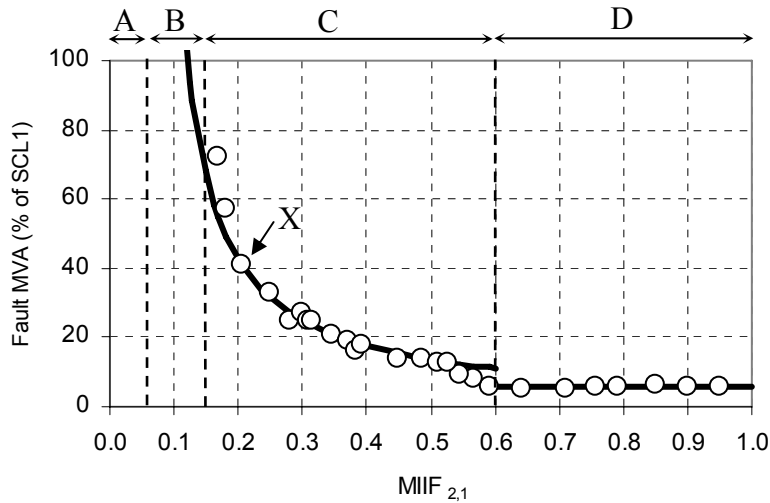


**Figure 5-11: Correlation between  $MIIF_{2,1}$  and CF-causing ac faults**

The results show that the MIIF could be a useful parameter in estimating the propensity for concurrent commutation failures. The correlation between the MIIF and immunity to concurrent commutation failure can be divided into four regions based on the value of MIIF:  $MIIF_{2,1} \leq 0.06$ ;  $0.06 < MIIF_{2,1} \leq 0.15$ ;  $0.15 < MIIF_{2,1} \leq 0.6$ ; and  $MIIF > 0.6$ . These regions are identified in Figure 5-11 with A, B, C, and D, respectively. Each of the regions is discussed below.

#### 5.4.4. Region A: $MIIF_{2,1} \leq 0.06$

In this MIIF range, the converters are decoupled as the  $MIIF \approx 0$ . Hence, there is very little voltage dip at the remote converter from a three-phase fault at the local converter; and consequently no concurrent CF is observed, regardless of the fault severity. The two converters are essentially not connected with each other. The majority of the HVDC systems in operation to date are in this category.



#### 5.4.5. Region B: $0.06 < \text{MIIF}_{2,1} \leq 0.15$

For this MIIF range, a three-phase fault at bus 1 will cause a commutation failure on the remote converter 2, but this is independent of the presence of converter 1. Simulation results showed that in this range of the MIIF, the occurrence of a commutation failure in system 1 has no impact on the commutation of the valves in system 2, and therefore the commutation failure behaviour of system 2 is independent of the status of the converter 1. This is in line with the recommendations given in [3] that suggest that for a  $\text{MIIF} < 0.15$  the interactions between converters could be ignored. A formula for calculation of the threshold fault level based on the MIIF is presented in Section 5.4.8.

#### 5.4.6. Region C: $0.15 < \text{MIIF}_{2,1} \leq 0.6$

In this MIIF range, the correlation between the MIIF and immunity to concurrent commutation failure is similar to Region B. The immunity to concurrent commutation failure increases as the MIIF decreases. A formula for calculation of the threshold fault level based on the MIIF is presented in Section 5.4.8.

#### 5.4.7. Region D: $\text{MIIF}_{2,1} > 0.6$

For these values of  $\text{MIIF}_{2,1}$ , the commutation failure in system 1 will most likely cause a concurrent commutation failure in system 2. For this  $\text{MIIF}_{2,1}$  range commutation failure occurs for the remote converter even if converter 1 is blocked after detection of a CF. For this MIIF range, converters could be considered to be on the same ac bus as far as the CF phenomenon is concerned.

Note that this is consistent with the earlier observations in Chapter 2 that as the MIIF approaches 1.0, the system becomes a single-infeed system as if both converters are connected to the same ac bus.

#### 5.4.8. An Equation to Represent the MIIF-CFII Correlation

The curve (solid line) in Figure 5-11 is a fit for the mathematical Equation in (5-2), which is heuristically obtained based on the study results presented in Section 5.4.3. Using the MIIF, Equation (5-2) calculates the fault level at bus 1 that results in a concurrent commutation failure on converter 2.

$$\begin{aligned}
 &\text{For } MIIF_{2,1} \leq 0.06 \\
 &\quad \text{fault level} = \infty \\
 &\text{For } 0.06 < MIIF_{2,1} \leq 0.6 \\
 &\quad \text{fault level} = [(MIIF_{2,1} / 0.06) - 1]^{-1} \times 100 (\%) \\
 &\text{For } 0.6 < MIIF_{2,1} \\
 &\quad \text{fault level} = 6 (\%)
 \end{aligned} \tag{5-2}$$

where :

fault level means  $(V_1^2 / Z_{fault})$  Per unitized to the short circuit capacity at the ac bus

Note that the term “fault level” as used in (5-2) and plotted in Figure 5-11, is a relative measure for the fault impedance and is essentially  $(V_1^2 / Z_{fault})$  per unitized to the short circuit capacity at the ac bus. Although alternative fitting equations could also be developed using curve fitting techniques to fit the simulation results of Figure 5-11, there is a particular appeal in using (5-2). This is because the fault level at the local converter (bus 1) of  $[(MIIF_{2,1} / 0.06) - 1]^{-1} \times 100\%$  of the  $SCL_1$  results in a voltage drop of approximately 6% at the remote converter (bus 2) using simplified steady state calculation. Hence, the commutation failure phenomenon can be related to a voltage depression of a specific magnitude.

Therefore, (5-2) can be used to give an estimate of the immunity to concurrent commutation failure at the remote converter caused by an ac fault at the local converter.

### 5.5. CF Phenomena in Multi-Infeed Systems with Different Ratings

To see if the approach used in Section 5.4 can be extended to MI systems with varying converter rating ratios, additional studies were conducted and are discussed here. The ratio of the ratings between two converters in a multi-infeed configuration is represented by the power base ratio (PBR) given in (2-7), which is repeated in (5-3) for convenience.

$$PBR_{j,i} = \frac{P_{dcj}}{P_{dci}} \quad (5-3)$$

To verify the validity of using the MIIF for concurrent CF studies, several multi-infeed configurations with  $PBR_{2,1}$  ranging from 0.1 to 2.0 are considered.

As discussed in Chapter 4, it should be noted that when conducting the simulations, dc side elements such as the smoothing reactor, the resistance, and the capacitance of the dc line were appropriately resized to offer the same per-unit values in all cases. For example, if the converter rating is reduced to 25% by reducing the rated dc current to 25% and keeping the rated dc voltage the same, the smoothing inductance in Henries must be increased by a factor of 4. This is because the dc side impedance base ( $Z_{base} = V/I$ ) is now 4 times larger and the same per-unit inductance means a larger actual inductance.

The results showing the correlation between concurrent CF and MIIF are plotted in Figure 5-12. The points for all power base ratios essentially cluster around the same curve as those shown in Figure 5-12.

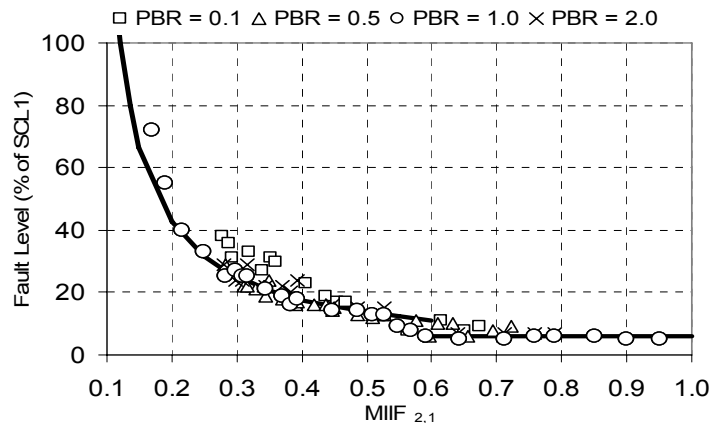


**Figure 5-12: Impact of system ratings on concurrent commutation failure**

The fitting Equation (5-2) heuristically derived in Section 5.4.8 is thus equally applicable even when the two dc converters do not have the same rating. Hence, it can be concluded that the concurrent commutation failure behaviour of multi-infeed systems can be predicted by the same characteristic regardless of the relative power ratings of the individual converters.

## 5.6. CF Prevention and Remedial Actions in MI Systems

Each converter in a multi-infeed HVDC system should be individually equipped with commutation failure prevention methods applicable to single-infeed systems. In addition to that, a coordinated strategy for recovery from faults is required to minimize the negative impacts of mutual interactions on the recovery process [40]. Increasing the safety margin for  $\gamma$  decreases the chance of commutation failure and increases the chance of successful recovery if

a CF occurs [42]. However, these benefits are obtained at the expense of increased reactive power demand as well as higher converter and transformer ratings.

A coordinated control design in multi-infeed systems [43],[44] has the potential to minimize the number of commutation failures and ensure that a single failure is not prolonged into a succession of failures. Detail design of such coordinated control should be optimized for each specific HVDC scheme and is not attempted in this thesis.

## **5.7. Summary and Conclusions of Chapter 5**

The analysis of CF in multi-infeed systems indicates that local commutation failures are essentially affected only by the local short circuit ratio, with the immunity level increasing as the local ESCR increases. With regard to concurrent CF, distortion of the voltage waveform due to a CF of the local converter and significant reduction in the ac voltage magnitude are the two distinct causes of CF for a remote converter. Voltage distortion could cause an anomalous CF on the remote converter that should be analyzed in detail in the planning process of MIHVDC systems.

For an MIIF  $< 0.15$ , the occurrence of the commutation failure in converter 2 is independent of the status of converter 1. On the other end of the spectrum, for an MIIF  $> 0.6$  a CF in converter 1 always causes a CF in converter 2. This is consistent with the general guideline that suggests as MIIF approaches zero, the two HVDC links could be analyzed as two single-infeed systems; and when MIIF

approaches 1 the system performance is as if the converters are connected to the same bus.

For a  $0.06 < \text{MIIF} < 0.6$ , the tendency towards concurrent CF is determined principally by the MIIF index, with the immunity level decreasing as the MIIF increases. A simple mathematical formula can be heuristically fitted to this behaviour. This study also concludes that the correlation between the MIIF and the CFII is valid for dc systems with different power ratings, which makes these indices powerful tools in the assessment of CF performance in multi-infeed HVDC systems.

## **6. Conclusions and Recommendations for Future Research**

This thesis makes a contribution to the understanding of the interaction phenomena in multi-infeed systems. The new indices and formulas developed in this thesis are helpful for the analysis and planning of the multi-infeed HVDC systems. The MIIF, MIESCR, and CFII indices are powerful tools for the analysis of transient overvoltage, PV stability, and commutation failure phenomena.

The possibility of anomalous commutation failure, reported in this thesis, should be considered in the planning of multi-infeed HVDC systems in order to prevent successive commutation failure and cascading outages of the HVDC links.

### **6.1. The Main Contributions of this Thesis**

The following contributions to the field are made by this thesis:

- The voltage interaction level between the ac converter buses was quantified using the MIIF index. A parametric study was conducted to assess the impact of ac system configuration on the MIIF. To make the parametric study feasible, new calculation methods and closed-form formulas were developed.
- In collaboration with Dr. Ioni Fernando, the MIESCR index was developed. When all the converters proportionally share the power order, the MIESCR has the same applications in multi-infeed systems as the ESCR has in single-infeed systems. Hence, the critical MIESCR value for PV stability is 1.5.
- It was proved that in the transient overvoltage (TOV) analysis of a multi-infeed system with any number of infeeds, the worst case TOV level could be obtained by replacing the ESCR with the MIESCR in the corresponding formulas. The worst case TOV occurs when all the converters in a multi-infeed system are simultaneously blocked.
- A commutation failure immunity index (CFII) that uses electromagnetic transient simulation to quantify the immunity of HVDC converters to ac-fault-induced commutation failure was developed.
- Anomalous concurrent commutation failure phenomena in multi-infeed systems were identified and their causes discussed.



- The applications of the new indices were demonstrated in the planning studies for an actual dc scheme in the Province of Alberta, Canada.
- A new component in PSCAD was developed that guides the multiple-run module in the PSCAD program in the calculation of the CFII. This component reduces the required number of runs by an order of magnitudes.

## **6.2. Summary of the Conclusions**

The conclusions of each chapter of this thesis are summarized in the final section of each chapter. A summary of all the conclusions is provided here for quick reference.

### **6.2.1. MIIF Calculation Methods, Range, and Critical Values**

The definition of MIIF is based on the dynamic simulation of the ac/dc system, but it is shown that using fault current calculations the MIIF formula provides a reasonably accurate estimate of the MIIF. It should be noted that  $MIIF_{i,j}$  is different from  $MIIF_{j,i}$ .

If the MIIF is less than 0.15, the interactions between the HVDC systems could be ignored and the studies could be performed as if the HVDC schemes are independent. As MIIF approaches 1.0, the dc schemes could be assumed to be on the same bus and the system could be analyzed as a single-infeed scheme.

It should be noted that the MIIF is not meant to replace detailed analysis of different phenomena in multi-infeed systems, but rather it is meant to give a high-level indication of possible issues.

### 6.2.2. MIESCR Definition and Application in Multi-infeed Systems

MIESCR is an index that quantifies the strength of the ac system in a multi-infeed case. The MIESCR could be applied in a similar manner to that in which ESCR is applied in single-infeed system.

The transient overvoltage, power-voltage stability, and commutation failure phenomena were analyzed. It was shown that both the ESCR and the MIESCR should be utilized in the analysis of multi-infeed systems. When the performance of only one converter is analyzed while the other converters are operating at nominal ratings, the ESCR index is applicable. If all the converters are simultaneously blocked or change the output power, the MIESCR index is applicable.

MIESCR varies in the  $\frac{ESCR_i}{\sum P_{dc_j}} \leq MIESCR_i \leq ESCR_i$  range, and the threshold

values are similar to the ESCR index:  $MIESCR > 3$  represents a strong ac system,  $2 < MIESCR < 3$  represents a weak or moderately strong system, and  $MIESCR < 2$  represents a very weak ac system. It is recommended that in a multi-infeed HVDC design the MIESCR be at least 2.5 to have a stable and acceptable performance.

The critical MIESCR value for PV stability is approximately 1.5. For this value of MIESCR the system is on the border of instability.

### 6.2.3. Commutation Failure in Single-Infeed Systems

The probability of the occurrence of a commutation failure due to an ac fault depends on many parameters of the ac/dc systems, and also on the severity of the fault and on the time instance of fault application. The impact of all the parameters is taken into account in the electromagnetic simulation of the ac/dc system resulting in the CFII.

The CFII is almost linearly correlated with the ESCR index. The higher the ESCR is, the higher the immunity of the HVDC converter to commutation failure is. Increasing the inductance of the smoothing reactor may increase or decrease the CFII. A faster current controller at the rectifier side would increase the CFII. It is also concluded that the CFII is not a function of the rating of the HVDC scheme.

### 6.2.4. Commutation Failure in Multi-Infeed Systems

In this thesis the commutation failure events in multi-infeed systems are divided into local commutation failures and concurrent commutation failures. If an ac fault causes a commutation failure only on the nearby local converter, the event is called a local commutation failure and its occurrence is mostly a function of the ESCR. If an ac fault causes a commutation failure not only on the nearby local converter but also on the remote converter, the event is categorized as a concurrent commutation failure. This study shows that the probability of a

concurrent commutation failure for the remote converter due to a fault on local converter is mostly a function of the MIIF between the two ac buses. For MIIF values less than 0.06, there is no chance of concurrent commutation failure due to a local fault. For MIIF values more than 0.6, a commutation failure on the local converter will always cause a commutation failure on the remote converter as if they are on the same bus.

It was shown in the studies that multi-infeed HVDC systems could experience anomalous concurrent commutation failure where a commutation failure unexpectedly occurs at low fault levels due to the voltage distortion and occurs at high fault levels due to the ac voltage drop.

The above characteristics are valid in systems comprising HVDC links with different ratings. A heuristic formula was developed based on the simulation results that represents the correlation between the concurrent CFII and the MIIF index for the MIIF values in the  $0.06 < \text{MIIF} < 0.6$  range.

### **6.3. Thesis Publications**

The following papers were entirely or partially written based on the research conducted during the progress of this thesis.

#### **6.3.1. Technical Brochure (CIGRÉ publication)**

1. B. Davies, A. Williamson, A. M. Gole, B. Ek, B. Long, B. Burton, D. Kell, D. Brandt, D. Lee, **E. Rahimi**, G. Andersson, H. Chao, I. T. Fernando, K. L. Kent, K. Sobrink, M. Haeusler, N. Dhaliwal, N. Shore, P. Fischer, and S. Filizadeh, “**Systems with multiple DC infeed,**” CIGRÉ Working Group B4.41, Dec. 2008, Publication 364.

### 6.3.2. Journal Paper

1. **E. Rahimi**, A.M. Gole, J.B. Davies, I.T. Fernando, K.L. Kent, "Commutation Failure Analysis in Multi-infeed HVDC Systems," IEEE Transactions on Power Delivery, Vol. 26, No. 1, pp. 378-384, January 2011.

### 6.3.3. Conference Papers

1. **E. Rahimi**, A.M. Gole, J.B. Davies, "Analysis of Multi-Infeed HVDC systems with inverter and rectifier connected to the same ac network," In Proc. 10th IEE International Conference on AC-DC Power Transmission, London, UK, 2010, Paper No. 37.
2. I.T. Fernando, K.L. Kent, J.B. Davies, **E. Rahimi**, A.M. Gole, "Parameters for Planning and Evaluation of Multi-Infeed HVDC Schemes," CIGRÉ Symposium on System Development and Asset Management under Restructuring, Osaka, Japan, November 01-04, 2007, Paper 326.
3. **E. Rahimi**, A.M. Gole, J.B. Davies, I.T. Fernando, K.L. Kent, "Commutation Failure in Single- and Multi-infeed HVDC Systems," In Proc. 8th IEE International Conference on AC-DC Power Transmission, London, UK, 2006, pp. 182-186.
4. **E. Rahimi**, A.M. Gole, J.B. Davies, I.T. Fernando, K.L. Kent, "Commutation Failure and Overvoltage Phenomena in Multi-Infeed HVDC Systems," In Proc. Colloquium of Role of HVDC, FACTS and Emerging Technologies in Evolving Power Systems, Bangalore, India, September 2005, pp. 54 – 73.
5. **E. Rahimi**, S. Filizadeh, A.M. Gole, "Commutation Failure Analysis Using Advanced Multiple-Run Methods," IPST 2005 conference, Montreal, QC, Jun. 19-23, 2005, Paper IPST05-160-17c.

6. Qahraman B., **Rahimi E.**, Gole A.M., "An Electromagnetic Transient Simulation Model for Voltage Sourced Converter Based HVDC Transmission," In Proc. 2004 Canadian Conference on Electrical and Computer Engineering, CCECE04.

#### **6.4. Recommended Future Research**

The concepts, methodologies, and indices developed in this thesis have great potential for further research in the area of multi-infeed HVDC systems. In this section, several topics that could be further researched using this thesis as a base to build upon are discussed.

##### **6.4.1. Application of the Indices in Cases in which HVDC Links are in Parallel with AC Lines**

There are several schemes in the world that, in addition to the HVDC link, have ac lines that transfer power from the sending end to the receiving end of the HVDC link [44]. Such a configuration is technically a multi-infeed system if the MIIF between the rectifier and inverter is high. This type of system configuration needs further research, especially if the MIIF between the sending and receiving end is relatively high ( $MIIF > 0.15$ ).

For example, in such a system configuration the calculation of the transient overvoltage is very complex. When there is no ac connection between the ends of an HVDC link, there is no path for a voltage disturbance to be transferred from one end to the other. However, the existence of an ac connection creates the

possibility that voltage fluctuations at the rectifier side will have an impact on the inverter side, and vice versa.

#### 6.4.2. Analysis of Multi-Infeed Schemes in which the Inverter and Rectifier of Independent Schemes are Connected to the same AC Network

One example of such a system, in which there is an ac interconnection between the rectifier and inverter of an HVDC link, is discussed in the section above. Under these circumstances, technically the rectifier absorbs power from the ac system and the inverter injects power to the same ac system.

Another example would be an ac system that covers a vast geographic area with a large amount of variable generation, such as wind generation, concentrated at one corner of the area. In this system configuration, if the variable generation is low (for example, a no-wind scenario) all the HVDC schemes will deliver power to the area. Whereas, in the case of high variable generation (for example, a high wind scenario), the dc links close to the cluster of generators will absorb power from the system (rectifiers) while the rest of the dc links will deliver power to the load area of the system (inverters). The interactions between the rectifiers and inverters in such a system configuration, the impact on commutation failure phenomena, the transient overvoltage, and the power-voltage stability in such systems need further analysis [46].

#### 6.4.3. Further Study to Evaluate the Impact of other HVDC Transmission Technologies on the Application of the Indices and the Validity of the Recommendations

The focus of this thesis is the application of HVDC technology for bulk power transmission, which at this time is carried out by conventional line-commutated converters. However, due to the advances in new technologies for power transmission, such as voltage sourced converter (VSC) technology [47]-[51], new technologies could be used in high power transmission schemes with ratings of several thousand megawatts [50]. The operation of VSC-based HVDC transmission technology is fundamentally different from the operation of conventional HVDC converter technology. VSC transmission offers many benefits that could be utilized in the overall design of a multi-infeed scheme. The performance of a multi-infeed system comprising conventional HVDC technology and VSC-based HVDC technology and its impact on transient overvoltage, commutation failure of the conventional converter, and voltage stability of the system is an interesting topic for further research.

#### 6.4.4. Analytical Proof for the Value of Critical MIESCR (CMIESCR) for a General Case with n HVDC Infeeds

It has been proven analytically that the critical value for the ESCR with regard to voltage and power stability could be obtained using Equation (3-2). The criteria for the critical ESCR is that the derivative of the dc power versus the dc current ( $\partial P_{dc} / \partial I_{dc}$ ) should be equal to zero at  $I_{dc} = 1.0$  pu.



Since the calculation of the  $\partial P_{dc} / \partial I_{dc}$  in multi-infeed systems is complex, in this thesis the critical MIESCR value was calculated using simulation tools. Many system configurations with varying parameters were tested and the CMIESCR value was calculated for those systems. Based on the study results for many cases it was concluded that the value for the CMIESCR is similar to the CIESCR and is around 1.5. Using a simulation tool is a valid method for proving a hypothesis, but technically the conclusion is only valid for the systems studied. However, an analytical proof for the CMIESCR creates more confidence in using the index and shows the limitations of the application of the index.

## References

- [1] Long, W.; Nilsson, S.; "HVDC Transmission: Yesterday and Today," IEEE Power and Energy Magazine, Vol. 5, No. 2, pp. 22-31, March/April 2007.
- [2] Asplund G., Carlsson L., Tollerz O., "50 Years of HVDC ", *ABB Review* 4/2003, pp. 06-13.
- [3] B. Davies, A. Williamson, A. M. Gole, B. Ek, B. Long, B. Burton, D. Kell, D. Brandt, D. Lee, E. Rahimi, G. Andersson, H. Chao, I. T. Fernando, K. L. Kent, K. Sobrink, M. Haeusler, N. Dhaliwal, N. Shore, P. Fischer, and S. Filizadeh, "Systems with multiple DC infeed," CIGRÉ Working Group B4.41, Dec. 2008, Publication 364.
- [4] E. W. Kimbark, *Direct Current Transmission*. New York: Wiley, 1971, vol. I.
- [5] J. Arrillaga, *High Voltage Direct Current Transmission*. 2nd Edition, IEE publications, 1998.
- [6] Hammons, T.J.; Woodford, D.; Loughtan, J.; Chamia, M.; Donahoe, J.; Povh, D.; Bisewski, B.; Long, W.; "Role of HVDC transmission in future energy development," IEEE Power Engineering Review, Vol. 20, No. 2, pp. 10-25, Feb. 2000.
- [7] Barthold. L.O., "Technical and Economic Aspects of Tripole HVDC," International Conference on Power System Technology, Powercon 2006, Chongqing, China, pp. 1-6, 22-26 Oct. 2006.
- [8] Lionel Barthold, R. Adapa, Harrison Clark, Dennis Woodford, "System Advantages in Conversion of AC Transmission Lines to DC," Presented in 10<sup>th</sup> International Conference on AC-DC Power Transmission, London, UK, Paper No. 1.

- [9] Aik, D.L.H., Andersson G., "Power Stability Analysis of Multi-Infeed HVDC Systems," *IEEE Trans. Power Delivery*, Vol. 13, pp. 923 – 931, July 1998.
- [10] Aik, D.L.H.; Andersson, G.; "Voltage Stability Analysis of Multi-Infeed HVDC Systems," *IEEE Trans. Power Delivery*, Vol. 12, pp. 1309 – 1317, July 1997.
- [11] Lee Hau Aik, D.; Andersson, G.; "Influence of load characteristics on the power/voltage stability of HVDC systems. Part 1: Basic equations and relationships," *IEEE Transactions on Power Delivery*, Vol. 13, Issue 4, pp. 1437-1444, October 1998.
- [12] Lee Hau Aik, D.; Andersson, G.; "Influence of load characteristics on the power/voltage stability of HVDC systems. Part 2: Stability Margin Sensitivity," *IEEE Transactions on Power Delivery*, Vol. 13, Issue 4, pp. 1445-1452, October 1998.
- [13] *High-Voltage Direct Current Handbook*, First Edition, Electric Power Research Institute, Palo Alto, California, 1994
- [14] Kundur P., "Power System Stability and Control," EPRI Power System Engineering Series, McGraw-Hill, 1994.
- [15] Barker, C.; Jenkins, A.; Davidson, C.; Ebockayuk, D.; Gold, J.; Kayibabu, B.; Kirby, N.; Li, M.; MacLeod, N.; Matthews, B.; McConnachie, I.; Mendiratta, G.; Monteiro, J.; Mukhedkar, R.; Oh'Eidhin, G.; Sadullah, S.; Stevenson, D.; Stott, T.; Whitehouse, R.; Wu, X.; "HVDC: Connecting to the future," Alstom Grid, 2010.
- [16] Lips H. P., "Aspects of Multiple Infeed of HVDC Inverter Stations into a Common A.C. System," *IEEE Trans. Power Apparatus and Systems*, Vol. PAS-92, pp. 775 – 779, March/April 1973.
- [17] Pilotto, L.A.S.; Szechtman, M.; Wey, A.; Long, W.F.; Nilsson, S.L.; "Synchronizing and Damping Torque Modulation Controllers for Multi-Infeed HVDC Systems," *IEEE Trans. Power Delivery*, Vol. 10, No. 3, pp. 1505 – 1513, July 1995.
- [18] Thio, C.V., Davies, J.B., Kent, K.L., "Commutation failures in HVDC transmission systems," *IEEE Trans. Power Delivery*, Vol. 11, pp. 946 – 957, April 1996.
- [19] E. Rahimi, A.M. Gole, J.B. Davies, I.T. Fernando, K.L. Kent, "Commutation Failure Analysis in Multi-infeed HVDC Systems," *IEEE Transactions on Power Delivery*, Vol. 26, No. 1, pp. 378-384, January 2011.
- [20] Nayak, O.B.; Gole, A.M.; Chapman, D.G.; Davies, J.B.; "Dynamic performance of static and synchronous compensators at an HVDC inverter bus in a very weak AC system," *IEEE Trans. Power Systems*, Vol. 9, No. 3, pp. 1350 – 1358, August 1994.
- [21] Xiao Jiang; Gole, A.M.; "A frequency scanning method for the identification of harmonic instabilities in HVDC systems," *IEEE Trans. Power Delivery*, Vol. 10, No. 4, October 1995.

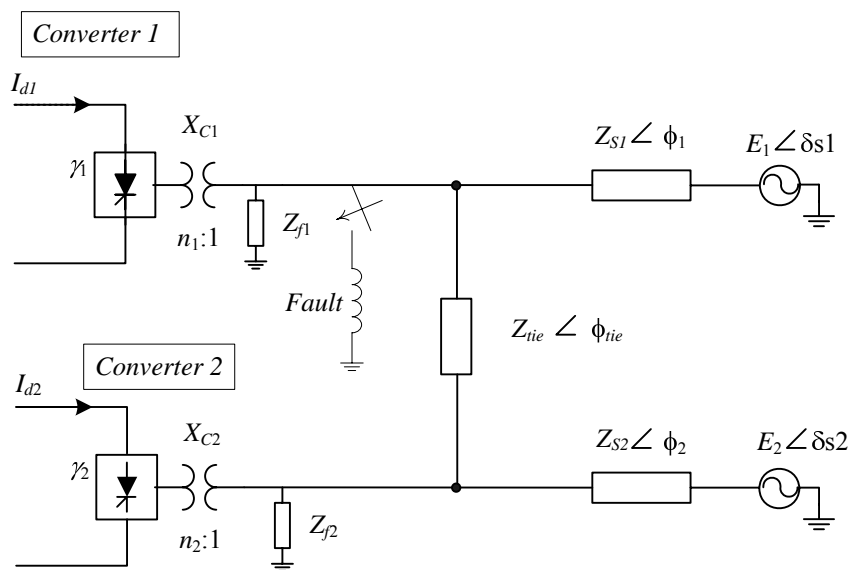
- [22] Reeve, J.; Lane-Smith, S.P.; "Multi-infeed HVDC transient response and recovery strategies," *IEEE Trans. Power Delivery*, Vol. 8, No. 4, pp. 1995-2001, Jan. 1993.
- [23] Nayak, O.B.; Gole, A.M.; Chapman, D.G.; Davies, J.B.; "Control sensitivity indices for stability analysis of HVDC systems," *IEEE Trans. Power Delivery*, Vol. 10, No. 4, pp. 2054- 2060, October 1995.
- [24] Claudio A. Cañizares, Fernando L. Alvarado, Christopher L. DeMarco, Ian Dobson, Willis F. Long, "Point of Collapse Methods Applied to Large AC/DC Power Systems," *IEEE Transactions on Power Systems*, Vol. 7, No. 2, pp. 673-683, May 1992.
- [25] Cañizares, C.A.; Alvarado F.L., "Point of Collapse and Continuation Methods for Large ac/dc Systems," *IEEE Transactions on Power Systems*, Vol. 8, No. 1, pp. 1-8, Feb 1993.
- [26] Chan-Ki Kim, Vijay K. Sood, Gil-Soo Jang, Seong-Joo Lim, Seok-Jin Lee, "HVDC Transmission: Power Conversion Applications in Power Systems," pp. 151-159, John Wiley and Sons, 2009.
- [27] Gole, A.M.; Meisingset, M.; "Capacitor Commutated Converters for Long-Cable HVDC Transmission," *Power Engineering Journal*, Vol. 16, No. 3, pp. 129-134, June 2002.
- [28] E. Rahimi, A.M. Gole, J.B. Davies, I.T. Fernando, K.L. Kent, "Commutation Failure and Overvoltage Phenomena in Multi-Infeed HVDC Systems". In *Proc. Colloquium of Role of HVDC, FACTS and Emerging Technologies in Evolving Power Systems*, Bangalore, India, September 2005, pp. 54 – 73.
- [29] I.T. Fernando, K.L. Kent, J.B. Davies, E. Rahimi, A.M. Gole, "Parameters for Planning and Evaluation of Multi-Infeed HVDC Schemes," *CIGRÉ Symposium on System Development and Asset Management under Restructuring*, Osaka, Japan, November 01-04, 2007, Paper 326.
- [30] E. Rahimi, A.M. Gole, J.B. Davies, I.T. Fernando, K.L. Kent, "Commutation Failure in Single- and Multi-infeed HVDC Systems," In *Proc. 8th IEE International Conference on AC-DC Power Transmission*, London, UK, pp. 182-186.
- [31] Paulo Fischer de Toledo, Bernt Bergdahl, Gunnar Asplund, "Multiple Infeed Short Circuit Ratio – Aspects Related to Multiple HVDC into One AC Network," in *Proc. IEEE/PES Transmission and Distribution Conference and Exhibition Asia Pacific*, Dalian, China, August 14-18, 2005.
- [32] Mercedes Sanchez Illanas, "Evaluation of a new definition for a Multi-Infeed Short Circuit Ratio," M.Sc. Dissertation, KTH Electrical Engineering, Electrical Power Systems, Stockholm, March 2007.

- [33] Szechtman M., et al "Commutation failures in HVDC transmission systems due to ac system faults". CIGRÉ WG 14.02, *Electra*, No. 169, pp. 59 – 85, December 1996.
- [34] K. R. Padiyar, "HVDC power transmission systems: technology and system interactions," New Age International (P) Limited Publishers, 2005
- [35] Szechtman M., Wess T., C.V. Thio, "First Benchmark Model for HVDC Control Studies". CIGRÉ WG 14.02, *Electra*, No. 135, pp. 54 – 73, April 1991.
- [36] EMTDC Manual, Winnipeg: Manitoba HVDC Research Center, 2003.
- [37] E. Rahimi, S. Filizadeh, A.M. Gole, "Commutation Failure Analysis Using Advanced Multiple-Run Methods", presented at the IPST 2005 conference, Montreal, QC, Jun. 19-23, 2005, Paper IPST05-160-17c.
- [38] A. M. Gole, S. Filizadeh, R. W. Menzies, P. L. Wilson, "Optimization-Enabled Electromagnetic Transient Simulation," *IEEE Trans. Power Delivery*, vol. 20, no. 1, pp. 512-518, Jan. 2005.
- [39] Changchun Zhou, Zheng Xu, "Study of Commutation Failure of Multi-infeed HVDC systems," in Proc. Int. Conference on Power System Technology, 2002.
- [40] Machida, T.; Yoshida, Y.; "A Method to Detect the Deionization Margin Angle and to Prevent the Commutation Failure of an Inverter for DC Transmission," *PAS-86*, No. 3, pp. 259-262, July 1967.
- [41] Bauman, J.; Kazerani, M.; "Commutation Failure Reduction in HVDC Systems Using Adaptive Fuzzy Logic Controller," *IEEE Trans. Power Systems*, Vol. 22, No. 4, Dec. 2007.
- [42] Meisingset, M.; Gole, A.M.; "A Comparison of Conventional and Capacitor Commutated Converters Based on Steady-State and Dynamic Considerations," in Proc. Seventh International Conference on AC-DC Power Transmission, pp. 49-54, 28-30 November 2001.
- [43] Karawita, C.; Annakkage, U.D.; "Multi-Infeed HVDC Interaction Studies Using Small-Signal Stability Assessment," *IEEE Trans. Power Delivery*, Vol. 24, No. 2, pp. 910-918, April 2009.
- [44] Verdolin, R.; Gole, A.M.; Kuffel, E.; Diseko, N.; Bisewski, B.; "Induced overvoltages on an AC-DC hybrid transmission system," *IEEE Trans. Power Delivery*, Vol. 10, No. 3, pp. 1514-1524, July 1995.
- [45] Yang, W.D.; Xu, Z.; Han, Z.X.; "Co-ordinated hierarchical control strategy for multi-infeed HVDC systems," *IEE Proceedings on Generation, Transmission and Distribution*, Volume: 149 , Issue: 2, pp. 242 – 248, 2002.
- [46] E. Rahimi, A.M. Gole, J.B. Davies, "Analysis of Multi-Infeed HVDC systems with inverter and rectifier connected to the same ac network," In Proc. 10th IEE

- International Conference on AC-DC Power Transmission, London, UK, 2010, Paper No. 37.
- [47] Qahraman B., Rahimi E., Gole A.M., "An Electromagnetic Transient Simulation Model for Voltage Sourced Converter Based HVDC Transmission," In Proc 2004 Canadian Conference on Electrical and Computer Engineering, CCECE04.
- [48] Papic, I., Zunko, P., "UPFC converter-level control system using internally calculated system quantities for decoupling," *Int. Journal of Electrical Power and Energy Systems*, Vol. 25, pp. 667-675, October 2003.
- [49] Schauder, C., Mehta, H., "Vector analysis and control of advanced static VAR compensators," *IEE Proceedings-Generation, Transmission and Distribution*, Vol. 140, pp. 299-306, July 1993.
- [50] Dragan Jovcic; "Thyristor-Based HVDC With Forced Commutation," *IEEE Trans. Power Delivery*, Vol. 22, No. 1, pp. 557-564, Feb. 2007.
- [51] N. Hörle, K. Eriksson, A. Maeland, T. Nestli, "Electrical supply for offshore installations made possible by use of VSC technology," *CIGRÉ 2002 Conference*, Paris, France, Aug 2002.

## Appendix A - HVDC Test System Data

The schematic diagram of a multi-infeed test system used in this thesis is given in the following.



Parameters of each HVDC link, tie-line impedance, and the ac source Thévenin impedances are given in Table A-1 below.

TABLE A.1: TEST SYSTEM PARAMETERS

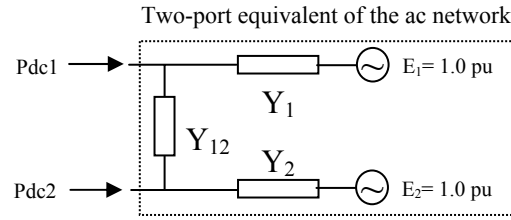
BASE MODEL: CIGRÉ HVDC BENCHMARK MODEL		
HVDC SYSTEM	DC Line Resistance = $5.0 \Omega$	
500 kV	DC Line +Smoothing Reactor = 1.194 H	
1000 MW	$\alpha = 15^\circ, \gamma = 15^\circ$	
RECTIFIER SIDE		
AC SYSTEM	FILTERS + CAPACITORS (MVAR)	TRANSFORMERS (EACH)
345 kV, 50 Hz	11 <sup>th</sup> harmonic: 252	345/213.5 kV
SCR: 2.5 at $84^\circ$	13 <sup>th</sup> harmonic: 252	603.73 MVA
	Capacitors: 125	$X_s = 0.18$ p.u.
INVERTER SIDE		
230 kV, 50 Hz	11 <sup>th</sup> harmonic: 252	230/209.2 kV
SCR: 2.5 at $75^\circ$	13 <sup>th</sup> harmonic: 252	591.79 MVA
	Capacitors: 125	$X_s = 0.18$ p.u.
TIE-LINE IMPEDANCE		
Z ( $\Omega$ /km)		X/R
0.41		6.0
SNUBBER CIRCUIT (SERIES RC)		
R		5000 $\Omega$
C		0.05 $\mu$ F
AC source impedances are modelled as L-L  R in which the impedance angle at 3 <sup>rd</sup> harmonic is equal to the impedance angle at fundamental frequency.		
Commutation failure is detected by observing when the absolute sum of the absolute values of the ac-valve side currents becomes less than twice the magnitude of the dc current [11].		



## **Appendix B – Derivation of the MIIF Formula**

In this appendix, the derivation of a closed-form formula for approximate calculation of the MIIF is presented:

$$MIIF_{2,1} = \frac{\Delta V_2 \%}{1\% \text{ voltage change in } V_1}$$



As shown in the above equation, the MIIF is basically the voltage drop at bus 2 for a 1% voltage drop at bus 1. Assuming the 1% drop as a voltage source at bus 1, the amount of voltage drop at bus 2, which is the MIIF, will be the voltage division of between  $Y_{12}$  and  $Y_2$ .

The following notation for the system parameters will be used in the derivation of the formula:

$S_1$  = Short circuit current at bus 1

$S_2$  = Short circuit current at bus 2

$S_{2,1}$  = Short circuit current for simultaneous fault at bus 1 and bus 2 (Base MVA)

$M_{2,1}$  =  $MIIF_{2,1}$

Assuming 1.0 pu voltage for the ac system, the following formulas could be used for short circuit capacities:

$$S_1 = Y_1 + \frac{Y_{12} \cdot Y_2}{Y_{12} + Y_2}$$

$$S_2 = Y_2 + \frac{Y_{12} \cdot Y_1}{Y_{12} + Y_1}$$

$$S_{2,1} = Y_1 + Y_2 = 1$$

$$M_{2,1} = \frac{Y_{12}}{Y_{12} + Y_2} \Rightarrow Y_{12} = \frac{M_{2,1}}{1 - M_{2,1}} \cdot Y_2$$

$$S_1 = Y_1 + \frac{Y_{12} \cdot Y_2}{Y_{12} + Y_2} = \frac{Y_{12} \cdot (Y_1 + Y_2) + Y_1 \cdot Y_2}{Y_{12} + Y_2} = M_{2,1} + \frac{Y_1 \cdot Y_2}{\frac{M_{2,1}}{1 - M_{2,1}} \cdot Y_2 + Y_2} = M_{2,1} + \frac{Y_1}{\frac{M_{2,1}}{1 - M_{2,1}} + 1} = M_{2,1} + Y_1 \cdot (1 - M_{2,1}) \Rightarrow Y_1 = \frac{S_1 - M_{2,1}}{1 - M_{2,1}}$$

$$S_2 = Y_2 + \frac{Y_{12} \cdot Y_1}{Y_{12} + Y_1} \Rightarrow S_2 \cdot (Y_{12} + Y_1) = Y_{12} \cdot Y_2 + Y_1 \cdot Y_2 + Y_{12} \cdot Y_1 = Y_{12} + Y_1 - Y_1^2 \Rightarrow Y_1^2 = (Y_{12} + Y_1) \cdot (1 - S_2)$$

$$Y_{12} + Y_1 = \frac{M_{2,1}}{1 - M_{2,1}} \cdot (1 - Y_1) + Y_1$$

$$Y_1^2 = \left( \frac{M_{2,1}}{1 - M_{2,1}} \cdot (1 - Y_1) + Y_1 \right) \cdot (1 - S_2) = \left( \frac{M_{2,1}}{1 - M_{2,1}} + Y_1 \cdot \frac{1 - 2 \cdot M_{2,1}}{1 - M_{2,1}} \right) \cdot (1 - S_2)$$

$$\left( \frac{S_1 - M_{2,1}}{1 - M_{2,1}} \right)^2 = \left( \frac{M_{2,1}}{1 - M_{2,1}} + Y_1 \cdot \frac{1 - 2 \cdot M_{2,1}}{1 - M_{2,1}} \right) \cdot (1 - S_2)$$

$$(S_1 - M_{2,1})^2 = (M_{2,1} + Y_1 \cdot (1 - 2 \cdot M_{2,1})) \cdot (1 - S_2) \cdot (1 - M_{2,1})$$

$$\begin{aligned} S_1^2 + M_{2,1}^2 - 2 \cdot S_1 \cdot M_{2,1} &= (M_{2,1} + Y_1 \cdot (1 - 2 \cdot M_{2,1})) \cdot (1 - M_{2,1} - S_2 + S_2 \cdot M_{2,1}) = M_{2,1} - M_{2,1}^2 - S_2 \cdot M_{2,1} + S_2 \cdot M_{2,1}^2 + (1 - 2 \cdot M_{2,1}) \cdot (1 - S_2) \cdot (S_1 - M_{2,1}) \\ &= M_{2,1} - M_{2,1}^2 - S_2 \cdot M_{2,1} + S_2 \cdot M_{2,1}^2 + (1 - 2 \cdot M_{2,1}) \cdot (S_1 - S_1 \cdot S_2 - M_{2,1} + S_2 \cdot M_{2,1}) \\ &= M_{2,1} - M_{2,1}^2 - S_2 \cdot M_{2,1} + S_2 \cdot M_{2,1}^2 + S_1 - S_1 \cdot S_2 - M_{2,1} + S_2 \cdot M_{2,1} - 2 \cdot M_{2,1} \cdot S_1 + 2 \cdot M_{2,1} \cdot S_1 \cdot S_2 + 2 \cdot M_{2,1}^2 - 2 \cdot S_2 \cdot M_{2,1}^2 \end{aligned}$$

$$S_1^2 = -S_2 \cdot M_{2,1}^2 + S_1 - S_1 \cdot S_2 + 2 \cdot M_{2,1} \cdot S_1 \cdot S_2$$

$$M_{2,1}^2 - 2 \cdot S_1 \cdot M_{2,1} + \frac{S_1}{S_2} \cdot (S_1 + S_2 - 1) = 0$$

$$M_{2,1} = S_1 - \sqrt{\frac{S_1}{S_2} (1 - S_1) \cdot (1 - S_2)}$$

$$Y_1 = \frac{S_1 - M_{2,1}}{1 - M_{2,1}}$$

$$Y_2 = 1 - Y_1$$

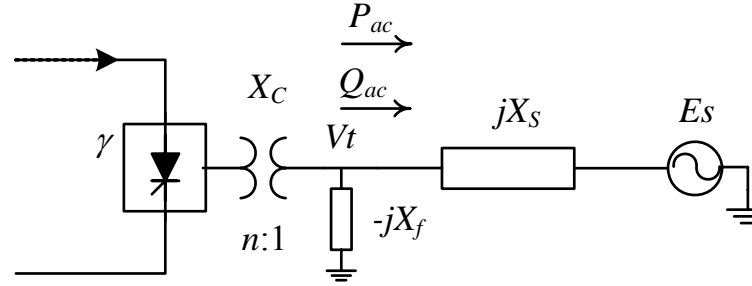
$$Y_{12} = \frac{M_{2,1}}{1 - M_{2,1}} \cdot Y_2$$

By replacing the 1 and 2 in the above equations, a similar formula could be developed for MIIF<sub>1,2</sub>.

## **Appendix C –TOV Formula in Single-Infeed Systems**

In this appendix, the derivation of a closed-form formula to calculate the transient overvoltage due to the blocking of an HVDC converter is discussed.

The schematic diagram of the inverter side of a single-infeed HVDC system is shown in the following figure:



Assuming that the HVDC converter is operating at nominal current and voltage and also assuming that system impedance is purely inductive, we have:

$$P_{dc} = P_{ac} = 1 \text{ pu}; \quad Q_{ac} = Q_f - Q_{dc}; \quad V_t = 1 \text{ pu}$$

$$I_{ac} = \left( \frac{P_{ac} + jQ_{ac}}{V} \right) = P_{ac} - jQ_{ac} = 1.0 - j \cdot (Q_f - Q_{dc})$$

$$E_s = V_t - j \cdot X_s \cdot I_{ac} = 1.0 - j \cdot X_s \cdot (1.0 - j \cdot (Q_f - Q_{dc}))$$

$$E_s = 1.0 - X_s \cdot (Q_f - Q_{dc}) - j \cdot X_s$$

After blocking the dc converter

$$V_{t\_after\_blocking} = E_s \cdot \frac{-jX_f}{-jX_f + jX_s} = (1.0 - X_s \cdot (Q_f - Q_{dc}) - j \cdot X_s) \cdot \frac{X_f}{X_f - X_s}$$

Also we have:

$$Q_f = \frac{1}{X_f}, \quad ESCR = \frac{1}{X_s} - \frac{1}{X_f} \Rightarrow X_s = \frac{1}{ESCR + \frac{1}{X_f}} = \frac{1}{ESCR + Q_f}$$

$$Vt\_after\_blocking = (1.0 - X_s \cdot (Q_f - Q_{dc}) - j \cdot X_s) \cdot \frac{1}{X_s \cdot ESCR}$$

$$Vt\_after\_blocking = \left( \frac{1}{X_s \cdot ESCR} - \frac{(Q_f - Q_{dc})}{ESCR} - \frac{j}{ESCR} \right)$$

$$Vt\_after\_blocking = \left( \frac{ESCR + Q_f}{ESCR} - \frac{(Q_f - Q_{dc})}{ESCR} - \frac{j}{ESCR} \right)$$

$$Vt\_after\_blocking = \left( 1.0 + \frac{Q_{dc}}{ESCR} - \frac{j}{ESCR} \right)$$

$$TOV = |Vt\_after\_blocking| - 1.0 \text{ (pu)}$$

$$TOV = \sqrt{1.0 + \frac{2 \cdot Q_{dc}}{ESCR} + \frac{1 + Q_{dc}^2}{ESCR^2}} - 1.0 \text{ pu}$$

For  $Q_{dc} = 0.5$  and  $Q_{dc} = 0.55$  the TOV formulas are:

$$TOV_{(Q_{dc}=0.5)} = \sqrt{1.0 + \frac{1.0}{ESCR} + \frac{1.25}{ESCR^2}} - 1.0$$

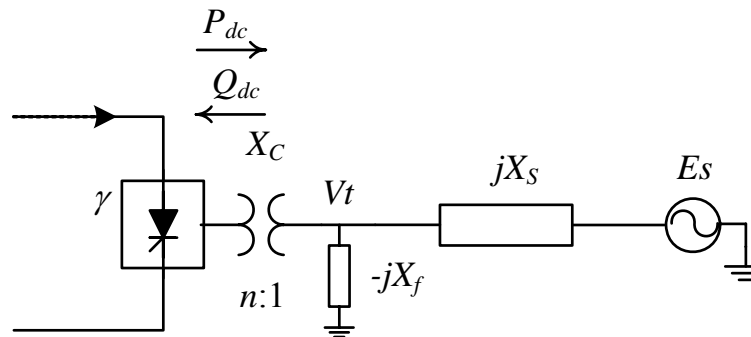
$$TOV_{(Q_{dc}=0.55)} \approx \sqrt{1.0 + \frac{1.1}{ESCR} + \frac{1.3}{ESCR^2}} - 1.0$$

## **Appendix D –TOV Formula in Multi-Infeed Systems**

A formula to calculate the transient over voltage (TOV) in single-infeed systems is derived in Appendix C. In this appendix, a formula for TOV calculation in multi-infeed systems is derived.

The calculation is carried out under similar assumptions as the calculation in a single-infeed system; it is assumed that the impedance of the ac system is purely inductive. It is also assumed that the HVDC schemes are operating at their nominal power prior to the blocking. The following formula gives the highest amount of overvoltage that occurs when all the dc links in the multi-infeed system are blocked simultaneously.

The following figure shows a typical converter bus and the current that is injected into the bus by the HVDC converter as well as the Thévenin ac source:



$$\text{Current injected by the HVDC converter} = \left( \frac{P_{dc} - jQ_{dc}}{V_t} \right)$$

$$\text{Current injected from the Thévenin equivalent voltage} = \frac{E_s}{jX_s}$$

Therefore, using the KCL ( $Y \cdot V = I$ ) on the converter ac bus we have:

$$\left( \frac{1}{jX_s} + \frac{1}{-jX_f} \right) \cdot V_t = \left( \frac{P_{dc} - jQ_{dc}}{V_t} \right) + \frac{E_s}{jX_s}$$



Without losing generality, it could be assumed that the system under study is system 1 and the voltage and power of link 1 is used in the per-unitizing of all other systems. With these assumptions, the following equation is valid at nominal operating conditions:

$$Y \cdot V = I_{HVDC} + I_{Source} = \frac{Pdc + jQdc}{\bar{V}} - jYs \cdot Es$$

In which Y is the system admittance matrix, V is a vector of complex numbers for bus voltages,  $I_{HVDC}$  is a vector of the current injected to the converter ac buses by HVDC converters,  $I_{Source}$  is the Thévenin equivalent current source, and  $Ys$  is the vector of the Thévenin inductances.

The above equation could be solved to calculate the Thévenin ac sources ( $Es$ ):

$$Es = -jYs^{-1}(Pdc + jQdc) + jYs^{-1}Y$$

By replacing  $Es$  in the equation and considering that after blocking of the dc converters  $Pdc$  and  $Qdc$  will be zero for all converters, the maximum TOV is calculated in the followings:

$$Y \cdot V_{TOV} = -jYs \cdot (-jYs^{-1}(Pdc + jQdc) + jYs^{-1}Y)$$

$$Y \cdot V_{TOV} = -Pdc - jQdc + Y$$

$$V_{TOV} = Y^{-1} \cdot (-Pdc - jQdc + Y)$$

$$V_{TOV} = 1 - Y^{-1}(Pdc + jQdc) = 1 - jZ \cdot (Pdc + jQdc) = 1 + Z \cdot Qdc - jZ \cdot Pdc$$

Based on the above equation for the TOV at the converter buses, the voltage at bus 1 after blocking all the converters is:

$$V_{1\_TOV} = 1 + Q_{dc1} \cdot (z_{11} + z_{12} \cdot \frac{Q_{dc2}}{Q_{dc1}} + \dots + z_{1n} \cdot \frac{Q_{dcn}}{Q_{dc1}}) - j \cdot (z_{11} + z_{12} \cdot P_{dc2} + \dots + z_{1n} \cdot P_{dcn})$$

Assuming that  $Q_{dcn}/Q_{dc1}=P_{dcn}/P_{dc1}$ , the above equation could be rewritten in the following form:

$$V_{1\_TOV} = 1 + Q_{dc1} \cdot (z_{11} + z_{12} \cdot P_{dc2} + \dots + z_{1n} \cdot P_{dcn}) - j \cdot (z_{11} + z_{12} \cdot P_{dc2} + \dots + z_{1n} \cdot P_{dcn})$$

Considering the Equation (3.7) for MIESCR, which is equivalent to MIESCR, we have:

$$z_{11} + z_{12} \cdot P_{dc2} + \dots + z_{1n} \cdot P_{dcn} = \frac{1}{MIESCR_1}$$

By replacing the above equation in the  $V_{1\_TOV}$  formula, we have:

$$V_{1\_TOV} = 1 + \frac{Q_{dc1}}{MIESCR_1} - j \cdot \frac{1}{MIESCR_1}$$

$$TOV_1 = \sqrt{1.0 + \frac{2 \cdot Q_{dc1}}{MIESCR_1} + \frac{1 + Q_{dc1}^2}{MIESCR_1^2}} - 1.0$$

Similarly, for any converter bus in the system it could be shown that:

$$TOV_i = \sqrt{1.0 + \frac{2 \cdot Q_{dci}}{MIESCR_i} + \frac{1 + Q_{dci}^2}{MIESCR_i^2}} - 1.0$$